

BL ✓
ETHOS ✓
7/1/14

FOR REFERENCE ONLY

0 1 AUG 2008

41 0674647 2



ProQuest Number: 10183501

All rights reserved

INFORMATION TO ALL USERS

The quality of this reproduction is dependent upon the quality of the copy submitted.

In the unlikely event that the author did not send a complete manuscript and there are missing pages, these will be noted. Also, if material had to be removed, a note will indicate the deletion.



ProQuest 10183501

Published by ProQuest LLC (2017). Copyright of the Dissertation is held by the Author.

All rights reserved.

This work is protected against unauthorized copying under Title 17, United States Code
Microform Edition © ProQuest LLC.

ProQuest LLC.
789 East Eisenhower Parkway
P.O. Box 1346
Ann Arbor, MI 48106 – 1346

Laser Processing of Inkjet Printed and RF Magnetron Sputtered SnO₂:Sb

Sharron Louise Wilson

A thesis submitted in part fulfilment of the requirements of Nottingham Trent
University for the degree of Doctor of Philosophy

This research programme was carried out in collaboration with Keeling &
Walker Ltd and PTL Ltd

School of Science and Technology
Nottingham Trent University

June 2008

Copyright Statement

This work is the intellectual property of the author, and may also be owned by the research sponsor(s) and/or Nottingham Trent University. You may copy up to 5% of this work for private study, or personal, non-commercial research. Any re-use of the information contained within this document should be fully referenced, quoting the author, title, university, degree level and pagination. Queries or requests for any other use, or if a more substantial copy is required, should be directed in the first instance to the author.

Abstract

The desire for flexible electronics, in particular, flexible displays is driving research into processing methods that would enable the application of a range of functional materials to low temperature substrates. Transparent Conducting Oxides are materials which typically require thermal annealing or deposition at elevated temperatures to obtain suitable characteristics. Sputter deposited Indium Tin Oxide (ITO or $\text{In}_2\text{O}_3:\text{SnO}_2$) is the most common transparent conductor material, but indium is relatively scarce and therefore expensive. Antimony Tin Oxide (ATO or $\text{SnO}_2:\text{Sb}$) is a promising alternative that, in the present study, has been formulated into an inkjet printable solution for direct-write patterning and for the first time the novel method of laser processing has been shown to improve the characteristics via a technique that could be used with low temperature substrates.

Films of inkjet printed $\text{SnO}_2:\text{Sb}$ have been laser processed using a KrF UV Excimer laser emitting at 248nm. The electrical and optical properties of the films have been investigated for a range of laser fluences and number of pulses. A morphological examination has also been undertaken using x-ray diffraction, scanning electron microscopy and transmission electron microscopy. Furthermore, RF magnetron sputtered films of $\text{SnO}_2:\text{Sb}$ deposited onto a flexible substrate (Cronar®) have been laser processed to provide a comparator. The electrical, optical and morphological characteristics of these films have also been investigated.

It has been demonstrated that the electrical properties of both inkjet printed and RF magnetron sputtered films of $\text{SnO}_2:\text{Sb}$ can be improved with laser processing. The conductivity of inkjet printed films was improved by two orders of magnitude, while RF magnetron sputtered films underwent a 1.5 fold improvement. Increases in crystallinity were observed for laser processed inkjet printed films and electron microscopy showed an area of densification consistent with the expected optical penetration depth. Shifts in the IR end of the transmission spectrum indicated an increase in carrier concentration. In contrast, no increases in crystallinity nor areas of densification were detectable with RF magnetron sputtered films and there was no apparent shift in the IR end of the transmission spectra. The mechanisms for improvement in the conductivity of the films are discussed in terms of increasing the carrier concentration and mobility of inkjet printed films, and reducing the defect regions for the RF magnetron sputtered films.

Acknowledgements

I am extremely grateful to Professor Wayne Cranton for his amazing support, help and encouragement throughout this project and also for providing the opportunity to undertake this study. Thanks also to Dr Robert Ranson for, amongst many other things, the patient hours he has spent explaining much of the equipment and techniques used during this study. Special thanks also go to Professor Clive Thomas for keeping me on my toes and for the numerous informative and entertaining lectures. Also to Dr Costas Tsakonis and Dr Demothenes Koutsogeorgis I would like to express my gratitude for their technical help and discussions.

Thanks also to the ELjet project partners Keeling & Walker Ltd, PTL Ltd and in the early days, The IFM Company for many informative discussions, the supply of inkjet printed samples and their financial support. With a note of thanks also to Dr Stuart Speakman, I have enjoyed and found helpful our numerous telephone discussions. My gratitude is also extended to the DTI, in particular Cathy Williams and the Engineering and Physical Sciences Research Council for their support, both financial and otherwise.

Many people have given me the benefit of their experience over the years and helped with analytical equipment, laboratory set-ups or measurements and I am grateful to the following for their assistance in this way: Steve Burton, David Elgin, Steve Furzeland, James Hind, Gary Hix, Chris Pateman, and Christophe Trabi.

To my fellow PhD students, Sook Voon Yap, Thomas Miller, Gabriel Boutaud and Carly Farrow thank you for making the past few years fun, but also particular thanks to Gabriel and Tom for all their technical assistance during my pregnancy.

I wish to extend many thanks to my friends and family, I am extremely grateful and feel very lucky to have received their support and encouragement. Very special thanks go to Shirley Wilson and my mum Susan Waring for enabling me to finish this thesis. Finally a big thank you to my wonderful, patient and kind husband Ivan for his understanding and encouragement and for the sacrifices he has had to make for me to complete this, I am forever indebted to him and our little boy Oscar.

List of Publications

S. L. Wilson, W. M. Cranton, R. Ranson, D. C. Koutsogeorgis, A. Mosley, C. B. Thomas, G. Boutaud, S. Wagland, E. A. Mastio, S. Lipiec, A. Spiller, J. Scott, and S. Stoute, "*P-169: Optimization of the Electrical and Optical Properties of Ink-Jet-Printed SnO₂:Sb using Thermal Annealing and Excimer-Laser Processing*," SID Symposium Digest of Technical Papers, vol. 36, pp. 530, 2005

W. M. Cranton, S. L. Wilson, R. Ranson, D. C. Koutsogeorgis, K. Chi, R. Hedgley, J. Scott, S. Lipiec, A. Spiller, and S. Speakman, "*Excimer laser processing of inkjet-printed and sputter-deposited transparent conducting SnO₂:Sb for flexible electronics*" Thin Solid Films, vol. 515, pp. 8534, 2007.

List of Presentations

Oral Presentations

14th December 2004: Science Engineering and Technology for Britain, House of Commons, UK.

5th January 2005: COMIT Faraday Presentations, Cambridge, UK

25th April 2006: East Midlands Engineering and Science Professionals Masters Prize Presentations, Loughborough, UK.

Poster Presentations

2nd June 2004: Photonics 2004, London, UK.

23rd – 25th May 2005: Society for Information Display International Symposium, Boston, USA.

22nd June 2005: Photonics 2005, London, UK.

List of Symbols

Symbol	Description	Unit
Bz	Magnetic Flux Density	T
E	Electric Field	V/cm
E_F	Fermi Level	eV
ϵ	Relative Permittivity	F/cm
ϵ_0	Permittivity of Free Space	F/m
ϵ_∞	Material Permittivity	F/m
F(E)	Probability of Finding Electron at Given Energy State	
I	Current	A
j_x	Current Density	A/cm ²
k	Boltzman Constant	J/K
k	Extinction coefficient	
m_e	Effective Mass of Electron	kg
n	Refractive Index	
n	Carrier Concentration	cm ⁻³
n_t	Density of Trapped Carriers	cm ⁻³
N	Density of Allowed States	cm ⁻³
N_T	Density of Ionised Impurity States	cm ⁻³
N_c	Density of States in the Conduction Band	cm ⁻³
ρ	Resistivity	Ω cm
q	Magnitude of Electric Charge	C
R	Hall Coefficient	
R _s	Sheet Resistance	Ω /sq
t	Film Thickness	nm
T	Absolute Temperature	K
τ_c	Mean Free Time	s
μ	Electron Mobility	cm ² /Vs
μ_d	Drift Mobility	cm ² /Vs
V	Voltage	V
V_H	Hall Voltage	V
v	Velocity	m/s
v_n	Drift Velocity	cm/s
ω_p	Plasma Resonance Frequency	Hz
σ	Conductivity	Ω^{-1} cm ⁻¹
λ	Wavelength	nm
ϕ_0	Photon Flux	W/m ²
α	Absorption Coefficient	cm ⁻¹

List of Abbreviations

ArF	Argon Fluoride
ATO	Antimony Tin Oxide
COJ	Continuous Inkjet
CVD	Chemical Vapour Deposition
DC	Direct Current
DOD	Drop On Demand
DTI	Department for Trade and Industry
EL	Electroluminescent
EPSRC	Engineering and Physical Sciences Research Council
FWHM	Full Width at Half Maximum
IR	Infrared
ITO	Indium Tin Oxide
KrF	Krypton Fluoride
LCD	Liquid Crystal Display
Nd:YAG	Neodymium-doped Yttrium Aluminium Garnet
NTU	Nottingham Trent University
OLED	Organic Light Emitting Display
PDA	Personal Digital Assistant
PE-CVD	Plasma Enhanced Chemical Vapour Deposition
PEDOT	Poly (3,4-ethylenedioxythiophene)
PEN	Polyethylene Naphthalate
PET	Polyethylene Terephthalate
PSI	Pounds per Square Inch
PSI	Phase Shift Interferometry (chapter 3)
RF	Radio Frequency
RTA	Rapid Thermal Annealing
SEM	Scanning Electron Microscopy
TCO	Transparent Conducting Oxide
TEM	Transmission Electron Microscopy
TFT	Thin Film Transistor
UV	Ultraviolet
VSI	Vertical Scanning Interferometry
XeCl	Xenon Chloride
XRD	X-ray Diffraction

Contents

1. INTRODUCTION TO PROJECT	1-1
1.1 INTRODUCTION	1-1
1.2 AIM.....	1-4
1.3 OBJECTIVES	1-4
1.4 THESIS SCOPE AND STRUCTURE.....	1-5
1.5 HISTORICAL CONTEXT	1-7
1.6 THE ELJET PROJECT.....	1-7
2. BACKGROUND REVIEW	2-1
2.1 SEMICONDUCTOR MATERIALS	2-1
2.1.1 <i>Crystalline structures</i>	2-1
2.2 CARRIER TRANSPORT MECHANISMS.....	2-2
2.2.1 <i>Introduction</i>	2-2
2.2.2 <i>Carrier Drift</i>	2-3
2.2.3 <i>Carrier Scattering</i>	2-4
2.2.4 <i>Carrier Diffusion</i>	2-5
2.2.5 <i>Recombination Processes</i>	2-6
2.2.6 <i>Trapping</i>	2-6
2.2.6.1 The Effect of Traps on Mobility.....	2-7
2.2.6.2 Passivation	2-8
2.2.6.3 Grain Boundaries	2-8
2.2.7 <i>The Hall Effect</i>	2-9
2.3 TRANSPARENT CONDUCTING OXIDES	2-11
2.3.1 <i>Introduction</i>	2-11
2.3.2 <i>Optical Properties</i>	2-12
2.3.2.1 Absorption coefficient.....	2-15
2.3.3 <i>Tin Oxide</i>	2-17
2.3.4 <i>Indium Tin Oxide vs Antimony Tin Oxide</i>	2-18
2.3.5 <i>Antimony-Tin Oxide</i>	2-19
2.3.5.1 Thermal Annealing of SnO ₂ :Sb.....	2-21
2.3.5.2 Summary	2-24
2.4 DEPOSITION METHODS FOR ATO.....	2-24
2.4.1 <i>Introduction</i>	2-24
2.4.2 <i>Sputtering</i>	2-24
2.4.3 <i>Alternative Deposition Processes</i>	2-26
2.4.3.1 Dip-Coating.....	2-27
2.4.3.2 Spray Pyrolysis.....	2-27
2.4.3.3 Chemical Vapour Deposition.....	2-28
2.5 PRINTING TECHNOLOGIES	2-29
2.5.1 <i>Inkjet Printing</i>	2-30

2.6	FLEXIBLE SUBSTRATES.....	2-32
2.7	LASER PROCESSING OF THIN FILMS	2-33
2.7.1	<i>Introduction</i>	2-33
2.7.2	<i>Applications</i>	2-34
2.7.3	<i>Interactions</i>	2-35
2.7.4	<i>Laser Processing of Transparent Conductors</i>	2-37
2.8	APPLICATIONS.....	2-38
2.8.1	<i>Electronic Displays</i>	2-38
2.8.2	<i>Solar Cells</i>	2-40
2.8.3	<i>Anti-reflection coatings</i>	2-40
3.	EXPERIMENTAL PROCEDURES	3-1
3.1	PROCESSING TECHNOLOGIES	3-1
3.1.1	<i>Laser Processing System</i>	3-1
3.1.1.1	Thermal model	3-3
3.1.2	<i>Sputtering System</i>	3-3
3.1.3	<i>Sputtering Targets</i>	3-5
3.1.3.1	Powder Targets.....	3-5
3.1.3.2	Sputtering parameters.....	3-7
3.1.4	<i>Thermal Processing</i>	3-7
3.2	METROLOGY SYSTEMS	3-7
3.2.1	<i>Optical Profiler</i>	3-7
3.2.1.1	Phase-Shifting Interferometry	3-8
3.2.1.2	Vertical-Scanning Interferometry.....	3-8
3.2.2	<i>Filmetrics</i>	3-9
3.2.3	<i>SEM</i>	3-10
3.2.4	<i>TEM</i>	3-11
3.2.5	<i>X-ray Diffraction</i>	3-12
3.2.5.1	The Debye-Scherrer Equation	3-14
3.3	ELECTRICAL CHARACTERISTICS.....	3-14
3.3.1	<i>Four Point Probe</i>	3-14
4.	ELECTRICAL AND OPTICAL PROPERTIES.....	4-1
4.1	THERMAL ANNEALING.....	4-1
4.1.1	<i>Thermal annealing in air of inkjet printed SnO₂:Sb on soda lime glass</i>	4-1
4.1.1.1	Film Stability.....	4-4
4.1.2	<i>Summary of inkjet printed ATO thermally annealed on soda lime glass</i>	4-5
4.1.3	<i>Thermal annealing in various atmospheres of inkjet printed ATO on borosilicate</i>	4-6
4.1.3.1	Sheet Resistance.....	4-7
4.1.3.2	Transmission	4-7
4.1.3.3	Hall Effect	4-9
4.1.3.4	Summary	4-9
4.1.4	<i>Thermal annealing of SnO₂:Sb on Quartz</i>	4-9

4.1.4.1	Sheet Resistance.....	4-10
4.1.4.2	Transmission	4-10
4.1.4.3	Summary	4-11
4.2	LASER PROCESSING	4-12
4.2.1	<i>ATO inkjet printed onto borosilicate</i>	4-12
4.2.1.1	Sheet Resistance.....	4-13
4.2.1.2	Transmission	4-14
4.2.2	<i>Laser Processing in Argon at Pressure</i>	4-15
4.2.3	<i>Thermal Annealing and Laser Processing on Borosilicate</i>	4-16
4.2.3.1	Summary	4-17
4.2.4	<i>ATO RF magnetron sputtered onto Cronar®</i>	4-17
4.2.4.1	Sputter Parameters	4-18
4.2.4.2	Sheet Resistance.....	4-21
4.2.4.3	Transmission	4-23
4.2.4.4	Summary	4-26
4.3	SUMMARY OF ELECTRICAL AND OPTICAL PROPERTIES	4-26
5.	ANALYSIS OF STRUCTURE.....	5-1
5.1	INTRODUCTION	5-1
5.2	FILM THICKNESS MEASUREMENTS	5-1
5.3	THE EFFECT OF THERMAL ANNEALING ON THE MORPHOLOGY OF INKJET PRINTED $\text{SnO}_2\text{:Sb}$ 5-3	
5.3.1	<i>SEM</i>	5-3
5.3.2	<i>TEM</i>	5-5
5.3.3	<i>XRD</i>	5-5
5.4	THE EFFECT OF LASER PROCESSING ON THE MORPHOLOGY OF INKJET PRINTED $\text{SnO}_2\text{:Sb}$	5-8
5.4.1	<i>The Thermal Model</i>	5-8
5.4.2	<i>SEM</i>	5-10
5.4.3	<i>TEM</i>	5-11
5.4.4	<i>XRD</i>	5-12
5.5	THE EFFECT OF LASER PROCESSING ON THE MORPHOLOGY OF RF MAGNETRON SPUTTERED $\text{SnO}_2\text{:Sb}$ ON A CRONAR® SUBSTRATE	5-13
5.5.1	<i>TEM</i>	5-13
5.5.2	<i>XRD</i>	5-15
5.6	SUMMARY.....	5-17
6.	DISCUSSION.....	6-1
6.1	INTRODUCTION	6-1
6.2	THERMAL ANNEALING.....	6-1
6.2.1	<i>Inkjet Printed $\text{SnO}_2\text{:Sb}$ on Soda Lime Glass</i>	6-1
6.2.2	<i>Inkjet Printed $\text{SnO}_2\text{:Sb}$ on borosilicate thermally annealed in various atmospheres</i>	6-3
6.2.2.1	Hall effect.....	6-5
6.2.3	<i>Dip-coated $\text{SnO}_2\text{:Sb}$ on quartz substrates thermally annealed at various temperatures</i> ..	6-6
6.3	LASER PROCESSING	6-7

6.3.1	<i>Laser Processed Inkjet Printed SnO₂:Sb on Borosilicate</i>	6-7
6.3.2	<i>Laser Processing in Argon at Pressure</i>	6-10
6.4	THERMAL ANNEALING AND LASER PROCESSING	6-10
6.5	RF MAGNETRON SPUTTERED SnO ₂ :Sb	6-11
6.6	SUMMARY.....	6-14
7.	CONCLUSIONS AND FURTHER WORK.....	7-1
7.1	CONCLUSIONS	7-1
7.2	FURTHER WORK	7-4
7.2.1	<i>Further Analytical Work</i>	7-4
7.2.2	<i>Alternative Processes</i>	7-7

APPENDIX A: Ramp Rate for Thermal Anneal

APPENDIX B: Comparison Between PTL and NTU Rs Measurements

APPENDIX C: Photographs of Water-Soaked Laser Processed SnO₂:Sb Films

APPENDIX D: Thermal Model Simulations

PUBLISHED ARTICLES

List of Figures

Figure 2-1: Schematic of the various crystalline structures of a solid.....	2-2
Figure 2-2: The effect of temperature on carrier mobility with respect to impurity and lattice scattering. (From [3]).....	2-5
Figure 2-3: Energy band diagram of a semiconductor with traps under a bias	2-7
Figure 2-4: The Hall effect	2-9
Figure 2-5: Typical transmission spectra for a transparent conducting oxide.....	2-13
Figure 2-6: Typical transmission and reflection response of a transparent conducting oxide to an increase in carrier concentration	2-15
Figure 2-7: Schematic of light propagating through a transparent conductor.....	2-16
Figure 2-8: Variation in absorption coefficient with wavelength of SnO ₂ :Sb deposited by spray pyrolysis	2-17
Figure 2-9: Schematic of the atomic structure of SnO ₂ (From [22])	2-17
Figure 2-10: Schematic of RF magnetron sputtering system used for thin film deposition during this project.....	2-26
Figure 2-11: Typical layout of thin film deposition by spray pyrolysis.....	2-28
Figure 2-12: Inkjet printing heads i) thermal Drop On Demand (DOD) and ii) Continuous inkjet (COJ) head[78].....	2-31
Figure 2-13: State diagram of possible energy transitions during laser processing.....	2-37
Figure 2-14: Fixed legend electroluminescent display made by screen printing.....	2-39
Figure 3-1: Laser processing experimental equipment	3-1
Figure 3-2: Calibration chart for online monitoring of laser energy at sample.....	3-2
Figure 3-3: RF Magnetron Sputtering System.....	3-4
Figure 3-4: Powder Target Press	3-6
Figure 3-5: Fringe intensity variation with focus of the optical profiler in VSI mode	3-9
Figure 3-6: Satisfying the Bragg condition for x-ray diffraction	3-12
Figure 3-7: Schematic of four point probe	3-15
Figure 4-1: Variation in R _s between batches in as-deposited inkjet printed ATO.....	4-3
Figure 4-2: Variation in R _s between batches of thermally annealed inkjet printed ATO ...	4-4
Figure 4-3: Comparison between the change in sheet resistance of inkjet printed SnO ₂ :Sb left in a vacuum and in atmosphere.	4-5
Figure 4-4: Change in R _s with thermal annealing in air, vacuum and nitrogen rich environment.....	4-6
Figure 4-5: Transmission spectra for inkjet printed ATO films; as-deposited and thermally annealed in air, vacuum and nitrogen	4-8
Figure 4-6: Variation in sheet resistance of dip coated ATO on Quartz substrates with temperature of thermal anneal.....	4-10

<i>Figure 4-7: Transmission spectra of dip coated ATO on quartz substrates thermally annealed at 400, 600, 800 and 1000°C (thickness unknown)</i>	<i>4-11</i>
<i>Figure 4-8: The variation in sheet resistance post laser processing as a function of number of pulses and laser energy. ◆ = 20mJ/cm², ■ = 40mJ/cm², and ▲ = 70mJ/cm².</i>	<i>4-13</i>
<i>Figure 4-9: Transmission spectra for inkjet printed ATO on borosilicate glass laser processed at 40mJ/cm² with 10, 100 and 1000 pulses</i>	<i>4-14</i>
<i>Figure 4-10: Change in sheet resistance following laser processing of inkjet printed SnO₂:Sb in pressurised argon</i>	<i>4-15</i>
<i>Figure 4-11: Change in sheet resistance of a thermally annealed film of inkjet printed SnO₂:Sb laser processed with 100 pulses at 80mJcm⁻²</i>	<i>4-16</i>
<i>Figure 4-12: Matrix of laser processing parameters; number of pulses at 25, 40, 70 and 100mJcm⁻²</i>	<i>4-18</i>
<i>Figure 4-13: Change in sheet resistance of sputter deposited ATO on Cronar® following laser processing at 25, 40, 70 and 100mJcm⁻²</i>	<i>4-21</i>
<i>Figure 4-14: Change in sheet resistance of sputter deposited ATO after 2000, 3000 and 10000 pulses at 25mJcm⁻²</i>	<i>4-22</i>
<i>Figure 4-15: Transmission spectra for RF magnetron sputtered ATO on Cronar® laser processed with 25mJ/cm²</i>	<i>4-24</i>
<i>Figure 4-16: Transmission spectra for RF magnetron sputtered ATO laser processed with 40mJ/cm²</i>	<i>4-25</i>
<i>Figure 4-17: Transmission spectra of RF magnetron sputtered ATO laser processed with 70mJ/cm²</i>	<i>4-25</i>
<i>Figure 4-18: Transmission spectra of RF magnetron sputtered ATO laser processed with 100mJ/cm²</i>	<i>4-26</i>
<i>Figure 5-1: Typical step height of ablated inkjet printed SnO₂:Sb</i>	<i>5-3</i>
<i>Figure 5-2: SEM images of the top surface of as-deposited and thermally annealed inkjet printed SnO₂:Sb</i>	<i>5-4</i>
<i>Figure 5-3: Cross section of as-deposited and thermally annealed inkjet printed SnO₂:Sb showing a film approximately 1µm thick</i>	<i>5-4</i>
<i>Figure 5-4: TEM cross section of as-deposited and thermally annealed inkjet printed SnO₂:Sb showing a film approximately 1µm thick</i>	<i>5-5</i>
<i>Figure 5-5: X-ray diffraction pattern from powdered SnO₂ and Sb₂O₃ used to produce the SnO₂:Sb ink</i>	<i>5-6</i>
<i>Figure 5-6: XRD of as-deposited and thermally annealed inkjet printed SnO₂:Sb</i>	<i>5-7</i>
<i>Figure 5-7: 300k magnification of uppermost surface of inkjet printed SnO₂:Sb</i>	<i>5-8</i>
<i>Figure 5-8: A modelled temperature and depth profile of SnO₂ following laser processing</i>	<i>5-9</i>

Figure 5-9: SEM images of laser processed inkjet printed SnO₂:Sb.....5-10

Figure 5-10: Cross sectional TEM of SnO₂:Sb laser processed with 1000 pulses at 70mJcm⁻² (x50000 magnification left, x100000 magnification right).....5-11

Figure 5-11: XRD of laser processed SnO₂:Sb inkjet printed onto borosilicate.....5-12

Figure 5-12: TEM cross-sectional image of as-deposited RF magnetron sputtered SnO₂:Sb5-13

Figure 5-13: TEM cross sectional images of laser processed RF Magnetron sputtered SnO₂:Sb processed with (L to R) 10, 100 and 1000 pulses at 40mJcm⁻²5-14

Figure 5-14: A higher magnification TEM cross-sectional image of the grain structure of RF magnetron sputtered SnO₂:Sb5-15

Figure 5-15: XRD of as-deposited and laser processed (100 pulses@120mJcm⁻²) SnO₂:Sb RF magnetron sputtered onto Cronar® (bottom) and Cronar® only (top).....5-16

Figure 6-1: Surface Profiler image of RF Magnetron Sputtered SnO₂:Sb following laser processing with 1000 pulses at 100mJcm⁻²6-13

List of Tables

<i>Table 2-1: Summary of deposition techniques and electrical characteristics of SnO₂.....</i>	<i>2-18</i>
<i>Table 2-2: Summary of deposition techniques and electrical characteristics of SnO₂:Sb</i>	<i>2-20</i>
<i>Table 4-1: Summary of samples used for investigation into consistency of Rs results with different batches of material</i>	<i>4-2</i>
<i>Table 4-2: Laser processing parameters of ATO inkjet printed onto borosilicate.....</i>	<i>4-12</i>
<i>Table 4-3: Temperature at the substrate for various RF magnetron sputtering powers...</i>	<i>4-19</i>
<i>Table 4-4: Sputter parameters and the resultant sheet resistance and transmission for the simple optimisation process</i>	<i>4-20</i>
<i>Table 4-5: Transmission at 550nm for as-deposited and laser processed RF magnetron sputtered ATO on Cronar®.....</i>	<i>4-24</i>
<i>Table 4-6: Summary of results for electrical and optical properties</i>	<i>4-29</i>
<i>Table 5-1: Thickness variation of inkjet printed SnO₂:Sb on borosilicate substrate</i>	<i>5-2</i>
<i>Table 5-2: Comparison of phase peaks for different XRD sources</i>	<i>5-16</i>
<i>Table 5-3: Summary of XRD findings including FWHM and particle size</i>	<i>5-18</i>
<i>Table 6-1: Comparison of the effect of laser processing on inkjet printed and RF magnetron sputtered SnO₂:Sb</i>	<i>6-15</i>

1. Introduction to Project

1.1 Introduction

The recent interest in flexible electronics is being driven to some extent by the maturing of some enabling technologies such that prototype devices can be made and demonstrated. However, there are many technological hurdles to overcome before flexible electronics, including flexible displays, become an economically viable product. The term *flexible* encompasses an array of meanings which can range from conformable devices that are flexed only once during manufacture, to rolling devices such as a display that rolls out from within a PDA (Portable Digital Assistant). The term does not distinguish between inorganic (i.e. Electroluminescent displays) and organic displays (i.e. OLEDs - Organic Light Emitting Displays) that are manufactured on flexible substrates, indeed hybrid organic/inorganic displays look likely to be a main contender in future flexible markets[1].

One of the challenges that faces researchers is the development of suitable substrates. Thin glass is a possibility for conformable displays, but certainly not for rollable devices. The use of glass also eliminates one of the perceived benefits of flexible electronics; their mechanical robustness. Some type of polymer substrate would be more adaptable, however they are temperature sensitive. This is problematic since many of the components that are used in flexible electronics require high temperature processing to enhance their material properties. For progress therefore, there must be a convergence of the two limits, with a reduction in manufacturing processing temperatures and an increase in the temperature tolerance of polymer substrates.

The majority of electronic displays use a transparent conducting layer to switch the pixels on and off. This layer is typically a film of ITO (Indium Tin Oxide)[2], although alternative oxide materials are available and include $\text{SnO}_2\text{:Sb}$; the material investigated within this body of work. Aside from the issue of indium being a scarce expensive resource, it is brittle under pressure[3]. ITO and its alternatives also require high processing temperatures to achieve the desired material properties. Organic alternatives to ITO are also under investigation, with PEDOT (poly (3,4-ethylenedioxythiophene)) perhaps being the most well known of these. However, these materials are often unreliable and irreproducible and will require a few more years of development before they could become commercially viable alternatives[1].

TFTs (Thin Film Transistors) are used for active matrix switching in many high resolution displays and are prone to failure and poor performance on flexible substrates[4]. Like the transparent conducting layer, the materials used in conventional TFTs require high temperature processing to achieve desirable performance levels. Thermal and humidity expansion of polymer substrates also cause problems with mask alignment during traditional photolithographic manufacturing processing.

Many researchers are investigating these and other issues surrounding the viability of flexible displays[5-8]. The research presented here concentrates on the transparent conducting layer of flexible electronics, in particular a cheaper alternative to ITO: ATO (Antimony Tin Oxide) or $\text{SnO}_2\text{:Sb}$.

With the move towards flexible devices there is a desire among the manufacturing sector to change operations to a roll to roll process, because it would be simpler and therefore cheaper than handling large glass panels. In tandem with this method of manufacture is the technology of printing functional materials, which is one deposition method investigated within this body of work, and which has the benefit of being a direct-write (see below) deposition method.

Inkjet printing is an attractive alternative deposition method since material can be deposited only where it is required. It therefore avoids the need for the traditional, expensive and time consuming photolithography mask and etch process. Savings are also made because material is used only where needed, reducing consumption of functional materials. However, the nature of the ink means that it is not possible to heat the substrate during deposition, which is one process that improves the conductive properties of transparent conducting materials. Alternatively there must be a post process anneal, neither of which are compatible with flexible substrates. Also investigated within this work is an alternative to the high temperature processing required to extract the optimum material properties, that alternative being laser processing.

Laser processing is widely used in the manufacture of polysilicon TFTs to induce a crystalline material[9-11] and interest in laser processing is growing. By selective absorption it is possible to limit processing depth, which makes lasers an attractive alternative to a conventional heating processing, particularly in the race for the flexible electronic display. Therefore the effect of a high power UV laser on inkjet printed SnO₂:Sb will be investigated. As an already established deposition technique

for both ITO and ATO, RF magnetron sputtering will provide a comparator for the inkjet printed material.

1.2 Aim

To investigate the effects of laser processing and thermal annealing on inkjet printed SnO₂:Sb and the effects of laser processing on RF magnetron sputter deposited SnO₂:Sb on glass and flexible substrates and to demonstrate the feasibility of laser processing as an alternative to conventional thermal annealing and ATO as an alternative to ITO.

1.3 Objectives

- Perform literature review of the science and technology of transparent conductors.
- Commission excimer laser processing system at NTU.
- Investigate printed Sb doped tin oxide (ATO) films in terms of conductivity, optical transmission and crystallinity.
- Investigate the effect of thermally annealing and laser processing the inkjet printed Sb doped tin oxide (ATO) films in terms of conductivity, optical transmission and crystallinity.
- Carry out a study to produce conductive films of ATO by RF magnetron sputtering for laser processing
- Perform laser processing study, comparing the properties of laser processed printed ATO on glass with laser processed ATO on Cronar@[12].

1.4 Thesis Scope and Structure

The remaining chapters within this thesis are as follows:

Chapter 2: Background Review

This chapter covers the essential theories and technologies used throughout this investigation. It includes an introduction to semiconductor materials and their carrier transport mechanisms, before looking at transparent conducting materials specifically. Electrical and optical properties are summarised and a comparison between ATO and ITO is made with a literature review of ATO deposition and optimisation included. In addition deposition methods, including printing, are discussed together with the issues surrounding flexible substrates. Finally there is a section on laser processing, laser interactions and applications.

Chapter 3: Experimental Procedures

This chapter describes the equipment used to carry out this investigation. The chapter starts with a description of the sputtering chamber and related equipment used for film deposition. It then describes the processing equipment, including the laser processing set-up. Characterisation equipment is described next with four point probe, transmission spectra and optical profilometry included. Finally there is a description of the equipment used for morphological analysis covering Scanning Electron Microscopy (SEM), Transmission Electron Microscopy (TEM) and X-ray Diffraction (XRD).

Chapter 4: Electrical and Optical Properties

The results chapter is in two halves with thermally annealed results followed by laser processed results. The effect on sheet resistance and transmission spectra are

reported for thermally annealed inkjet printed films on soda lime glass, borosilicate and quartz. Films that have been thermally annealed at different temperatures and in different environments are also reported. The results on laser processed films include inkjet printed ATO on borosilicate in air and under pressure, thermal and laser processing of inkjet printed films on borosilicate and RF magnetron sputtered ATO on Cronar®.

Chapter 5: Analysis of Structure

X-ray diffraction, Scanning Electron Microscopy and Transmission Electron Microscopy results are contained within this chapter. XRD and SEM analysis of thermally annealed and laser processed inkjet printed films are included, as are TEM analysis of laser processed inkjet printed films. TEM images of laser processed RF magnetron sputter deposited films are presented and analysis of the XRD traces is also included.

Chapter 6: Discussion

The discussion chapter provides analysis of the results published in chapters 4 and 5. It includes suggestions for processing mechanisms based on findings and also compares the results found here with those published elsewhere. There is also a summarised comparison between the results for laser processed inkjet printed ATO and laser processed RF magnetron sputtered ATO.

Chapter 7: Conclusions and Further Work

The conclusion chapter summarises the findings of this body of work and suggests further directions for investigation.

1.5 Historical Context

Historically, the Displays Research group at Nottingham Trent University has a good deal of experience in electroluminescent (EL) based displays[13-17]. More recent work by the group investigated methods of improving the electroluminescent output of displays by traditional thermal annealing and novel laser-processing[18-20]. The skills and knowledge of laser processing built up through the EL based work has here been applied to transparent conducting oxides with the aim of optimising the electrical and optical characteristics of inkjet printed and RF Magnetron Sputtered SnO₂:Sb, such that it may be applied to temperature sensitive substrates such as polyester.

1.6 The ELJet Project

The work carried out for this project is a major part of a DTI LINK project called ELJet (Electroluminescent Displays by inkjet printing). Funded by the DTI, EPSRC (through a COMIT Faraday Partnership CASE studentship) and originally three companies: Keeling & Walker[21], Patterning Technologies Limited[22] and The IFM Company. The project has set out to use respective expertise to solve a multi-disciplinary problem.

Keeling & Walker are the world's leading producer of tin oxide. In particular they have extensive experience in the manufacture of Antimony Tin Oxide (ATO). While the transparent conductor of choice amongst the display's community is Indium Tin Oxide this is an expensive material due to the limited supply of Indium (See Chapter 2, section 2.3.4). As such, Antimony Tin Oxide as a cheaper alternative has been the

focus of the work in this body of work. The raw materials for both the ink and the sputter target used in this investigation have been supplied by Keeling & Walker.

Patterning Technologies Limited is a printing company specialising in inkjet printing of industrial processes to reduce manufacturing costs. They have developed the ATO ink and the printing process that has been used for this project.

The IFM Company were a display manufacturing company who were initially involved in the project to manufacture displays using the optimised inkjet printed thin films. Unfortunately, the company ceased trading in March 2005.

Nottingham Trent University was responsible for the characterisation of the inkjet printed ATO and investigating a laser processing technique suitable for use on a temperature sensitive substrate. This is the subject of the research presented here.

References

- [1] G. P. Crawford, *Flexible Flat Panel Displays*: John Wiley & Sons, 2005.
- [2] C. G. Granqvist and A. Hultaker, "Transparent and conducting ITO films: new developments and applications," *Thin Solid Films*, vol. 411, pp. 1, 2002.
- [3] K. Sierros, "Mechanical properties of oxide coated polymer substrates for flexible displays.," in *Metallurgy and Materials*, vol. PhD. Birmingham: Birmingham University, 2007.
- [4] J. H. Cheon, J. H. Bae, and J. Jang, "Mechanical stability of poly-Si TFT on metal foil," *Solid-State Electronics*, vol. In Press, Corrected Proof.
- [5] Z. L. Pei, X. B. Zhang, G. P. Zhang, J. Gong, C. Sun, R. F. Huang, and L. S. Wen, "Transparent conductive ZnO:Al thin films deposited on flexible substrates prepared by direct current magnetron sputtering," *Thin Solid Films*, vol. 497, pp. 20, 2006.
- [6] Y. Z. You, Y. S. Kim, D. H. Choi, H. S. Jang, J. H. Lee, and D. Kim, "Electrical and optical study of ITO films on glass and polymer substrates prepared by DC magnetron sputtering type negative metal ion beam deposition," *Materials Chemistry and Physics*, vol. 107, pp. 444, 2008.
- [7] T.L. Li and S.L.C. Hsu, "Preparation and properties of a high temperature, flexible and colorless ITO coated polyimide substrate," *European Polymer Journal*, vol. 43, pp. 3368, 2007.
- [8] A. C. Mofor, A. S. Bakin, B. Postels, M. Suleiman, A. Elshaer, and A. Waag, "Growth of ZnO layers for transparent and flexible electronics," *Thin Solid Films*, vol. 516, pp. 1401, 2008.

- [9] M. Stehle, "Excimer laser treatment for large surface," *Journal of Non-Crystalline Solids*, vol. 218, pp. 218, 1997.
- [10] T. Sameshima, "Status of Si thin film transistors," *Journal of Non-Crystalline Solids*, vol. 227-230, pp. 1196, 1998.
- [11] I.H. Song and M.K. Han, "Low temperature poly-Si TFTs for display application," *Current Applied Physics*, vol. 3, pp. 363, 2003.
- [12] Dupont, http://www2.dupont.com/Products/en_RU/Cronar_en.html, 26th March 2008.
- [13] W. M. Cranton, D. M. Spink, R. Stevens, and C. B. Thomas, "Growth and dielectric characterization of yttrium oxide thin films deposited on Si by r.f.-magnetron sputtering," *Thin Solid Films*, vol. 226, pp. 156, 1993.
- [14] E. K. Evangelou, N. Konofaos, M. R. Craven, W. M. Cranton, and C. B. Thomas, "Characterisation of the BaTiO₃/p-Si interface and applications," *Applied Surface Science*, vol. 166, pp. 504, 2000.
- [15] S. O. Barros, R. Stevens, and W. Cranton, "Enhancement of the laterally emitting thin film electroluminescent device optical outcoupling via the fabrication of novel geometry structures," *Optical Engineering*, vol. 40, pp. 934, 2001.
- [16] E. A. Mastio, W. M. Cranton, and C. B. Thomas, "Lattice misfit versus performance of thin film electroluminescent structures," *Journal of Applied Physics*, vol. 89, pp. 1605, 2001.
- [17] S. Otero-Barros, R. Stevens, and W. Cranton, "Enhancement of the LETFEL device optical outcoupling via the fabrication of novel geometry structures," presented at Liquid Crystal Materials, Devices, and Flat Panel Displays, San Jose, CA, USA, 2000.

- [18] D. C. Koutsogeorgis, E. A. Mastio, W. M. Cranton, and C. B. Thomas, "Pulsed KrF laser annealing of ZnS:Mn laterally emitting thin film electroluminescent displays," *Thin Solid Films*, vol. 383, pp. 31, 2001.
- [19] E. A. Mastio, W. M. Cranton, C. B. Thomas, E. Fogarassy, and S. de Unamuno, "Pulsed KrF laser annealing of RF sputtered ZnS:Mn thin films," *Applied Surface Science*, vol. 138-139, pp. 35, 1999.
- [20] E. A. Mastio, E. Fogarassy, W. M. Cranton, and C. B. Thomas, "Ablation study on pulsed KrF laser annealed electroluminescent ZnS:Mn/Y₂O₃ multilayers deposited on Si," *Applied Surface Science*, vol. 154-155, pp. 35, 2000.
- [21] Keeling & Walker, www.keelingwalker.co.uk, 26th March 2008.
- [22] PTL Limited, www.pattech.com, 26th March 2008.

2. Background Review

2.1 Semiconductor Materials

In the study of the effects of laser processing on transparent conductors, it is necessary to have an understanding of material properties and conduction mechanisms of semiconductors and how the two are interlinked. A general discussion follows with further details on the effects of doping and trapping states as recombination centres.

2.1.1 Crystalline structures

Many solid materials are crystalline, i.e. their atoms or molecules are regularly ordered. A solid is created when the kinetic energy of a group of molecules or atoms becomes so small they become permanently attached to one another (e.g. when the temperature is sufficiently reduced). The net attractive interactions between the atoms form them into a three dimensional array – a solid. The movement of the atoms is restricted to vibrations about a particular point to the extent that the atoms are now ordered, either almost, or fully periodically homogeneous. The degree of homogeneity is dependent upon the distribution of the atoms or molecules when they form into a solid. Three arrangements can occur: a single crystal material, a polycrystalline material or an amorphous material. The three arrangements are schematically depicted in Figure 2-1 for a two dimensional case.

A single crystal material is said to be at its absolute thermal equilibrium; it is in a stable state with the lowest internal energy. In this case the atoms or molecules will align in a three dimensional periodic array. External conditions such as temperature,

pressure and cooling rate can result in a material with random breaks in the periodicity, in this case a polycrystalline material is formed and the material is divided into small single crystal sections (grains) that intersect with one another. These materials are stable, but are not at their lowest internal energy and so are said to be in local thermal equilibrium. Amorphous materials have no periodicity, that is, upon cooling the atoms or molecules did not form into a periodic array (e.g. glass, which is too viscous for the atoms to align during the cooling process). Because of the random nature of the structure, amorphous materials have the same properties in all directions, i.e. they are isotropic.

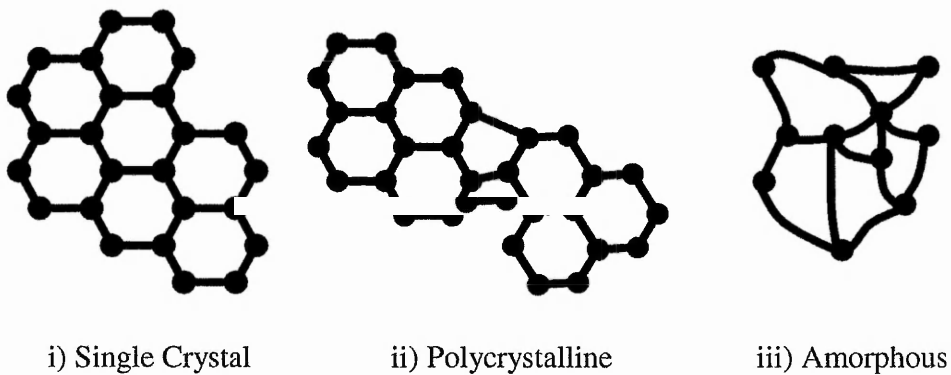


Figure 2-1: Schematic of the various crystalline structures of a solid

2.2 Carrier Transport Mechanisms

2.2.1 Introduction

Carrier transport mechanisms can be quite complex; only an overview of issues critical to the subject matter are given here. For particularly interested readers there are many textbooks that deal with the subject including the following references[1, 2].

2.2.2 Carrier Drift

Considering an n-type semiconductor with a uniform doping distribution in thermal equilibrium; electrons in the conduction band are effectively free to move. Without an applied external force, the electrons will randomly move about the material colliding with lattice and impurity atoms such that over a sufficient period of time the net movement of the electron will be zero. The average distance between collisions is known as the mean free path and the average time between collisions is known as the mean free time τ_c (s).

The application of an electric field E (V/cm) will cause the electron to be accelerated along the orientation of the field, but in the opposite direction, during the time in between collisions. Thus a net displacement of the electron occurs. This displacement is quantified by the drift velocity v_n (cm/s). Between collisions, the force experienced by the electron upon the application of the electric field is given by $-qE$, where q = magnitude of electric charge (C). The momentum applied to the electron during this time is given by the force \times time and so is $-qE\tau_c$. Given that all the momentum is given up at the time of collision this can be equated with the momentum gained by the electron during this time: $m_e v_n$, where m_e is the effective mass of the electron (kg), to determine the drift velocity.

$$\text{Drift velocity } (v_n) = - \left[\frac{q\tau_c}{m_e} \right] E \quad \text{Eq 2-1}$$

To simplify this we say that the drift velocity is proportional to the applied electric field and that this proportionality is determined by the effective mass of the electron

and the mean time between collisions. This is known as the electron mobility μ ($\text{cm}^2/\text{V}\cdot\text{s}$), so:

$$\mu \equiv \frac{q\tau_c}{m_e} \quad \text{Eq 2-2}$$

$$\text{and } v_n = -\mu E \quad \text{Eq 2-3}$$

From these equations we can see that an important factor in determining the mobility of an electron is the mean free time between collisions. This is mainly determined by scattering mechanisms within the lattice and more specifically, lattice scattering and impurity scattering.

2.2.3 Carrier Scattering

Lattice scattering is the result of thermal vibrations of the lattice atoms at temperatures above 0°K and is therefore a dominant process at higher temperatures. It causes a decrease in mobility due to lattice scattering proportional to $T^{-3/2}$. Impurity scattering is as a result of passing electrons being attracted to impurity ions. These can be from dopant ions, an atomic vacancy (where an atom is missing from the lattice) or from dislocations in the lattice. Impurities will have an *effective area* associated with them, which determines the probability of scattering. Also known as the cross-section, it is a measure of the range of the ion potential as seen by the carrier. The amount of impurity scattering is dependent upon the concentration of ionised impurities N_T (cm^{-3}) and unlike lattice scattering, reduces with increasing temperature. As the temperature increases the carriers travel faster and are less likely to be affected by the ionised impurity. Mobility due to impurity scattering is therefore dependent upon temperature and impurity concentration and varies as a

function of $T^{3/2}/N_T$. Figure 2-2 shows the combined effects of scattering mechanisms on mobility as a function of temperature.

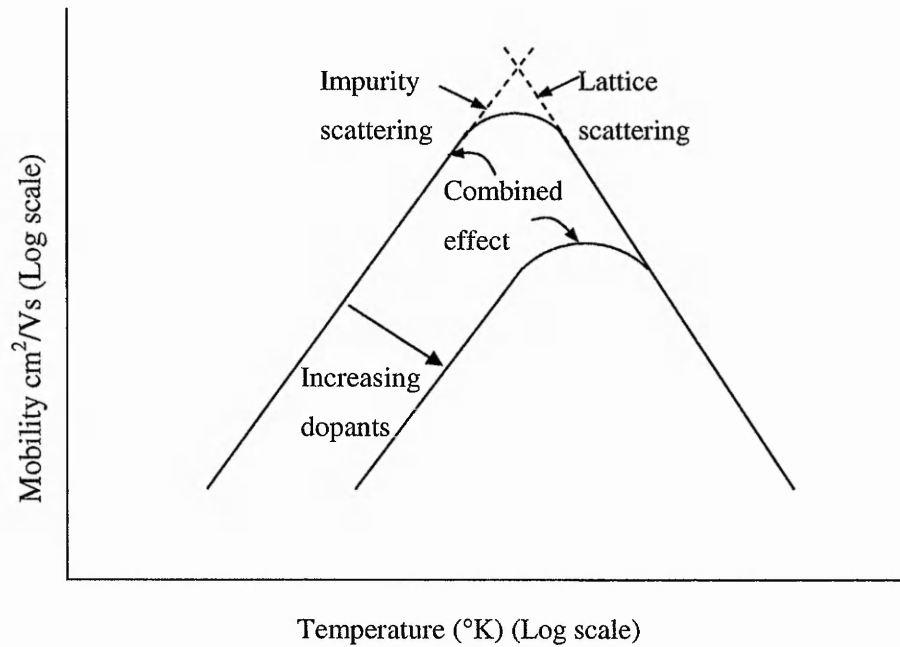


Figure 2-2: The effect of temperature on carrier mobility with respect to impurity and lattice scattering. (From [3])

2.2.4 Carrier Diffusion

Carrier diffusion occurs when for a given material, there are areas of high carrier concentration and areas of low carrier concentration. The carriers will diffuse from high to low carrier concentration areas. The current generated by this is called the diffusion current and is as a result of the random thermal motion of carriers in a concentration gradient.

2.2.5 Recombination Processes

If a direct bandgap semiconductor is considered whilst in thermal equilibrium, then the lattice vibrations due to thermal energy can sometimes be sufficient to break an atomic bond. When this happens an electron-hole pair is generated and the thermal energy allows the electron into the conduction band, whilst the hole can contribute to conduction in the valence band. This is known as carrier generation. Conversely, when an electron in the conduction band loses its energy and falls into the valence band, the electron-hole pair recombine and are said to be annihilated. This is recombination. Clearly for a semiconductor in thermal equilibrium, the rate of generation is equal to the rate of recombination. The recombination process is responsible for electron hole pair annihilation. It is therefore an undesirable effect in terms of conductivity.

Where trapping states are present from impurities or vacancies etc, electrons in the conduction band can more readily fall to the trapping state where they will recombine with an energised hole causing an annihilation of an electron hole pair. It is easier for this to occur since the energy exchanges required are smaller than that for a valence band-conduction band transition.

2.2.6 Trapping

As previously mentioned, ionised states can attract passing carriers. Ionised states can be created by impurities, dangling bonds, atomic vacancies etc and are called traps[4]. For example, a dangling bond will want an extra electron and although it is neutrally charged when empty, it nevertheless has a coulombic attraction associated

with it. Trapping states also have a cross section associated with them, the smaller the cross section, the less likely an electron will be trapped and vice-versa.

2.2.6.1 The Effect of Traps on Mobility

For the purposes of this work, the importance of trapping is the effect on the mobility of the material. If we consider the following semiconductor in Figure 2-3 containing traps with an applied bias:

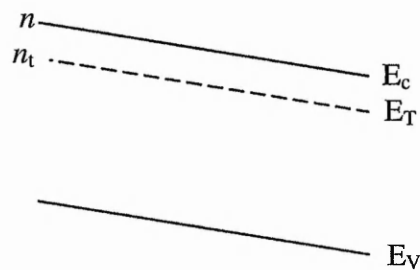


Figure 2-3: Energy band diagram of a semiconductor with traps under a bias

Where n = density of free charge (cm^{-3}) and n_t = density of trapped charge (cm^{-3})

Letting:

μ_d = Drift mobility (assuming both free and trapped carriers contribute to conduction) ($\text{cm}^2/\text{V}\cdot\text{s}$)

μ = Drift mobility of free charge ($\text{cm}^2/\text{V}\cdot\text{s}$)

Then we can say:

$$(n + n_t)\mu_d = n\mu \quad \text{Eq 2-4}$$

$$\text{So } \mu_d = \frac{n}{n + n_t}\mu \quad \text{Eq 2-5}$$

If the semiconductor contains many traps then we can say that $n_t \gg n$ so:

$$\mu_d \approx \frac{n}{n_t}\mu \quad \text{Eq 2-6}$$

Relating this to the density of states equations:

$$n = N_c \exp\left(\frac{E_F - E_c}{kT}\right) \text{ and } n_t = N_t \exp\left(\frac{E_T - E_c}{kT}\right) \quad \text{Eq 2-7 \& Eq 2-8}$$

Where N_c and N_t are the density of states in the conduction band and density of traps respectively.

$$\text{So } \mu_d \approx \frac{N_c}{N_t} \exp\left(\frac{E_F - E_T}{KT}\right) \quad \text{Eq 2-9}$$

i.e. The mobility reduces with increasing density of traps.

2.2.6.2 Passivation

Dangling bonds are a common problem in semiconductor manufacture and passivation is a commonly used technique to overcome them[5]. This usually involves the introduction of hydrogen into the manufacturing process, typically in the form of AsH_3 , SiH_4 , NH_3 or for vacuum systems, residual H_2O . The hydrogen attaches itself to a dangling bond and effectively eliminates the trap. The scope of the project and insufficient time did not allow for passivation techniques to be attempted on the materials discussed in this thesis.

2.2.6.3 Grain Boundaries

Grain boundaries also have a significant effect on carrier mobility and are a dominant characteristic of the conduction mechanisms. At the interfaces, there are high densities of interface states that trap and scatter carriers due to disorder and trapped charges. The result of this is a space charge region with an associated potential barrier that carriers must overcome.

It has been shown[6-8] that the grain boundary mobility can be written as:

$$\mu_g = \mu_0' T^{-1/2} \exp\left(\frac{-e\phi_b}{KT}\right) \quad \text{Eq 2-10}$$

where $\mu_0 = M/n_cKT$ and M is a barrier dependent factor[7], n_c is the number of crystallites per unit length along the film and ϕ_b is the height of the potential barrier.

2.2.7 The Hall Effect

In 1879 E. H. Hall[9] discovered what became known as the *Hall effect* and which can be used to determine the mobility and type (n or p) of a semiconductor. Hall was investigating the nature of the forces on a conductor carrying a current in the presence of a magnetic field. He discovered that when a magnetic field is applied perpendicular to the direction of current flow that an electric field is set up perpendicular to both the magnetic field and the current direction. The magnitude of this electric field was proportional to the product of the current density and the magnetic flux density. The value R , the Hall coefficient, is therefore defined by:

$$V_H = Rj_x B_z \quad \text{Eq 2-11}$$

Where V_H is the Hall voltage (V), j_x is the current density (A/cm^2) and B_z is the magnetic flux density (T). Figure 2-4 shows how the Hall voltage is generated and the relative directions of the magnetic field and the current for electron carriers.

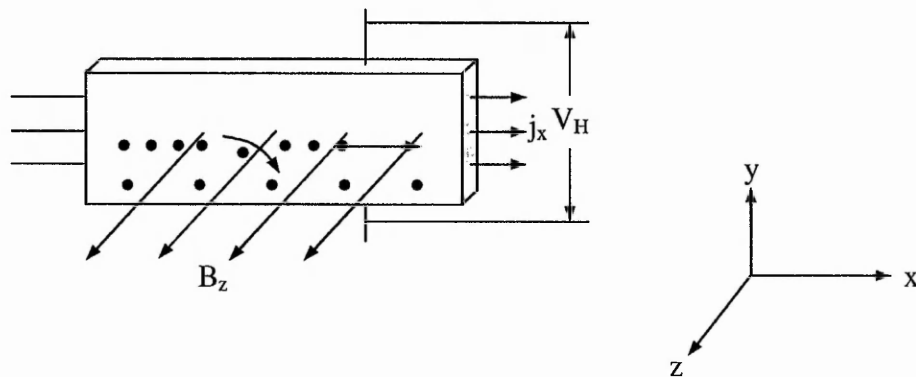


Figure 2-4: The Hall effect

The value of R will reveal the carrier concentration and how this is so becomes evident when the current is considered as a stream of electrons travelling through a conductor within a magnetic field. An electron travelling at a velocity v (m/s) would be subject to a Lorentz force $(B \times v)q$. If the electrons were travelling in free space, they would be deflected in a direction perpendicular to plane of B and v . In practice the constraints of travelling in a solid means that only a small proportion of the electrons will be deflected and that they will set up an electric field which will counter balance the Lorentz force. The remaining electrons will therefore be free to continue to flow through the conductor.

The electric field (E) required to counterbalance the Lorentz force can be given by:

$$qE = (B \times v)q \quad \text{Eq 2-12}$$

Since current density is given by $j = nqv$ Eq 2-13

Combining equations gives:

$$E = \frac{1}{nq} Bj \quad \text{Eq 2-14}$$

So $R = \frac{1}{nq}$ Eq 2-15

The direction of the field E , is dependent upon the charge of q , so for negative q :

$$R = -\frac{1}{nq} \quad \text{Eq 2-16}$$

Another parameter that can be found from the Hall coefficient is the carrier mobility,

μ , defined as the electron drift velocity per unit electric field; i.e. $\mu = \frac{v}{E}$.

Since $j = \sigma E$, we can say that:

$$\sigma = nq \frac{v}{E} \quad \text{Eq 2-17}$$

So $\sigma = nq\mu$ Eq 2-18

Or:

$$\mu = \sigma |R| = \text{Hall Mobility} \quad \text{Eq 2-19}$$

Investigations using the Hall effect are very useful for determining the mobility and carrier concentration of a material and are instrumental in determining the effect of deposition method, post deposition processing etc.

2.3 Transparent Conducting Oxides

2.3.1 Introduction

Transparent Conducting Oxides (TCOs) have been extensively studied[10-14] because their excellent transparency and conductive properties are ideal for use in applications such as electronic displays, solar cells and photodetectors, where they typically form electrodes. An excellent summary of research, characteristics and techniques relating to transparent conducting oxides can be found in the textbook entitled *Semiconducting Transparent Thin Films* by Hartnagel, Dawar, Jain and Jagadish[15]. Most research into TCOs is based on tin or indium oxides, combinations of them or doped tin oxides. Whilst there are a range of materials suitable for use as transparent conductors including: indium oxide, tin oxide, zinc oxide and cadmium stannate, the vast majority of current research involves tin oxide or doped tin oxides. This is because their wide band gap makes them electrically and optically attractive. Thin layers of metals (~100-200Å) also show conductive and

transparent properties, however the films are not very stable. Semiconductor based materials are the popular choice since they are more stable and hard in comparison to metal films. An overview of the optical properties of transparent conductors follows with a material specific discussion on the electrical properties in section 2.3.3 Tin Oxide.

2.3.2 Optical Properties

The properties of a transparent conductor are curious because they conduct electricity but are also transparent in the visible region. In a material such as tin oxide, absorption takes place in the UV part of the spectrum and reflection in the infra red (mid). This leaves transmission through the mid part to the optical spectrum that is visible to the human eye. Figure 2-5 shows a typical transmittance spectra for a transparent conducting oxide[15].

The absorption in the shorter, UV, wavelengths is because of the fundamental band gap of the material. For absorption to take place, the incident photon must have sufficient energy to excite an electron to a higher energy state within the same energy band, or the energy must be great enough to excite the electron to the next energy band. For the former to take place a free electron energy state must exist for the electron to be excited to. The latter phenomenon creates an absorption band, the lower frequency edge of which relates to the critical energy at which this will occur. This is known as the absorption edge.

The reflection in the longer infrared wavelengths is due to free electron plasma absorption, where the free carriers act collectively and are deemed to be a

plasma[16]. After initial absorption, the carriers polarise and cause the incident light to reflect. The Figure 2-5 shows the two critical points, λ_{gap} , the bandgap absorption wavelength and λ_{pl} , the free electron plasma resonance wavelength. It has been shown that a correlation can be drawn between the optical and electrical properties of the material using Drude's theory for free electrons in a metal[17]. The key optical properties of the TCO are the values of n and k , the refractive index and extinction co-efficient. They determine the reflectance and absorption of the surface and are, in turn, dependent upon n and μ , the carrier concentration and the mobility.

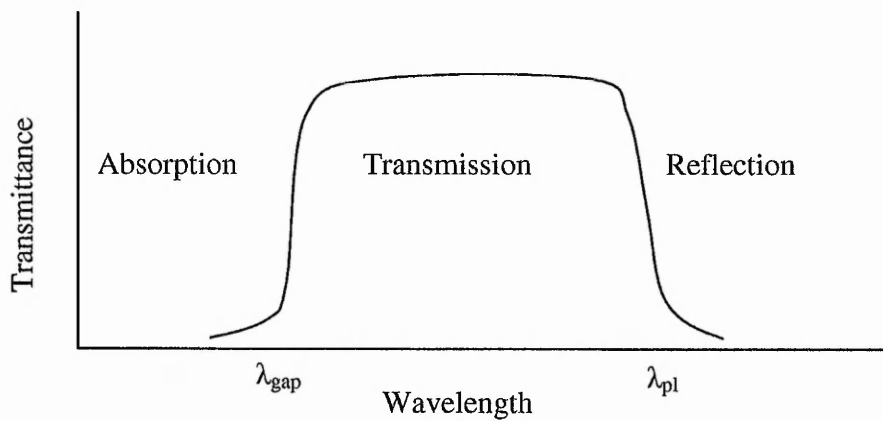


Figure 2-5: Typical transmission spectra for a transparent conducting oxide

According to Drude theory, free electron interaction with an electromagnetic field will lead to a polarisation field within the material which will affect the relative permittivity ϵ (F/cm) of the material. ϵ can be expressed as follows:

$$\epsilon = (n - ik)^2 \quad \text{Eq 2-20}$$

With the real part:

$$\epsilon^1 = n^2 - k^2 = \epsilon_{\infty} \left(1 - \frac{\omega_p^2}{\omega^2 + \gamma^2} \right) \quad \text{Eq 2-21}$$

and the imaginary part:

$$\varepsilon'' = 2nk = \frac{\omega_p^2 \gamma \varepsilon_0}{\omega(\omega^2 + \gamma^2)} \quad \text{Eq 2-22}$$

Where ε_∞ = material permittivity (F/m)

ω_p = plasma resonance frequency (Hz)

$$\text{and } \gamma = \frac{1}{\tau_c} \quad \text{Eq 2-23}$$

Since ω_p and τ_c are related to n and μ as follows:

$$\tau_c \equiv \frac{\mu m_e}{q} \quad \text{Eq 2-24}$$

$$\omega_p = \left(\frac{4\pi n q^2}{\varepsilon_0 \varepsilon_\infty m_e} \right)^{\frac{1}{2}} \quad \text{Eq 2-25}$$

These equations can be used to model the transmission spectra and show that n determines the position of the plasma wavelength (λ_{pl}) and influences the subsequent reflection gradient and that μ also influences the gradient of the reflection part of the spectrum. Simonis et al[17] showed that increasing the carrier concentration resulted in a shift in the wavelength of the free electron plasma absorption towards the visible and an increase in the gradient of the reflection slope. The free electron plasma absorption wavelength was shown to be independent of the mobility, but the gradient of the reflection slope increased with increasing mobility, making a more selective material. Figure 2-6 shows the effect of increasing the carrier concentration on the reflectance and transmittance of a transparent conducting oxide.

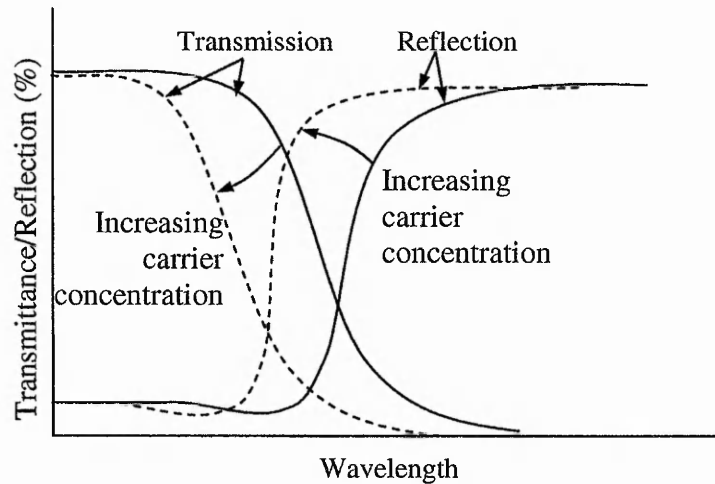


Figure 2-6: Typical transmission and reflection response of a transparent conducting oxide to an increase in carrier concentration

2.3.2.1 Absorption coefficient

The absorption coefficient of a material is an important parameter because it affects the depth of penetration of light into an absorbing medium[18]. Assuming that a transparent conducting material is illuminated with a light source, where the energy of the light is greater than the energy gap such that the light could be absorbed, given also that the photon flux is ϕ_0 (W/m^2); then it can be said that the proportion of the light absorbed as it travels through the material is proportional to the intensity of the flux. In a distance Δx , the number of photons absorbed is given by $\alpha\phi(x)\Delta x$, where α (cm^{-1}) is a constant of proportionality known as the absorption coefficient. By considering the schematic of a transparent conducting oxide shown in Figure 2-7, we can determine that photon flux decays exponentially.

We can say that:

$$\phi(x + \Delta x) - \phi(x) = \frac{d\phi(x)}{dx} \Delta x \quad \text{Eq 2-26}$$

which is $= -\alpha\phi(x)\Delta x$ (minus because the flux is reducing)

or, removing Δx ,

$$\frac{d\phi(x)}{dx} = -\alpha\phi(x) \quad \text{Eq 2-27}$$

Where at $x=0$, $\phi = \phi_0$ and:

$$\phi(x) = \phi_0 e^{-\alpha x} \quad \text{Eq 2-28}$$

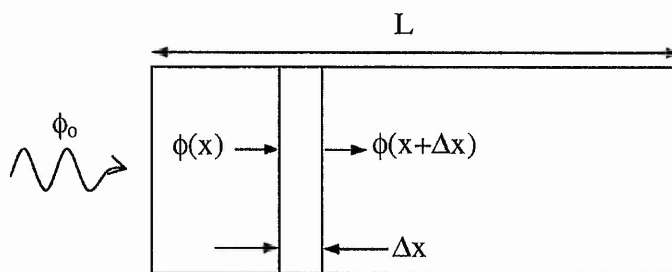


Figure 2-7: Schematic of light propagating through a transparent conductor

Unsurprisingly, the absorption coefficient is a function of wavelength so careful selection of the appropriate wavelength experimental tool is necessary. Figure 2-8 shows the typical variation in absorption coefficient with wavelength as observed by S. Shanthi et al[19]. For the material of interest here, namely $\text{SnO}_2\text{:Sb}$, the absorption coefficient at 193nm and 248nm is approximately $1.5 \times 10^5 \text{cm}^{-1}$ and $0.7 \times 10^5 \text{cm}^{-1}$ [20] respectively. This is in agreement with that reported by E Shanthi et al [21] for a carrier concentration of $7.9 \times 10^{20} \text{cm}^{-3}$. The penetration depths associated with these absorption coefficients are 66nm and 148nm[20] respectively, therefore a KrF UV laser, which emits at 248nm, is the experimental tool of choice to maximise the depth of the processed area.

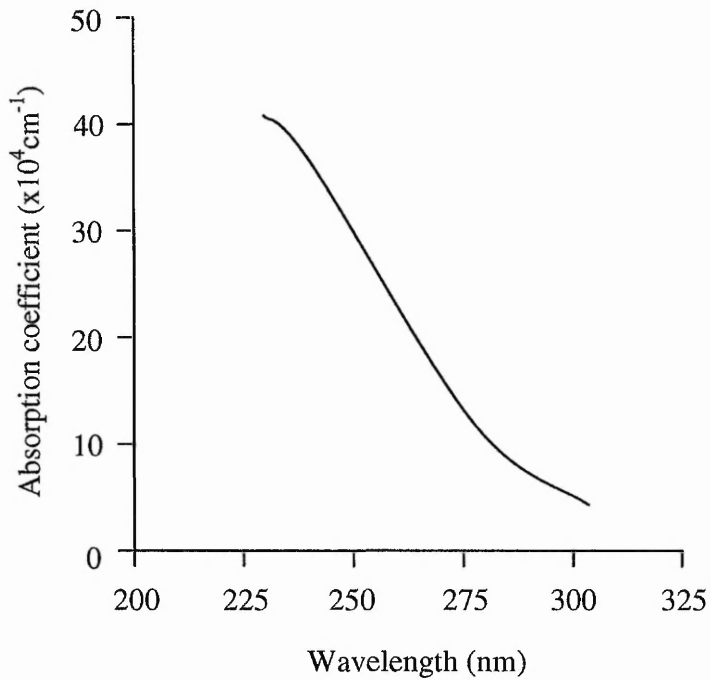


Figure 2-8: Variation in absorption coefficient with wavelength of SnO₂:Sb deposited by spray pyrolysis

2.3.3 Tin Oxide

SnO₂ has a tetragonal rutile structure. A unit cell contains two tin and four oxygen atoms as shown in Figure 2-9.

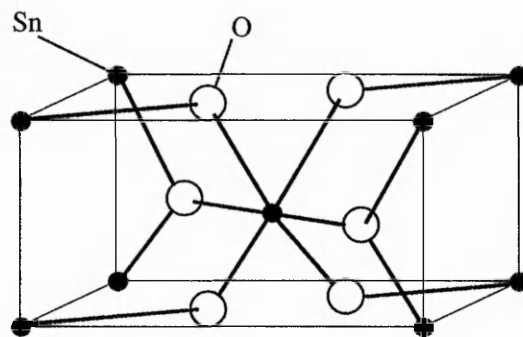


Figure 2-9: Schematic of the atomic structure of SnO₂ (From [22])

The lattice parameters for the structure are $a = b = 4.737 \text{ \AA}$ and $c = 3.185 \text{ \AA}$ and the bandgap has been measured to be 3.6 eV [18].

The tin atoms (cation) are surrounded by six oxygen atoms (anion) and each oxygen atom has three tin atoms around it, approximately in the shape of an equilateral triangle. The conduction mechanism of SnO₂ is primarily due to an imperfect crystal structure creating oxygen vacancies. From these vacancies, electrons are made available for conduction. To further increase conductivity, SnO₂ is often doped with antimony, fluorine or indium, where extra electrons are created when the dopant is substituted for the cation. The key parameters for tin oxide used as a transparent conductor are transmission, carrier concentration, mobility and resistivity (or sheet resistance). The values of these parameters are very much dependent upon the deposition method and the post deposition processing. Both of these will be discussed later in this chapter. Table 2-1 shows some typical values of these parameters for tin oxide deposited using various methods.

Deposition Technique	Sheet Resistance (Ω/sq)	Electrical Conductivity ($\Omega^{-1}\text{cm}^{-1}$)	Carrier Concentration N (cm^{-3})	Hall Mobility ($\text{cm}^2\text{V}^{-1}\text{s}^{-1}$)	Reference
Spray	6.3	-	1.53×10^{20}	8.5	[24]
Sputtered	-	1.6×10^2	1.3×10^{20}	7.72	[25]
CVD	23	2.6×10^2	1.27×10^{20}	12.8	[26]

Table 2-1: Summary of deposition techniques and electrical characteristics of SnO₂

2.3.4 Indium Tin Oxide vs Antimony Tin Oxide

The work presented in this thesis concentrates upon tin oxide doped with antimony although Indium Tin Oxide (ITO) is the most commonly used TCO. ITO is usually found in the form of In₂O₃ doped with SnO₂. In₂O₃ has a highly complex crystal

structure because the unit cell contains 40 atoms, the band structure is therefore not fully calculated[27]. It is often a non-stoichiometric compound with oxygen vacancies creating native donors resulting in an n-type semiconductor. Its prevalent use amongst the displays industry is attributed to its inherent stability, low resistivity and excellent transparency. Deposition is usually by DC sputtering[28-30], Spray Pyrolysis[31-33] or vacuum evaporation[34, 35], therefore a further patterning process is required for pixelation, much like ATO. With typical resistivity values of $3 \times 10^{-4} \Omega \text{cm}$ and transmission values of $>90\%$, it is unsurprising that it is the transparent conductor of choice. However the desire to find an alternative is great, since the cost of Indium is high. Listed on the London Metal Exchange in May 2007, the cost of Indium was \$680 per kg, whereas Antimony was \$5.40 per kg (price quoted in tonnes). The cost issue is further compounded when it is considered that ITO is Indium Oxide doped with Tin and therefore approximately 90% Indium, while ATO is Tin Oxide doped with Antimony, therefore Antimony is usually not more than 10%.

2.3.5 Antimony-Tin Oxide

The electrical and optical properties of any TCO are highly dependent upon many processing factors, including the deposition method [36-40], deposition temperature [41, 42] and post processing [20, 39, 43-47]. It has also been observed that the electrical properties of $\text{SnO}_2:\text{Sb}$ are also highly dependent upon the amount of Sb doping [14, 48-53]. Some typical electrical parameters for $\text{SnO}_2:\text{Sb}$ are shown in Table 2-2.

It appears that the optimum percentage of Sb is dependent upon deposition method, but the consensus for all deposition methods is that at lower doping concentrations Sb^{5+} substitutes with the Sn^{4+} since their ionic radii match ($r_{\text{Sn}}=0.071\text{nm}$, $r_{\text{Sb}}=0.065\text{nm}$). This generates an extra carrier and therefore increases the conductivity. Whilst absolute values vary with deposition method, studies have shown that between 1 and 10 wt% Sb doping is optimum for low resistivity. At higher levels of doping, Sb^{3+} is present in greater numbers creating traps for the increased carrier concentration and the conductivity decreases. It has also been demonstrated that the crystallinity reduces with increasing doping, thus reducing mobility and increasing grain boundary scattering [50, 51].

Deposition Technique	Sheet Resistance (Ω/sq)	Resistivity (Ωcm)	Carrier Concentration N (cm^{-3})	Hall Mobility ($\text{cm}^2\text{V}^{-1}\text{s}^{-1}$)	Reference
Spray Pyrolysis	6.75	4×10^{-3}	7.55×10^{23}	1.65	[53]
ac Sputtered	59	1.5×10^{-3}	4.2×10^{20}	10	[36]
Sol-Gel Dip Coating	90	4.5×10^{-3}	$3.1-7.8 \times 10^{20}$	2-5	[54]

Table 2-2: Summary of deposition techniques and electrical characteristics of $\text{SnO}_2:\text{Sb}$

The effect of substrate deposition temperature has also been studied. It has been reported that film crystallinity is poor at low temperatures below 350°C [42] and therefore resistivity is high. In the same study the critical temperature was determined to be 400°C , while above that the resistivity was observed to increase due to complete oxidation of the film. More recent studies[14, 55] have investigated deposition of $\text{SnO}_2:\text{Sb}$ onto temperature sensitive substrates, such as polyimide, which deforms at temperatures greater than 200°C . XRD spectra showed increasing

crystallinity with increasing temperature, up to 200°C, with slightly better crystallinity achieved on a glass substrate. This was attributed to a better quality of interface.

2.3.5.1 Thermal Annealing of SnO₂:Sb

The as-deposited electrical properties of SnO₂:Sb can be improved upon by the post deposition processing. Classical Thermal Annealing (CTA), Rapid Thermal Annealing (RTA) and laser processing have been studied and found to be successful [39, 43, 46]. Plasma treatment has also been studied, but found to be less useful. Classic and rapid thermal annealing will be discussed here, while laser processing will be discussed further on in this chapter.

The effects of thermal annealing on films of SnO₂:Sb are complex and depend upon many factors including deposition method, deposition temperature, thickness, dopant concentration and post deposition treatment. More specifically, changes in conductivity and optical transparency can be observed with thermal annealing depending upon the environment at the time of annealing. Studies of thermal annealing of these materials have included annealing in nitrogen, oxygen, air and a vacuum, with wide ranging effects. These include grain size increase, oxygen chemisorption or desorption, sintering or incorporation of the Sb dopant into the lattice.

Several authors have investigated the effect of the annealing environment during classic thermal annealing. Sabnis et al[56] carried out a temperature cycling investigation in nitrogen and found that their dc glow discharge sputtered films of SnO₂:Sb increased in conductivity and were more stable. The improvements were

attributed to an increase in grain size and the Sb dopant being incorporated into the lattice.

Shanthi et al[57] performed an extensive study on spray pyrolysed SnO₂:Sb including annealing in a vacuum, air and in hydrogen, oxygen, nitrogen and argon atmospheres. They found that oxygen played an important role in the annealing process; in general, inducing an increase in resistivity. The resistivity of films annealed in hydrogen, nitrogen or argon was observed to reduce. They attribute the changes in resistivity to changes in mobility since they saw little change in carrier concentration. It was suggested that chemisorption and desorption of oxygen from grain boundaries was responsible for modulating the potential barrier height and decreasing and increasing the carrier mobility respectively.

Beensh-Marchwicka et al[45] investigated the effect of annealing on the phase composition of dc reactive ion sputtered SnO₂:Sb films. The preferred orientation of the doped films was SnO₂ (110), which remained the case following annealing. Annealing in air produced a small increase in crystallinity, however none was observed for films annealed in a vacuum or nitrogen. Following annealing in nitrogen and air the resistivity of the films reduced.

More recently Huang et al[46] investigated the effects of classical thermal annealing on RF reactive magnetron sputtered SnO₂:Sb films. Their study investigated the effects of thermal annealing in O₂ and N₂ atmospheres at 300, 400 and 500°C. It was found that both mobility and carrier concentration increased with increasing temperatures for both atmospheres. Crystallinity was improved with increasing

temperature following annealing in an O₂ atmosphere, but an initial improvement in crystallinity could not be increased with higher temperatures in an N₂ atmosphere.

Van Bommel et al[58] and Zhang et al[59] investigated the change in resistivity with thermal annealing at increasing temperatures in air. Both observed decreases in resistivity with increasing temperature, followed by an increase with further temperature increases. Van Bommel et al produced spin coated films of SnO₂:Sb, the resistivity of which decreased with increasing temperature up to 800°C, above which it steadily increased. It is thought that the increase after 800°C is due to the segregation of Sb to the surfaces of the grain, thus decreasing the carrier mobility. More recently Zhang et al found that dip coated films of SnO₂:Sb followed a similar trend, however they observed the increase at approximately 500°C and attribute it to oxygen chemisorption decreasing the carrier concentration.

Rapid Thermal Annealing of transparent conducting oxides has also been investigated, but not extensively. Boudiar et al[43] used a series of 12 infrared lamps with repeated heating cycles of less than a minute to rapid thermal anneal dip coated SnO₂:Sb. They found it was possible to obtain good electrical and optical properties using RTA and found it particularly useful for very thin layers of 100-150nm, where classical thermal annealing showed no benefit. Densification and crystallite size increase was found to be more homogeneous with RTA than classical annealing. Daoudi et al[60] found that RTA of ITO films resulted in a lower resistivity than by classic thermal annealing. Rutherford Backscattering determined that the RTA films were more dense than the classically annealed films and this was suggested as the reason for the improved resistivity. No information on the temperature reached by

the substrate during this process was available so it is not possible to determine if this method is compatible with temperature sensitive substrates.

2.3.5.2 *Summary*

While many researchers have investigated many techniques for the deposition of SnO₂:Sb, some of the deposition methods and perhaps all of the post-deposition methods discussed above involve heating of the substrate layer and so are not suitable for temperature sensitive substrates such as PEN and PET. With a desire for flexible substrates from both manufactures and consumers, there is a pressing need for a low temperature post process which will decrease resistivity. Flexible substrates and UV laser processing of SnO₂:Sb will be discussed later in this chapter.

2.4 Deposition Methods for ATO

2.4.1 Introduction

The electrical and optical properties of a transparent conductor can vary hugely depending upon the deposition method. This is because these properties are highly dependent upon microstructure, stoichiometry and impurities present. Popular deposition methods for ATO are sputtering, chemical vapour deposition and spray pyrolysis. A brief description of each of these methods is given below together with typical electrical and optical characteristics using each method. Each of the methods described requires a subsequent mask and etch process to obtain patterned electrodes.

2.4.2 Sputtering

Sputtering is one of the most popular methods of deposition where the purity and homogeneity of the films is important[61]. The material to be sputtered is pressed

into a target. The target is usually placed on a plate that acts as a cathode. The anode typically holds the substrate onto which the material is to be deposited. This is housed in a vacuum chamber, into which a gas flows, for the deposition of SnO₂:Sb this is usually Ar with a 1-10% concentration of O₂. A voltage is applied between the cathode and anode to create a plasma in the gas. The target is then bombarded with ions which 'knock off' particles of the material which diffuse away and coat the substrate. There are different types of sputtering: DC, rf and magnetron (magnetically enhanced gas discharge). DC sputtering, where a direct voltage is applied to the cathode and anode; is used for conductive targets. RF sputtering is used for both conducting and insulating materials and uses a high frequency (13.56MHz) signal generator across the electrodes. Magnetron sputtering can be combined with the previous types to increase deposition rates and reduce deposition temperature. A schematic of the RF magnetron sputtering system used for depositions in this body of work is shown in Figure 2-10. A more in depth description of this equipment is given in chapter 3. The main disadvantages of sputtering are the need for a vacuum, substrate heating and comparatively high equipment costs.

Sputter deposition of SnO₂:Sb has been widely investigated [14, 36, 45, 46, 55, 62-64]. The lowest resistivity value reported is $1.3 \times 10^{-3} \Omega \text{cm}$ for films deposited by reactive rf magnetron sputtering[64] with an Sb concentration of 8%, O₂ concentration of 15.4% and substrate temperature of 530°C, however transmittance was poor at 62.8% (averaged transmittance over photopic vision spectra). Similar values of resistivity were achieved by Jager et al[36] and Hao et al[14] with a better transmittance of >88% (250nm thick film) and >70% respectively (~ 335nm thick

film). There are many parameters which affect film quality, these include O₂ concentration, Sb concentration, substrate temperature, gas flow speed, partial pressure and rf power applied. These parameters will be discussed further in Chapter 4.

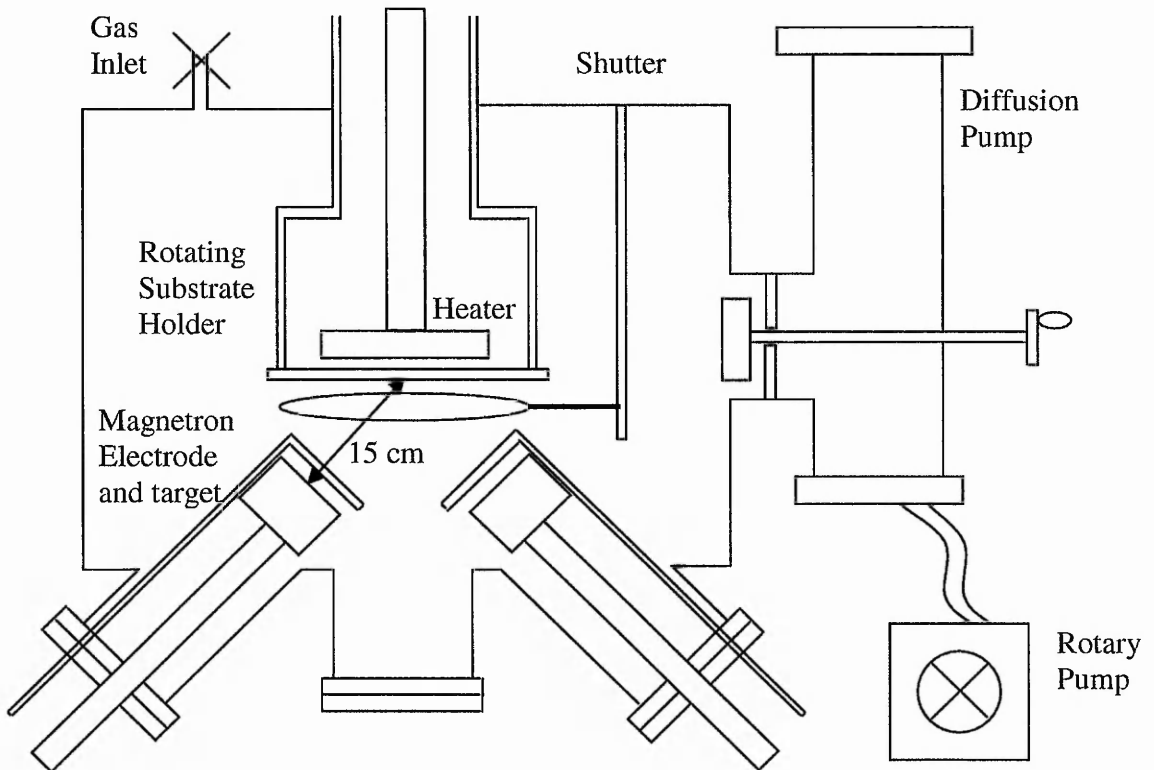


Figure 2-10: Schematic of RF magnetron sputtering system used for thin film deposition during this project

2.4.3 Alternative Deposition Processes

There are many thin film deposition techniques that have been used to deposit transparent conducting oxide materials, each producing films with unique properties. There follows a summary of the more popular alternative deposition techniques, with references to general texts for the more interested readers. Table 2-2 also gives

a summary of the typical electrical and optical properties for each deposition method.

2.4.3.1 Dip-Coating

Dip-coating is a common and relatively simple method used to deposit thin films of material[59, 65]. It involves the immersion, dwell and withdrawal of the substrate layer into a solution. Immersion should be carried out smoothly and at a fixed rate. A dwell time is then allowed for the solution to adhere to the substrate. Finally withdrawal occurs, with shorter rates for thinner samples and faster rates for thicker samples. The details of the technique used by Keeling & Walker Ltd[66] for the samples investigated in this project are confidential. Zhang et al[59] achieved a transmission of 80-90% with a sheet resistance of 85-100 Ohm/sq on dip-coated samples. Terrier et al[66] report a sheet resistance of 45 Ohm/sq with transmission between 65% and 80%.

2.4.3.2 Spray Pyrolysis

Spray pyrolysis is a popular deposition method and has been widely used to deposit SnO₂:Sb[10, 21, 52, 53]. Rajpure et al[53] report resistivity values as low as $0.4 \times 10^{-4} \Omega \text{cm}$ with an average 80% transmission while Jain et al [52] report higher transmission values of 90%, but with resistivity at $1.53 \times 10^{-3} \Omega$. Spray pyrolysis involves a metallic compound being dissolved into a liquid which is sprayed onto a pre-heated substrate[67]. The metallic compound undergoes a pyrolytic decomposition to form the film on the substrate. It is a relatively simple technique that can easily be scaled up for large scale manufacture. There are a number of critical parameters that directly affect the final film quality. The spray nozzle used to atomise the chemical solution into fine droplets needs to be of particular dimensions

and also requires a filtered gas carrier. The solution and the carrier gas need to be fed in at predetermined pressures and substrate temperature must be carefully maintained. Deposition time, distance from nozzle to substrate and solution composition also affect the final film quality.

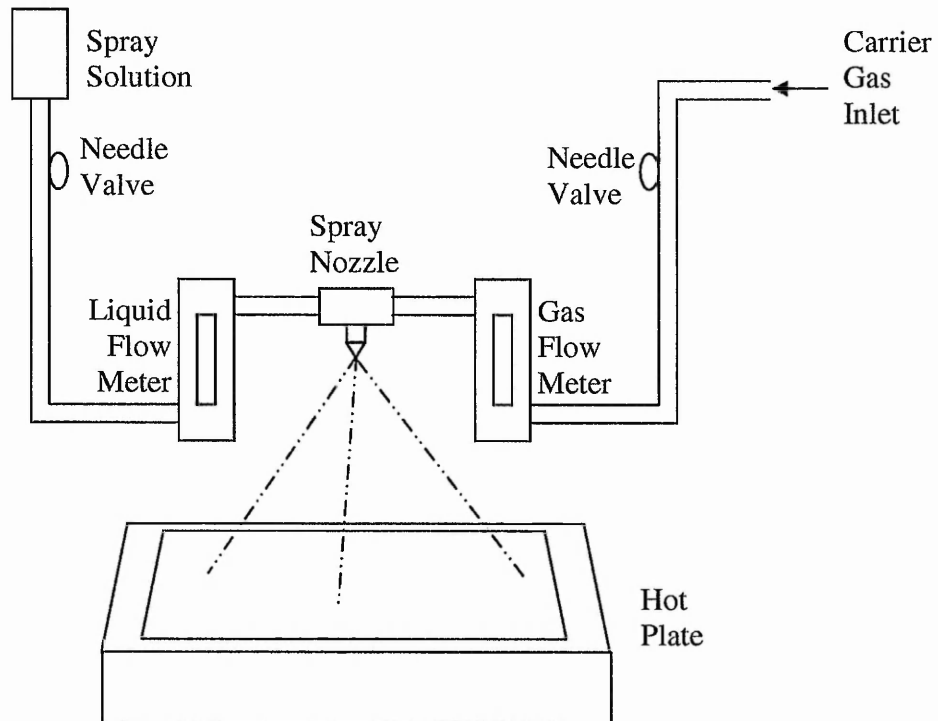


Figure 2-11: Typical layout of thin film deposition by spray pyrolysis

Resistivity values as low as $1.53 \times 10^{-3} \Omega \text{cm}$ [52] and $0.4 \times 10^{-4} \Omega \text{cm}$ [53] have been reported for spray pyrolysed $\text{SnO}_2:\text{Sb}$. A schematic for the equipment layout for spray pyrolysis is shown in Figure 2-11[67].

2.4.3.3 Chemical Vapour Deposition

Chemical Vapour Deposition (CVD) is the deposition of a solid form onto a substrate from a gaseous form[68]. The substrate is housed in a furnace and heated; since the temperature of the substrate is critical to the quality of the film grown. A carrier gas is used to transport the material to be deposited by creating a vapour

containing the condensate material. This is fed to the substrate, where a reaction occurs and the material decomposes. Gas flow rate, substrate temperature and system geometry should be optimised for the best quality film. It is a simple method of deposition that has the advantage of not requiring a vacuum and is therefore relatively easy to scale up. There are different types of CVD including Plasma-Enhanced CVD (PE-CVD) where a plasma is used to help the reaction of the condensate material. It has the advantage of using much lower temperatures, around 300°C compared to 800°C. Typical resistivity values published for PE-CVD SnO₂:Sb are $9 \times 10^{-2} \Omega \text{cm}$ [69].

2.5 Printing Technologies

The desire to print electronic components is driving research into printing techniques and material science. One of the greatest advantages of printing is that it is an additive process. The deposition methods discussed in the previous sections are all subtractive; i.e. they blanket deposit the material over the entire substrate, then remove, 'subtract' unwanted material. In order to create a pattern of pixels or a fixed legend display, the material must be etched away where it is not required. This usually requires a post deposition photolithographic mask and etch process. In terms of manufacturing, the less manufacturing steps to produce a product, the cheaper the cost of producing the product. As such, an additive deposition process, such as printing would cut the number of manufacturing steps and therefore cut the cost of production. It is also a more efficient use of the deposited material.

A further advantage to printing is the inherent low cost of the procedure due to the prevalence of home and work printers. Deposition methods such as sputtering

requires specialised vacuum equipment that costs £100,000s to buy and not inconsiderable amounts to maintain and run. There is also the problem of running a vacuum procedure in an automated manufacturing process. While the types of printer found in the home or work place may not be suitable for large scale manufacturing processes much of the printing during this project was carried out using a simple off the shelf inkjet printer, so it is clear that the process can be made very simple.

2.5.1 Inkjet Printing

While inkjet printing first gained enormous popularity in the 1970s, the seeds leading to this innovation were planted in 1878 by Lord Rayleigh when he first described the mechanisms by which a stream of liquid breaks up into droplets[70]. In 1951 Elmqvist[71] filed the first of many patents associated with inkjet printing which led directly to the development of a mingograph; a chart recorder for analogue voltage signals. As technology grew in sophistication, it was demonstrated that droplets of uniform size and spacing could be created by applying a shock wave to the inkjet head[72] and so inkjet printing as we know it was born. For further reviews of early inkjet printing developments Heinzl et al[73] and Kuhn et al [74] are recommended.

Inkjet printing works in one of two ways, either continuous inkjet (COJ), or drop on demand (DOD). DOD is the most appropriate for functional materials as COJ involves recirculation of the ink and risks contamination and it requires the ink to be chargeable. A simple schematic of a COJ and DOD jet head are shown in Figure 2-12.

US patents submitted by Zoltan[75] and Kyser and Sears[76] saw them amongst the pioneers of DOD printing technology. DOD inkjet printing is carried out with one of two heads, either a thermal head or a piezo actuated head. Thermal heads work by having a series of electrically heated chambers. A pulse of current is sent to the elements creating a steam bubble which propels a drop of ink out of the head onto the paper. For the purposes of this work, thermal heads were not suitable because the thermal process was not compatible with the ATO ink and the material clogged the nozzle head.

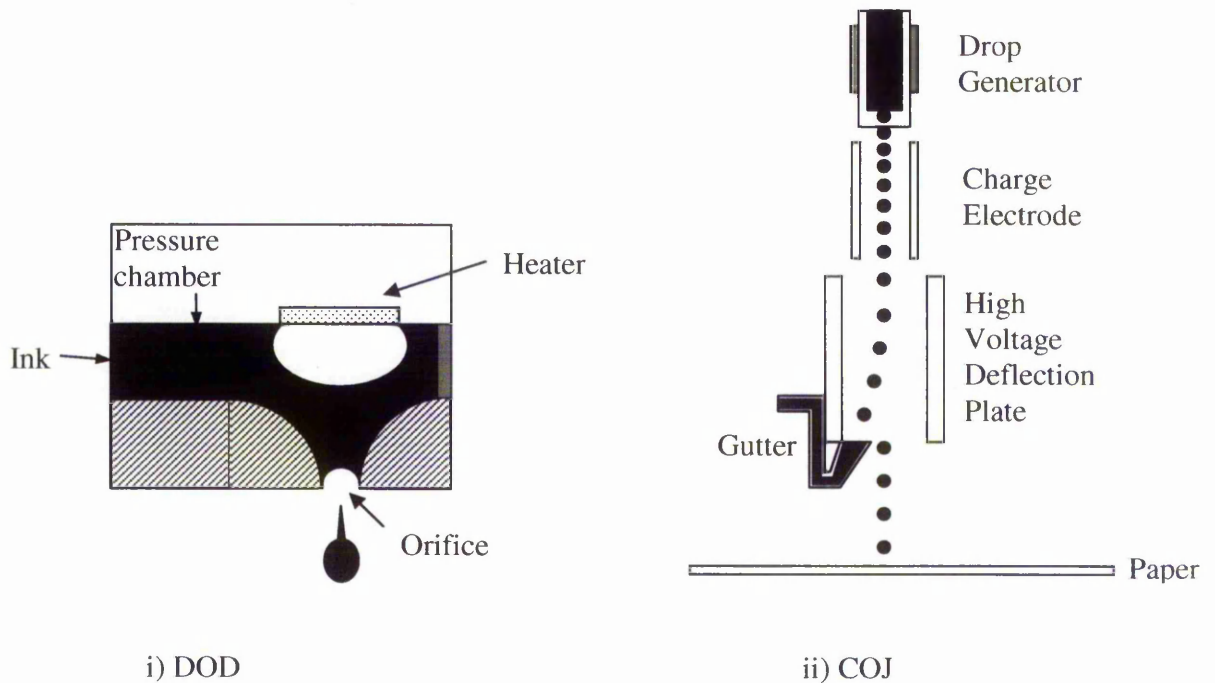


Figure 2-12: Inkjet printing heads i) thermal Drop On Demand (DOD) and ii) Continuous inkjet (COJ) head[78]

Piezo heads contain a piezo crystal which changes shape with the application of a voltage. The shape changes induced in the crystal create a mechanical pressure pulse in the ink reservoir forcing individual ink drops out of the nozzle. There are four modes of piezo operation: shear, bend, push and squeeze and the nature of the piezo

design means that higher viscosity inks, a range of solvents, heat sensitive inks and nano-particulate based inks can be jetted.

The details of the inkjet printer used for this investigation are confidential to PTL Ltd[77]. However, an excellent summary of inkjet printing technology past, present and future can be found at www.imaging.org[78].

2.6 Flexible substrates

Flexible substrates are another highly desirable innovation for the displays industry and consumer[79]. Display manufacturers would like to use flexible displays so that they can move to a roll-to-roll manufacturing process. Currently large panels of glass (Generation 7 = 2.2x2.2m panels) are used to manufacture displays, which creates a considerable manual handling problem. Every 18 months, the size of the glass substrates doubles such that new manufacturing plants must be built. Breakages reduce yields and the not inconsiderable weight of the glass means high shipping costs.

It is generally considered that flexible displays would also benefit the consumer, since flexible substrates would enable cheaper, more robust, lightweight and compact portable electronic devices. Advertisers could use an existing network of flexible displays to download advertising to saving them the cost of printing and shipping and to enable localised advertising, or last minute special offers.

The case for flexible substrates is compelling; however, it is clearly not without its problems since they are not yet a high street norm. One of the problems with flexible

substrates is temperature sensitivity, particularly with respect to transparent conductors. For tin oxides, and antimony-doped and indium-doped tin oxides a post-deposition thermal anneal is carried out to improve the conductivity. While precise temperatures vary from material to material and by deposition method, it is usual to see annealing temperatures such as 400°C for up to one hour. Various mechanisms have been cited[45] as being responsible for improvements in conductivity and these include; sintering, increased crystallinity, transformation of SnO phase material into SnO₂ (which is less resistive) and chemisorption and desorption of oxygen from grain boundaries.

There are specialised flexible materials that can withstand temperatures up to 200°C such as Teonex® by Dupont[80], but this is not high enough to induce the desired conductivity improvements. As such, if flexible substrates are to become commonplace in the market, alternative processes need to be developed. A summary of laser processing as an alternative follows in the next section.

2.7 Laser Processing of Thin Films

2.7.1 Introduction

The unique nature of laser light is driving an increase in research into the use of the laser as a material processing tool. There is little risk of contamination since lasers are chemically pure. The coherence of a laser beam enables strong focusing capabilities so that precision through localised absorption is achievable leaving neighbouring areas untouched, it also offers the advantage of high energy density capabilities. High temporal resolution can also be used to confine heating with rapid cooling by short pulse utilisation. Matching of the wavelength and beam power with

the optical and thermal properties of the material also facilitates control of heating, including depth. Finally. For the purposes of this work, the wavelengths associated with the KrF and ArF are compatible with the absorption spectrum of ATO and the absorption co-efficient prevents the laser radiation from reaching and damaging the substrate[81].

2.7.2 Applications

Perhaps due to its many unique and useful properties lasers have been applied to many applications including welding, cutting, marking, drilling, photolithography and micromaching, not to mention the many medical and measurement applications. William Steen[82] and John Ion[83] have both produced excellent texts on the subject for more interested readers.

It is well known that laser processing has been successfully used since the 1970s to convert amorphous silicon to poly-silicon for the purposes of TFTs in display applications[84]. Excimer lasers are usually the laser of choice because of their high energy UV output. This includes lasers such as XeCl (308nm), KrF (248nm) and ArF (193nm).

In the field of microelectronic manufacture there has been much research into laser processing[85] often as an alternative to rapid thermal annealing. These include laser-annealing of ion implanted dopants and laser-induced diffusion of dopants which have reduced transient enhanced diffusion because of the nano-scale ramp-up and down times. Excellent spatial resolution also results in very abrupt profiles and controlled processing. Silicon carbide is one such material; its properties are

particularly suited to high temperature, high frequency and high power applications. However its high melting point is a hindrance to the traditional thermal annealing used for incorporation and diffusion of dopants and laser-processing has been demonstrated as an excellent method to overcome this issue[86].

Slightly outside the area of semiconductors (although also applied to semiconductors) is the area of laser cleaning. Lasers are used to clean materials or compounds in areas such as optics, microelectronics, art and historic building[85]. Often the essential criteria are to keep surfaces free of chemicals and to maintain a controlled surface morphology and both of these can be achieved using either dry or steam laser cleaning.

The recent growth in research into methods of improving the characteristics of transparent films without traditional thermal annealing[81, 87, 88] has coincided with the desire for flexible electronics and displays and new applications for lasers are appearing all the time.

2.7.3 Interactions

An overview of interactions is given here, however for interested readers a fuller description can be found in Laser-Beam Interactions with Materials by Allmen and Blatter[89]. In an ideal scenario insulators and semiconductor materials without any excitement contain only electrons bound within a lattice, they can be considered to be transparent except at particular resonances. The resonance values correspond to energies between permitted energy states and therefore energy values where an electron transition can take place. The most significant of which are interband

transitions; those between the valence and conduction band, since these generate free carriers. With the introduction of an electric field in the form of incident laser light, the electrons will behave as harmonic oscillators responding to the oscillating force of the incident field at these resonances. These oscillations produce a macroscopic polarisation within the material. This small field is superposed onto the original field and the ratio of this combined field to the original field gives the dielectric function of a given material, i.e. its optical response at any given wavelength.

In addition to resonances due to electron transitions there are phonon resonances - resonances from lattice vibrations - usually in the infrared for non-metals. The absorption spectra of such a material often shows peaks in the infrared from phonon coupling, with poor absorption in the interim wavelengths until the photon energy approaches that which corresponds with the energy gap. In a simplistic summary, there are two absorption mechanisms that determine the appropriateness and effect of the laser, one from carrier absorption and one from lattice absorption. The laser of choice for this body of work is a KrF laser emitting at 248nm, this corresponds to a photon energy of 5eV, which is larger than reported band-gap figures for SnO₂ of approximately 4.1-4.2eV[90, 91] and so ideal for carrier absorption. It is therefore also likely that carrier absorption, rather than phonon coupling, is the dominant absorption mechanism.

With large carrier concentrations of $10^{17} - 10^{18} \text{ cm}^{-3}$, the free carriers can be thought of as a collective and separate to the lattice, in this case they are referred to as a plasma. The plasma acts as a conduit between the laser energy and the lattice,

absorbing the laser pulses and ultimately transferring this energy to the lattice.

Figure 2-13 shows a state diagram with possible transitions[89].

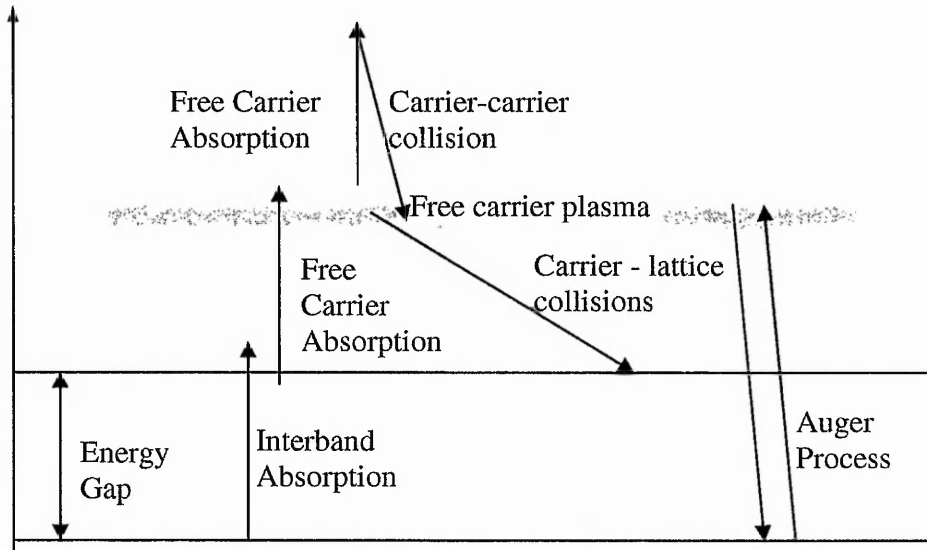


Figure 2-13: State diagram of possible energy transitions during laser processing

Ultimately, the distribution of optically excited free carriers is more complex than that of thermally excited carriers, which follow a typical Boltzman distribution. There are free carriers to be found high up in the conduction band and in states deep in the valence band. Excited carriers will relax via carrier-carrier and carrier-lattice collisions.

2.7.4 Laser Processing of Transparent Conductors

Nagase et al[87] have reported successful laser processing of Zinc Oxide (ZnO) films used for its luminescent properties. Laser processing with a KrF laser produced ZnO with high crystallinity and strong orientation.

Sandu et al[20, 81] have used both the ArF and KrF lasers to process sol-gel derived ATO on glass with the KrF being the more successful due to greater penetration depths. The films were deposited by sol-gel dip coating which were subsequently dried in air at 200°C for 5 hours. They reported a reduction in sheet resistance values to 30kOhm/sq (Approximately 0.6Ωcm assuming film thickness ~ 190nm) after 1000 pulses at 78mJcm⁻² which they attributed to increased crystallisation.

Chung et al[88] working with a XeCl laser and Indium Tin Oxide (ITO) have deposited the film using DC magnetron sputtering onto glass substrates and achieved a reduction in sheet resistance from 200kΩ/sq to 35kΩsq.

Aegerter et al found a four fold decrease in resistivity following a scan with a continuous wave CO₂ laser. The process resulted in a reduction in film thickness and therefore a densification of the film which was attributed as the cause of reduction in resistivity.

The author is unaware of any published work on laser processing of TCOs deposited onto flexible substrates, however this process is alluded to in each of the references described above.

2.8 Applications

2.8.1 Electronic Displays

Electronic displays are the primary target application for laser processed inkjet printed transparent conductors. Nearly all modern electronic display types require a

transparent conducting layer[92, 79]. An example of its use is in an electroluminescent device, as shown in Figure 2-14.



Figure 2-14: Fixed legend electroluminescent display made by screen printing

A schematic of an electroluminescent display, shown in Figure 2-15, shows how the TCO layer is built into the structure of the device.

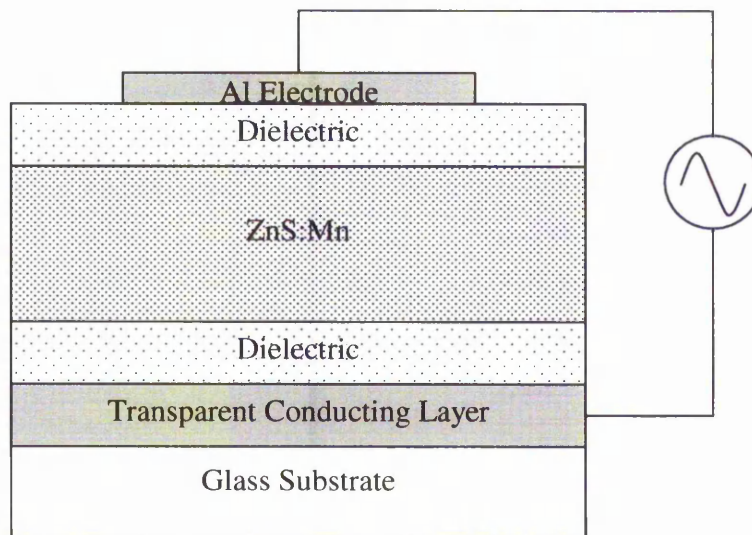


Figure 2-15: Schematic of an AC Electroluminescent device

Essential parameters for display applications include transmission, sheet resistance and surface roughness. Transmission should be $\geq 85\%$ and is usually quoted for 550nm; the peak of the human visual system. Ideal sheet resistance values will vary from application to application, but should be of the order of $100\Omega/\text{sq}$. Surface roughness is critical for display technologies such as Liquid Crystal Displays (LCD) and Organic Light Emitting Diodes (OLED), where a surface roughness of 1nm is required. In other applications such as electroluminescent devices, the surface roughness is not so critical.

2.8.2 Solar Cells

Interest in transparent conductors for solar cell applications has grown in recent years because transparent conductive oxides have a number of benefits that make them particularly useful in solar cells[93]. Their transparency allows direct transmission of the solar radiation onto the active medium with little or no losses. They can act as both a contact to the active medium and simultaneously an anti-reflection coating. They also have the benefit of easing the manufacturing process because they require lower temperatures to form the heterojunction.

Solar cells utilising TCOs have been developed with the TCO as an active element in a heterojunction cell, or solely as a transparent electrode. These combined characteristics make TCO based solar cells more suitable for large scale, worldwide applications and research in these areas continues.

2.8.3 Anti-reflection coatings

Antireflection coatings are frequently seen on displays to prevent eye strain from glare[79] The application of such a layer can be multi-functional since anti-static and

electromagnetic wave shielding are often a requirement too. A transparent conducting layer, with good transparency and very modest sheet resistance values of $10^2 - 10^3 \Omega/\text{sq}$. The current preferred method of depositing these coatings is by sputter deposition, which as already discussed above, is not ideal in terms of cost nor practicality. Recent research has focussed on simpler deposition methods of materials such as ATO and ITO for this application.

References

- [1] J. R. Hook and H. E. Hall, *Solid State Physics*, 2nd ed. England: John Wiley & Sons Ltd, 2005.
- [2] S. M. Sze and K. K. Ng, *Physics of Semiconductor Devices*, 3rd ed. New Jersey: John Wiley & Sons Inc, 2007.
- [3] B. L. Anderson and R. L. Anderson, *Fundamentals of Semiconductor Devices*, McGraw-Hill Professional, 2004.
- [4] D. K. Schroder, *Semiconductor Material and Device Characterization*, 2nd ed. John Wiley & Sons, 1998.
- [5] R. K. Willardson, Norbert H. Nickel & E. R. Weber, *Hydrogen in Semiconductors II*, Academic Press, 1999.
- [6] J. Y. W. Seto, "The electrical properties of polycrystalline silicon films," *Journal of Applied Physics*, vol. 46, pp. 5247, 1975.
- [7] R. L. Petritz, "Theory of Photoconductivity in Semiconductor Films," *Phys. Rev.*, vol. 104, pp. 1508, 1956.
- [8] J. W. Orton, B. J. Goldsmith, M. J. Powell, and J. A. Chapman, "Temperature dependence of intergrain barriers in polycrystalline semiconductor films," *Appl. Phys. Lett.*, vol. 37, pp. 557, 1980.
- [9] E. H. Hall, "On a new action of the magnet on electric currents," *American Journal of Mathematics*, vol. 2, pp. 287-282, 1879.
- [10] S. Shanthi, C. Subramanian, and P. Ramasamy, "Preparation and properties of sprayed undoped and fluorine doped tin oxide films," *Materials Science and Engineering B*, vol. 57, pp. 127, 1999.
- [11] Sung-Soon Park and J. D. Mackenzie, "Sol-gel-derived tin oxide thin films," *Thin Solid Films*, vol. 258, pp. 268, 1995.

- [12] X. Hao, J. Ma, D. Zhang, X. Xu, Y. Yang, H. Ma, and S. Ai, "Transparent conducting antimony-doped tin oxide films deposited on flexible substrates by r.f. magnetron-sputtering," *Applied Physics A: Materials Science & Processing*, vol. 75, pp. 397, 2002.
- [13] G. Gasparro, J. Putz, D. Ganz, and M. A. Aegerter, "Parameters affecting the electrical conductivity of SnO₂:Sb sol-gel coatings," *Solar Energy Materials and Solar Cells*, vol. 54, pp. 287, 1998.
- [14] X. Hao, J. Ma, D. Zhang, Y. Yang, X. Xu, F. Chen, and H. Ma, "Electrical and optical properties of SnO₂:Sb films prepared on polyimide substrate by r.f. bias sputtering," *Applied Surface Science*, vol. 189, pp. 157, 2002.
- [15] A. L. D. Hartnagel H, A.K. Jain, C. Jagadish, "*Semiconducting Transparent Thin Films*," 1995.
- [16] E. Hecht, *Optics*, 4th ed: Addison Wesley, 2002.
- [17] F. Simonis, M. van der Leij, and C. J. Hoogendoorn, "Physics of doped tin dioxide films for spectral-selective surfaces," *Solar Energy Materials*, vol. 1, pp. 221, 1979.
- [18] J. Wilson and J. F. B. Hawkes, *Optoelectronics - An introduction*, 2nd ed. Cambridge: Prentice Hall International (UK) Ltd, 1989.
- [19] S. Shanthi, C Subramanian, P Ramasamy, "Investigations on the Optical Properties of undoped, Fluorine Doped and Antimony Doped Tin Oxide Films" *Cryst. Res. Technol.*, Vol. 34, pp. 1037-1046, 1999.
- [20] C. S. Sandu, V. S. Teodorescu, C. Ghica, B. Canut, M. G. Blanchin, J. A. Roger, A. Brioude, T. Bret, P. Hoffmann, and C. Garapon, "Densification and crystallization of SnO₂:Sb sol-gel films using excimer laser annealing," *Applied Surface Science*, vol. 208-209, pp. 382, 2003.

- [21] E. Shanthi, V. Dutta, A. Banerjee, and K. L. Chopra, "Electrical and optical properties of undoped and antimony-doped tin oxide films," *Journal of Applied Physics*, vol. 51, pp. 6243, 1980.
- [22] Z. M. Jarzebski and J. P. Marton, "Physical Properties of SnO₂ Materials," *Journal of The Electrochemical Society*, vol. 123, pp. 199C, 1976.
- [23] S. Munnix and M. Schmeits, "Surface electronic structure of SnO₂(110)," *Solid State Communications*, vol. 43, pp. 867, 1982.
- [24] V. Vasu and A. Subrahmanyam, "Electrical and optical properties of sprayed SnO₂ films: Dependence on the oxidizing agent in the starting material," *Thin Solid Films*, vol. 193-194, pp. 973, 1990.
- [25] A. De and S. Ray, "A study of the structural and electronic properties of magnetron sputtered tin oxide films," *Journal of Physics D: Applied Physics*, vol. 24, pp. 719, 1991.
- [26] G. Sanon, R. Rup, and A. Mansingh, "Growth and characterization of tin oxide films prepared by chemical vapour deposition," *Thin Solid Films*, vol. 190, pp. 287, 1989.
- [27] C. G. Granqvist and A. Hultaker, "Transparent and conducting ITO films: new developments and applications," *Thin Solid Films*, vol. 411, pp. 1, 2002.
- [28] Ho-Chul Lee and O. Ok Park, "Behaviors of carrier concentrations and mobilities in indium-tin oxide thin films by DC magnetron sputtering at various oxygen flow rates," *Vacuum*, vol. 77, pp. 69, 2004.
- [29] J. Strumpfel and C. May, "Low ohm large area ITO coating by reactive magnetron sputtering in DC and MF mode," *Vacuum*, vol. 59, pp. 500, 2000.
- [30] A. Kawada, "Indium-tin oxide deposition by d.c. reactive sputtering on a low softening point material," *Thin Solid Films*, vol. 191, pp. 297, 1990.

- [31] A. K. Saxena, S. P. Singh, R. Thangaraj, and O. P. Agnihotri, "Thickness dependence of the electrical and structural properties of $\text{In}_2\text{O}_3:\text{Sn}$ films," *Thin Solid Films*, vol. 117, pp. 95, 1984.
- [32] H. Haitjema and J. J. P. Elich, "Physical properties of pyrolytically sprayed tin-doped indium oxide coatings," *Thin Solid Films*, vol. 205, pp. 93, 1991.
- [33] S. M. Rozati and T. Ganj, "Transparent conductive Sn-doped indium oxide thin films deposited by spray pyrolysis technique," *Renewable Energy*, vol. 29, pp. 1671, 2004.
- [34] J. L. Yao, S. Hao, and J. S. Wilkinson, "Indium tin oxide films by sequential evaporation," *Thin Solid Films*, vol. 189, pp. 227, 1990.
- [35] V. S. Vaishnav, P. D. Patel, and N. G. Patel, "Preparation and characterization of indium tin oxide thin films for their application as gas sensors," *Thin Solid Films*, vol. 487, pp. 277, 2005.
- [36] B. Szyszka, S. Jager, J. Szczyrbowski, and G. Brauer, "Comparison of transparent conductive oxide thin films prepared by a.c. and d.c. reactive magnetron sputtering," *Surface and Coatings Technology*, vol. 98, pp. 1304, 1998.
- [37] C. Goebbert, H. Bisht, N. Al-Dahoudi, R. Nonninger, M. A. Aegerter, and H. Schmidt, "Wet Chemical Deposition of Crystalline, Redispersable ATO and ITO Nanoparticles," *Journal of Sol-Gel Science and Technology*, vol. 19, pp. 201, 2000.
- [38] Yung-Jen Lin and Ching-Jiunn Wu, "The properties of antimony-doped tin oxide thin films from the sol-gel process," *Surface and Coatings Technology*, vol. 88, pp. 239, 1997.

- [39] M. A. Aegerter, A. Reich, D. Ganz, G. Gasparro, J. Putz, and T. Krajewski, "Comparative study of SnO₂:Sb transparent conducting films produced by various coating and heat treatment techniques," *Journal of Non-Crystalline Solids*, vol. 218, pp. 123, 1997.
- [40] C. Terrier, J. P. Chatelon, R. Berjoan, and J. A. Roger, "Sb-doped SnO₂ transparent conducting oxide from the sol-gel dip-coating technique," *Thin Solid Films*, vol. 263, pp. 37, 1995.
- [41] E. Elangovan, K. Ramesh, and K. Ramamurthi, "Studies on the structural and electrical properties of spray deposited SnO₂:Sb thin films as a function of substrate temperature," *Solid State Communications*, vol. 130, pp. 523, 2004.
- [42] S. Shanthi, C. Subramanian, and P. Ramasamy, "Growth and characterization of antimony doped tin oxide thin films," *Journal of Crystal Growth*, vol. 197, pp. 858, 1999.
- [43] T. Boudiar, C. S. Sandu, B. Canut, M. G. Blanchin, V. S. Teodorescu, and J. A. Roger, "Interest of Rapid Thermal Annealing (RTA) for the Elaboration of SnO₂:Sb Transparent Conducting Oxide by the Sol-Gel Technique," *Journal of Sol-Gel Science and Technology*, vol. 26, pp. 1067, 2003.
- [44] T. M. Hammad, "The effect of different plasma treatments on the sheet resistance of sol-gel ITO and ATO thin films," *Chinese Journal of Physics*, vol. 40, pp. 532-536, 2002.
- [45] G. Beensh-Marchwicka, L. Krol-Stepniewska, and A. Misiuk, "Influence of annealing on the phase composition, transmission and resistivity of SnO_x thin films," *Thin Solid Films*, vol. 113, pp. 215, 1984.

- [46] Jow-Lay Huang, Yi Pan, Jia Yuan Chang, and Bao-Shun Yau, "Annealing effects on properties of antimony tin oxide thin films deposited by RF reactive magnetron sputtering," *Surface and Coatings Technology*, vol. 184, pp. 188, 2004.
- [47] T. Kololuoma, A. H. O. Karkkainen, and J. T. Rantala, "Novel synthesis route to conductive antimony-doped tin dioxide and micro-fabrication method," *Thin Solid Films*, vol. 408, pp. 128, 2002.
- [48] M. I. B. Bernardi, L. E. Soledade, I. A. Santos, E. R. Leite, E. Longo, and J. A. Varela, "Influence of the concentration of Sb_2O_3 and the viscosity of the precursor solution on the electrical and optical properties of SnO_2 thin films produced by the Pechini method," *Thin Solid Films*, vol. 405, pp. 228, 2002.
- [49] A. F. Carroll, "Effects of additions to SnO_2 thin films," *Journal of Electrochemical Society*, vol. 123, pp. 1889-1893, 1976.
- [50] D. J. Goyal, C. Agashe, B. R. Marathe, M. G. Takwale, and V. G. Bhide, "Effect of dopant incorporation on structural and electrical properties of sprayed $\text{SnO}_2\text{:Sb}$ films," *Journal of Applied Physics*, vol. 73, pp. 7520, 1993.
- [51] S. Shanthi, C. Subramanian, P. Ramasamy, "Investigations on the Optical Properties of Undoped, Fluorine Doped and Antimony Doped Tin Oxide Films," *Crystal Research and Technology*, vol. 34, pp. 1037-1046, 1999.
- [52] G. Jain and R. Kumar, "Electrical and optical properties of tin oxide and antimony doped tin oxide films," *Optical Materials*, vol. 26, pp. 27, 2004.
- [53] K. Y. Rajpure, M. N. Kusumade, M. N. Neumann-Spallart, and C. H. Bhosale, "Effect of Sb doping on properties of conductive spray deposited SnO_2 thin films," *Materials Chemistry and Physics*, vol. 64, pp. 184, 2000.

- [54] J. A. Roger, C. Terrier, and J. P. Chatelon, "Electrical and optical properties of Sb:SnO₂ thin films obtained by the sol-gel method," *Thin Solid Films*, vol. 295, pp. 95, 1997.
- [55] J. Ma, X. Hao, S. Huang, J. Huang, Y. Yang, and H. Ma, "Comparison of the electrical and optical properties for SnO₂:Sb films deposited on polyimide and glass substrates," *Applied Surface Science*, vol. 214, pp. 208, 2003.
- [56] A. Sabnis and L. Feisel, "Heat Treatment of Dc-Sputtered Tin Dioxide Thin Films," *IEEE Transactions on Parts, Hybrids, and Packaging*, vol. 12, pp. 357-360, 1976.
- [57] E. Shanthi, A. Banerjee, V. Dutta, and K. L. Chopra, "Annealing characteristics of tin oxide films prepared by spray pyrolysis," *Thin Solid Films*, vol. 71, pp. 237, 1980.
- [58] M. J. Van Bommel, W. A. Groen, H. A. M. Van Hal, W. C. Keur, and T. N. M. Bernards, "The electrical and optical properties of thin layers of nano-sized antimony doped tin oxide particles," *Journal of Materials Science*, vol. 34, pp. 4803, 1999.
- [59] D. Zhang, L. Tao, Z. Deng, J. Zhang, and L. Chen, "Surface morphologies and properties of pure and antimony-doped tin oxide films derived by sol-gel dip-coating processing," *Materials Chemistry and Physics*, vol. 100, pp. 275, 2006.
- [60] K. Daoudi, C. S. Sandu, V. S. Teodorescu, C. Ghica, B. Canut, M. G. Blanchin, J. A. Roger, M. Oueslati, and B. Bessais, "Rapid thermal annealing procedure for densification of sol-gel indium tin oxide thin films," *Crystal Engineering*, vol. 5, pp. 187, 2002.

- [61] K. Wasa and S. Haber, *Handbook of Sputter Deposition Technology: Principle, Technology and Applications*: William Andrew, 1992.
- [62] N. Miyata and H. Kitahata, "Preparation and properties of antimony-doped tin oxide films deposited by R.F. reactive sputtering," *Thin Solid Films*, vol. 125, pp. 33, 1985.
- [63] K. Suzuki and M. Mizuhashi, "Structural, electrical and optical properties of r.f.-magnetron-sputtered SnO₂:Sb film," *Thin Solid Films*, vol. 97, pp. 119, 1982.
- [64] B. Stjerna, "Optical and electrical properties of radio frequency sputtered tin oxide films doped with oxygen vacancies, F, Sb or Mo," *Journal of Applied Physics*, vol. 76, pp. 3797-3817, 1994.
- [65] Keeling & Walker Ltd, 2008, www.keelingwalker.co.uk, 27th April 2008.
- [66] C. Terrier, J.P. Chatelon, J.A. Roger, "Electrical and optical properties of Sb:SnO₂ thin films obtained by the sol-gel method," *Thin Solid Films*, vol. 295, pp. 95-100, 1997.
- [67] J. B. Mooney and S. B. Radding, "Spray Pyrolysis Processing," *Annual Review of Materials Science*, vol. 12, pp. 81-101, 1982.
- [68] A. Sherman, *Chemical Vapor Deposition for Microelectronics: Principles, Technology & Applications*, William Andrew, 1987.
- [69] Keun-Soo Kim, Seog-Young. Yoon, Won-Jae. Lee, and Kwang Ho Kim, "Surface morphologies and electrical properties of antimony-doped tin oxide films deposited by plasma-enhanced chemical vapor deposition," *Surface and Coatings Technology*, vol. 138, pp. 229, 2001.
- [70] F. R. S Rayleigh, "On the instability of jets," *Proc. London Math. Soc.*, vol. 10 pp. 4-13, 1878.

- [71] R. Elmqvist, "Measuring instrument of the recording type", US Patent 2566443, 1951.
- [72] R. G. Sweet, "High Frequency recording with electrostatically deflected ink-jets," *Rev. Sci, Instrum.*, vol. 36, pp. 131, 1965.
- [73] J. Heinzl and C. H. Hertz, "Ink-jet printing," *Adv. Electronics and Electron Physics*, vol. 65, pp. 91, 1985.
- [74] L. Kuhn and A. Myers, Ink-jet printing, *Scientific American*, vol. 240, pp. 162-178, 1979.
- [75] S. L. Zoltan, (Celvite Corp.), "Pulse droplet ejection system," US Patent 3683212, 1974.
- [76] E. L. Kyser and S. B. Sears (Silonics Inc), "Method and apparatus for recording with writing fluids and drop projection means therefore," US Patent 3946398, 1976.
- [77] PTL Limited, 2008, "www.pattech.com," 27th April 2008.
- [78] The Society for Imaging Science and Technology, 2008, http://www.imaging.org/resources/web_tutorials/inkjet.cfm, 27th April 2008.
- [79] Gregory P. Crawford, "*Flexible Flat Panel Displays*," John Wiley & Sons, 2005.
- [80] DuPont, 2008, http://www2.dupont.com/Automotive/en_US/products_services/teijinFilms/teonex.html, 27th April 2008.
- [81] C. S. Sandu, V. S. Teodorescu, C. Ghica, P. Hoffmann, T. Bret, A. Brioude, M. G. Blanchin, J. A. Roger, B. Canut, and M. Croitoru, "Excimer Laser Crystallization of SnO₂:Sb Sol-Gel Films," *Journal of Sol-Gel Science and Technology*, vol. 28, pp. 227, 2003.

- [82] William Steen, "*Laser Material Processing*," Springer-Verlag London Ltd; 3rd Rev. edition, Oct 2003.
- [83] John Ion, "*Laser Processing of Engineering Materials: Principles, Procedure and Industrial Application*," Butterworth-Heinemann, 2006.
- [84] M. Stehle, "Excimer laser treatment for large surface," *Journal of Non-Crystalline Solids*, vol. 218, pp. 218, 1997.
- [85] Jacques Perriere, Eric Millon, Eric Fogarassy, "*Recent advances in the laser processing of materials*," Elsevier, 2006.
- [86] L. Fedorenko, A. Medvid', M. Yusupov, V. Yukhimchuck, S. Krylyuk, A. Evtukh, "Nanostructures on SiC surface created by laser microablation," *Applied Surface Science*, vol 254, pp. 2031-2036, 2008.
- [87] T. Nagase, T. Ooie, and J. Sakakibara, "A novel approach to prepare zinc oxide films: excimer laser irradiation of sol-gel derived precursor films," *Thin Solid Films*, vol. 357, pp. 151, 1999.
- [88] W. Chung, M. O. Thompson, P. Wickboldt, D. Toet, and P. G. Carey, "Room temperature indium tin oxide by XeCl excimer laser annealing for flexible display," *Thin Solid Films*, vol. 460, pp. 291, 2004.
- [89] Martin Allmen & Andreas Blatter, "*Laser-Beam Interactions with Materials Physical Principles and Applications*," 2nd ed., Springer, 1994.
- [90] H. H. Afify, R. S. Momtaz, W. A. Badawy, and S. A. Nasser, "Some physical properties of fluorine-doped SnO₂ films prepared by spray pyrolysis," *Journal of Materials Science: Materials in Electronics*, vol. 2, pp. 40, 1991.
- [91] V. Casey and M. I. Stephenson, "A study of undoped and molybdenum doped, polycrystalline, tin oxide thin films produced by a simple reactive

- evaporation technique," *Journal of Physics D: Applied Physics*, vol. 23, pp. 1212-1215, 1990.
- [92] ShinTson Wu, "*Introduction to Flat Panel Displays*," John Wiley & Sons, 2008.
- [93] Klaus Ellmer, Andreas Klein, Bernd Rech, "*Transparent Conductive Zinc Oxide: Basics and Applications in Thin Film Solar Cells*," Springer-Verlag Berlin and Heidelberg GmbH & Co., 2008

3. Experimental Procedures

3.1 Processing Technologies

3.1.1 Laser Processing System

The laser processing of transparent conductors during this project has been carried out using a Krypton Fluoride (KrF) laser. Specifically, a LPX300i from Lambda Physik, emitting at 248nm with a maximum energy density of approximately $1.5\text{J}\cdot\text{cm}^{-2}$ and pulse duration of 20ns. It is a gas laser, meaning that its lasing medium is a gas mixture. The laser is housed in a class 1000 clean room environment in a laser controlled area with the lasing gases being supplied by individual gas cylinders. The set-up of the experimental equipment is shown in Figure 3-1.

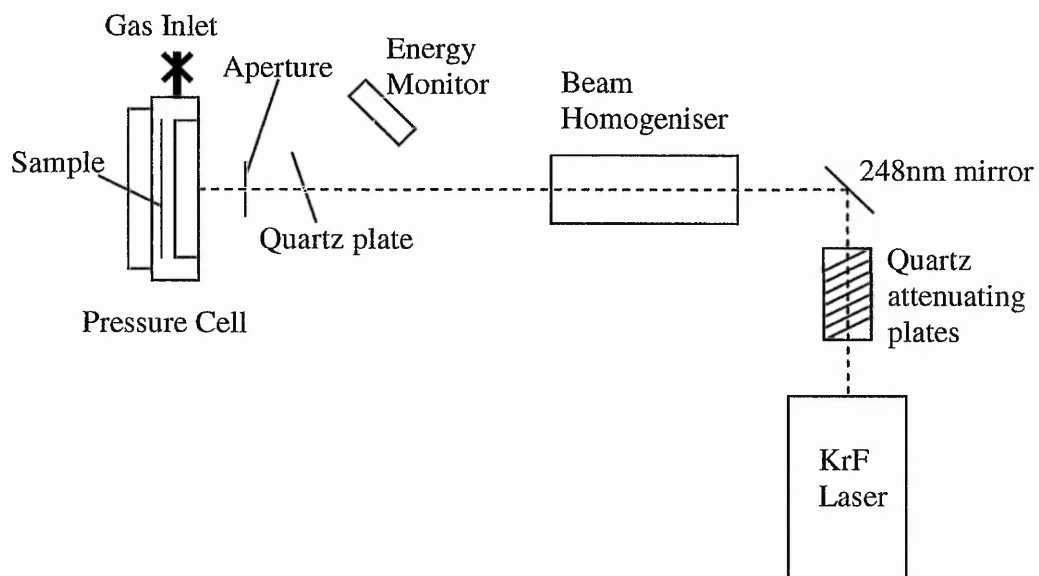


Figure 3-1: Laser processing experimental equipment

The laser beam is reflected down the table by a 248nm mirror. It enters the homogeniser, which takes the raw, non-uniform beam, expands it and using an 8x8 array of lenslets, splits it and recombines it to create a uniform 10x10mm square

beam. This is focussed to a point 1m from a condensing lens within the homogeniser onto the pressure cell. The condensing lens can be replaced by a series of condensing lenses to create a range of beam sizes depending upon application and energy density required. The pressure cell, with its thick quartz window, houses the sample and enables processing at pressure and various atmospheres. A square aperture is used to remove *beam satellites* that are a product of the homogeniser optics. Inherently, the laser energy will fluctuate so the laser energy is monitored using a single quartz plate to reflect a small (approximately 8%) portion of the incident beam. The reflected beam is measured with an energy monitor and has been calibrated so that the energy incident upon the sample can be calculated from this measurement. The calibration chart is shown in Figure 3-2.

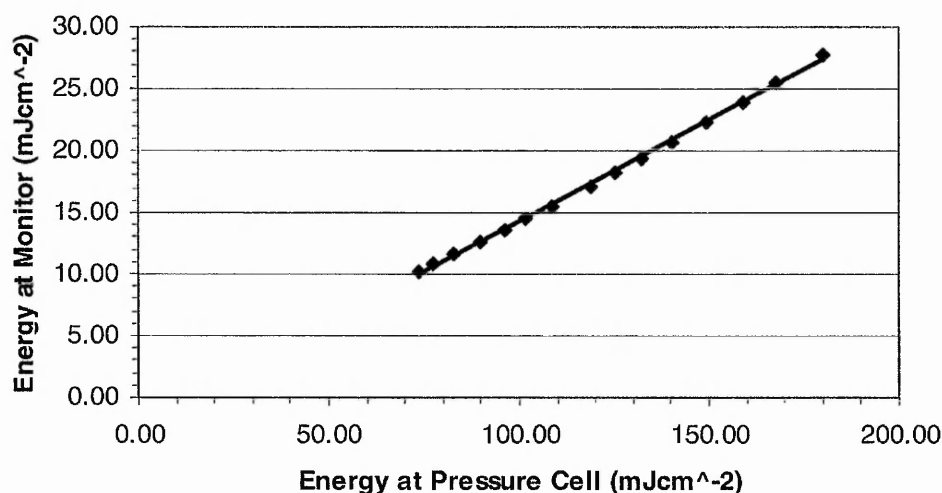


Figure 3-2: Calibration chart for online monitoring of laser energy at sample

The energy density of the beam can be roughly controlled by varying the high power value of the laser. Further fine adjustments are made using a set of quartz plates positioned in the beam path next to the laser aperture. For the lowest energy density

values, a centred variable aperture is placed in the raw beam to reduce its dimensions and therefore energy density.

The laser parameters varied for the purposes of this study were laser fluence (energy density) Jcm^{-2} and number of pulses.

3.1.1.1 Thermal model

It is theoretically possible to determine the heating effect of the laser with knowledge of some fundamental characteristics of the material being processed. A thermal model has been devised by the University Louis Pasteur (Strasbourg, France) together with the CNRS (French National Centre for Scientific Research) to determine the temperature profile in one-dimension immediately following laser processing. Further details of the thermal model can be found in the doctoral thesis by Emmanuel Antoine Mastio[1]. Analysis using this model was carried out on the ATO films and the results can be found in Section 5.4.

3.1.2 Sputtering System

Thin films of ATO were sputter deposited as a comparison to the inkjet printed samples. Sputter deposition is a well established method of film deposition and as such makes a useful comparator to the inkjet printed films.

The films were fabricated using a RF Magnetron sputtering chamber. Sputtering is a popular method of deposition, in particular where the quality of the film is important. Films produced by sputtering can be controlled to high purity, good adhesion strength, and good homogeneity[2]. The sputtering process works by creating a gas plasma (in this case using an oxygen/argon mix) by applying a voltage

between a cathode and an anode. The cathode tends to be the target holder, while the anode is usually the substrate holder. The cathode contains a target of the material to be deposited, in this case, $\text{SnO}_2\text{:Sb}$. The ions impact upon the target causing material particles to be ejected, these are then diffused away depositing a thin film layer onto the substrate. Radio Frequency (RF, as opposed to DC) sputtering requires a high frequency generator (13.56MHz) to be connected between the cathode and anode. Furthermore, to obtain faster deposition at lower deposition rates, magnetically enhanced gas discharge (magnetron sputtering) is employed. A schematic of the RF magnetron sputtering system used during this project is shown in Figure 3-3.

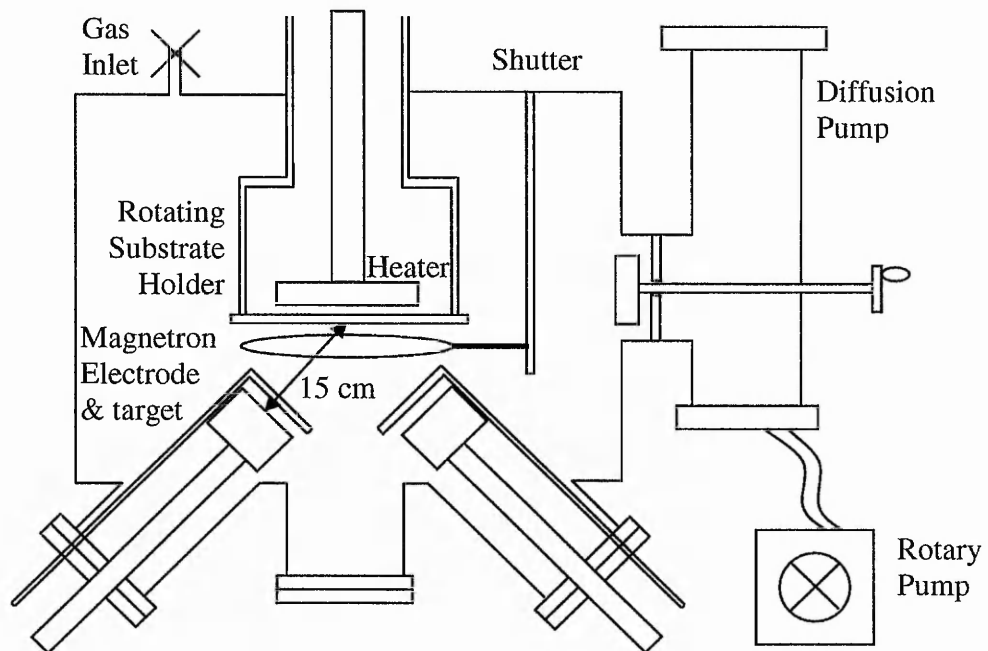


Figure 3-3: RF Magnetron Sputtering System

All of the sputter deposited thin film were grown using this system. A high vacuum was obtained using an oil diffusion pump backed up by a rotary pump. A typical chamber pressure prior to the argon being released into the chamber was 1.2×10^{-7}

mbar. The substrate layer was loaded using a load lock and arm. Once the substrate layer had been loaded onto the arm, the load lock was roughed out (to $\sim 1 \times 10^{-2}$) before the arm was opened up to the main chamber. The substrate layer was loaded onto the substrate holder above which a heater is suspended. The heater was lowered to just above the substrate layer and the substrate holder switched on to rotate.

3.1.3 Sputtering Targets

Two targets were used for the depositions during this project. A pressed powder target made from a powder material supplied by project partners Keeling & Walker Ltd composed of SnO_2 doped with 6wt% Sb_2O_3 , and a commercially produced hot pressed solid target from Testbourne, also composed of SnO_2 doped with 6wt% Sb_2O_3 . All targets used were 3" diameter, 5mm thick discs suitable for mounting into the electrodes.

3.1.3.1 Powder Targets

Powder targets are cheaper and easier to manufacture when compared to solid targets. Unlike their solid counterparts, they do not require any heating in order to bond. However, the low density nature of the powder targets, means that they sputter at a much faster rate than the solid targets and are prone to sputtering through, potentially causing damage to the target electrode. This is also problematic because each time the target sputters through it must be replaced by a new one. Since the whole deposition process needs to be carried out in a vacuum, this proves to be very time consuming. The powder target is made using a hydraulic press system specifically designed for pressing powders. A schematic of the system is shown in Figure 3-4.

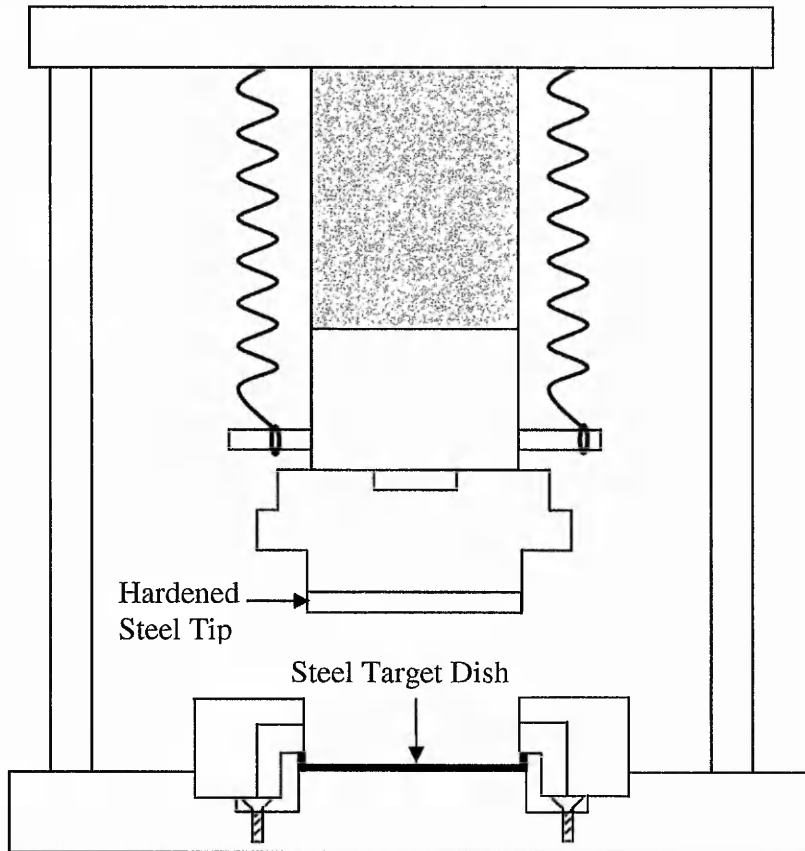


Figure 3-4: Powder Target Press

The powder is placed into the steel target dish and compressed initially by hand using a steel rule, this is repeated until the dish is completely full. It is important that the powder is evenly distributed and smoothed over since any imperfections are likely to cause “hotspots”. These hotspots cause the target to sputter through, usually within minutes, rendering the target useless. The excess powder is removed and the punch moved into position over the dish. A hydraulic pump is used to manoeuvre the punch in place, which is also gently rotated to smooth out any imperfections. The powder was compressed to a pressure of 300bar. The pressure was maintained for 10 minutes, with further pumping when necessary. After this time the hydraulic press was dismantled and the powder target carefully removed.

Once in place in the chamber and the chamber has been pumped to a sufficiently low pressure, each of the targets are individually pre-sputtered to remove the top layer of the target contaminated with oxygen. For solid targets this was typically carried out for 2-3 hours. For a powder target, it was typically 1 hour since its low density nature meant material from the target was removed at a much faster rate.

3.1.3.2 Sputtering parameters

An experimental programme was devised to determine the optimum sputter parameters for use with the commercial solid target. The programme (a response surface 3 level factorial quadratic design) and results from this are detailed in Section 4.2.4 of Chapter 4.

3.1.4 Thermal Processing

The substrate for an electronic display is typically some type of glass and as such it is a suitable material to undergo a thermal annealing process. Annealing typically takes place over 1 hour which for high volume manufacturing is far from ideal. All the thermal annealing for this project was carried out in a Carbolite CWF 1200 furnace. The samples were ramped up in temperature to around 440°C before being slowly cooled. The exact heating and cooling ramp used is shown in the Appendix A.

3.2 Metrology Systems

3.2.1 Optical Profiler

The optical profiler used for this research was a WYKO NT1100 surface profiler. It was used to image the surface of the inkjet printed ATO enabling surface roughness and step height measurement to be made. It has two modes of operation: Phase-

Shifting Interferometry (PSI) and Vertical Scanning Interferometry (VSI). PSI mode was used for surface images and VSI was used for step height measurements to accurately determine film thickness.

3.2.1.1 Phase-Shifting Interferometry

For Phase-Shifting Interferometry (PSI), the system produces a white light which is filtered (centred at 632nm) and then passed through a beam splitter. Half of the beam travels to the sample surface and half to a reference surface. The reflected beams from the sample surface and the reference surface are then recombined and interference fringes can be observed. When the measurement is being taken, the reference surface is moved a known, small quantity to create a phase shift between the two reflected beams. This shifting is repeated to different phase shifts and the intensity of the resultant interference fringes each time is recorded. Providing the fringe pattern is sampled enough, this method is accurate for resolving heights where the surface height variation between two adjacent pixels is less than $\lambda/4$, where λ is the wavelength of the incident light. A maximum range of 160nm can be measured in PSI mode to a resolution, with a single measurement, of 3Å.

3.2.1.2 Vertical-Scanning Interferometry

Vertical-Scanning Interferometry (VSI) is used to measure steps and rough surfaces where height changes of up to several millimetres are present. A white light source is passed through a neutral density filter preserving its short coherence length. As with the PSI mode, the beam is split and reflected off the sample surface and reference surface. The two reflected beams are recombined to create fringes.

In VSI mode the interferometric objective moves vertically, sampling the interference fringes at precise intervals. For a single data point, the intensity of the fringes is greatest at the point of focus since the white light source has a short coherence length and they are therefore only present in a narrow depth of field. Figure 3-5 shows the intensity with respect to focus and shows how its maximum is at the point of focus.

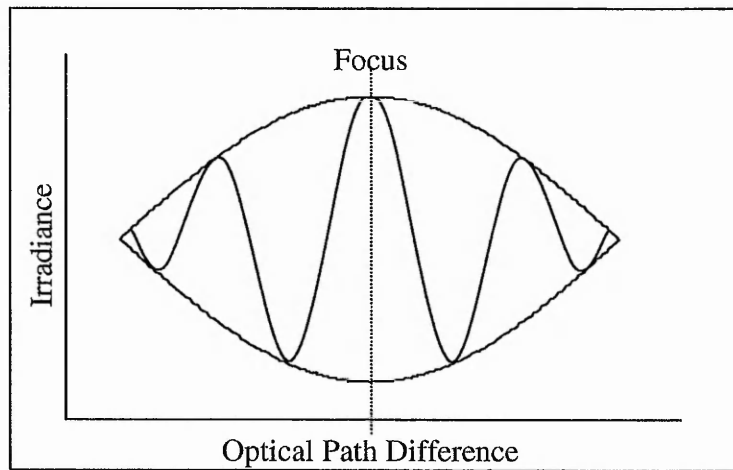


Figure 3-5: Fringe intensity variation with focus of the optical profiler in VSI mode

The vertical position corresponding to the peak intensity for each sample point is recorded and the three dimensional map is created. In VSI mode, vertical ranges of up to 2mm can be measured, for a single measurement, with a resolution of 3nm.

3.2.2 Filmetrics

A Filmetrics F20 spectrometer was used to measure the transmission spectra of the ATO thin film layers. The spectrometer measured transmission between 400-1000nm and used a tungsten-halogen bulb to generate the white light. The light was delivered to and collected from the sample by a fibre optic bundle, before being passed into a diffraction grating. The diffraction grating split the light into

approximately 512 composite wavelengths, the intensity of which was measured using a linear photodiode array. The integration of the current generated by the light incident on the pixels was used to determine transmission.

The lamp was switched on 10 minutes prior to use to allow it to warm up. The spectrometer was then set to transmission mode and a baseline measurement was taken with no medium in place. The reference material was quoted as air with a refractive index of 1. The baseline measurement was verified by performing a data acquisition with no medium in place (with an expected outcome of 1 across the spectrum). Measurements of the transmission spectra of the substrate were then carried out, followed by the transmission spectra of the area of interest of the ATO thin film. Typically, unless otherwise stated, three measurements were taken for a given area and an average spectral response is reported. The substrate transmission losses were added to the ATO transmission spectra to obtain a transmission of the thin film of ATO.

3.2.3 SEM

A Jeol JSM 840A scanning electron microscope (SEM) was used to inspect the surface and edge profiles of the inkjet printed ATO. An excellent introduction to the subject can be found in Scanning Electron Microscopy and X-ray Microanalysis[3].

An SEM consists of an electron gun in a vacuum column. Electrons are emitted from the gun and fired through a series of magnetic lenses to create a very fine spot. The sample is placed at the bottom of the column and a set of scanning coils deflect the electron beam to scan across the sample. The sample must be conductive otherwise

charge builds up and no image can be taken. Samples are therefore often coated with a thin layer of gold (a few nm) in a sputtering system prior to SEM. As the electron beam scans across the sample, secondary electrons are knocked loose from the surface into a detector. The final image is built up by counting and amplifying the electrons incident upon the detector from each spot.

3.2.4 TEM

Transmission Electron Microscopy was used to examine the cross sectional morphology of the as-deposited and laser processed thin films of ATO. Unless otherwise stated, the TEM analysis was carried out on a Jeol JEM 2010A on samples which had been deposited onto flexible substrates and which had been prepared in resin and subsequently microtomed to thickness of 10-100nm. TEMs are particularly useful at imaging details at a resolution of 1nm. Further information on the general technique can be found in Transmission Electron Microscopy: A Textbook for Materials Science[4].

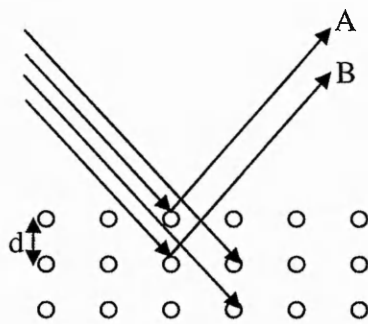
The sample sits on a small copper grid, a few millimetres in diameter. The sample needs to be so thin, as to be transparent to the electron beam. Electrons are accelerated from an electron gun at high voltages of 100-400kV which are imaged on the sample by a condensing lens. An objective lens magnifies the sample by several hundred fold to form an intermediary image which is subsequently further enlarged by a projection lens onto a fluorescent screen where it may be viewed and/or captured. Typically, the image taken by the TEM will be tens of thousands of times magnified. Such high resolution is possible because the wavelength associated

with an electron is much smaller than that associated with light, for example the wavelength associated with a 200kV electron is approximately 0.0028nm[5].

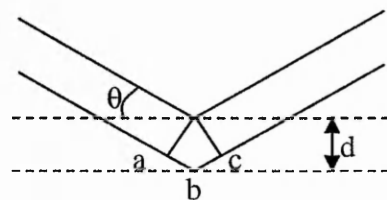
3.2.5 X-ray Diffraction

X-ray diffraction is a useful tool for determining the crystalline structure of a material. It was observed that crystals only reflected x-rays at certain angles and in 1912 when WL Bragg proposed what is now commonly known as the Bragg law. For an informative text on the practical application of x-ray diffraction 'X-ray Diffraction: A Practical Approach' is recommended[6].

When an x-ray is incident upon a crystal, most of the radiation is scattered and destructively interfere with one each other. However, when certain conditions are met, the x-rays are reflected. Consider the x-rays A and B in Figure 3-6i. If they were to constructively interfere with each other, the x-rays would appear to reflect. This occurs when the path difference between A and B is an exact multiple of the wavelength of the incident radiation and the peaks of the waves are aligned with each other. Figure 3-6ii shows the geometry of this. The extra distance travelled by B is the path a-b-c.



i) X-ray interaction with crystalline material



ii) Geometry satisfying the Bragg condition

Figure 3-6: Satisfying the Bragg condition for x-ray diffraction

For the Bragg condition to be satisfied the distance $a-b-c = n\lambda$, where $n =$ an integer.

$a-b = b-c$, and $ab = d\sin\theta$, so $a-b-c=2d\sin\theta$.

Once a peak has been detected, it is possible to determine the corresponding plane spacing which will correspond to well documented planes of a particular material.

The angle between the transmitted and Bragg diffracted rays is always 2θ , as such x-ray diffraction results are often quoted in 2θ .

Taller peaks indicate the presence of a larger number of grains of material of a particular planar orientation compared to shorter peaks. Narrow peaks indicate the presence of larger grains. Therefore a sample of finely ground material will give a broader peak compared to the same sample more coarsely ground.

X-ray diffraction was used to determine the crystalline structure of the powder, as-deposited inkjet printed $\text{SnO}_2\text{:Sb}$, thermally annealed $\text{SnO}_2\text{:Sb}$ and laser processed $\text{SnO}_2\text{:Sb}$. The XRD system used for the above was a Philips PW 1049/10 XRD system, using a $\text{CrK}\alpha$ Source ($\lambda = 2.22897 \text{ \AA}$). Experimental conditions were 40kV, 25mA, with diffraction intensity examined over an angular range of $2\theta = 5^\circ - 65^\circ$, incremented in 0.01° steps. All the peaks in this body of research were identified from the Powder Diffraction File. Education Indexes: Inorganic and organic phases[7].

Further XRD was carried out on RF magnetron sputtered films of $\text{SnO}_2\text{:Sb}$ using a PANalytical X'Pert PRO diffraction system with $\text{CuK}\alpha 1$ source (wavelength =

1.54056Å). The experimental conditions for these samples were 45kV, 40mA, with diffraction intensity examined over an angular range of $2\theta = 20^\circ - 80^\circ$, incremented in 0.004° steps.

3.2.5.1 *The Debye-Scherrer Equation*

The Debye-Scherrer equation can be used to estimate the particle size of the material from the position and width of its diffraction peaks[8].

The size, D, of the particle is given by:

$$D = \frac{0.9\lambda}{\beta \cos \theta} \quad \text{Eq 3-1}$$

Where:

λ = wavelength of incident radiation ($\lambda_{\text{Cu}} = 1.54\text{\AA}$, $\lambda_{\text{Cr}} = 2.23\text{\AA}$)

β = FWHM in radians (Full Width at Half Max height of peak)

θ = The position of the max diffraction/2

The Debye-Scherrer equation has been used throughout chapter 5 to corroborate the results from the SEM and TEM .

3.3 Electrical Characteristics

3.3.1 **Four Point Probe**

The four-point probe is a standard technique for measuring the sheet resistance of a flat conductive surface where sheet resistance is measured in Ohms per square (Ω/sq) and the size of the square is independent[9]. The system used for this project consisted of a linear-four-point probe, a voltmeter and a current source. The four equidistant probes are lowered onto the film and a current is passed through the two outer probes. As a result of the current, a voltage is built up between the inner probes

which is measured by the voltmeter. Figure 3-7 shows a schematic of the probe system used.

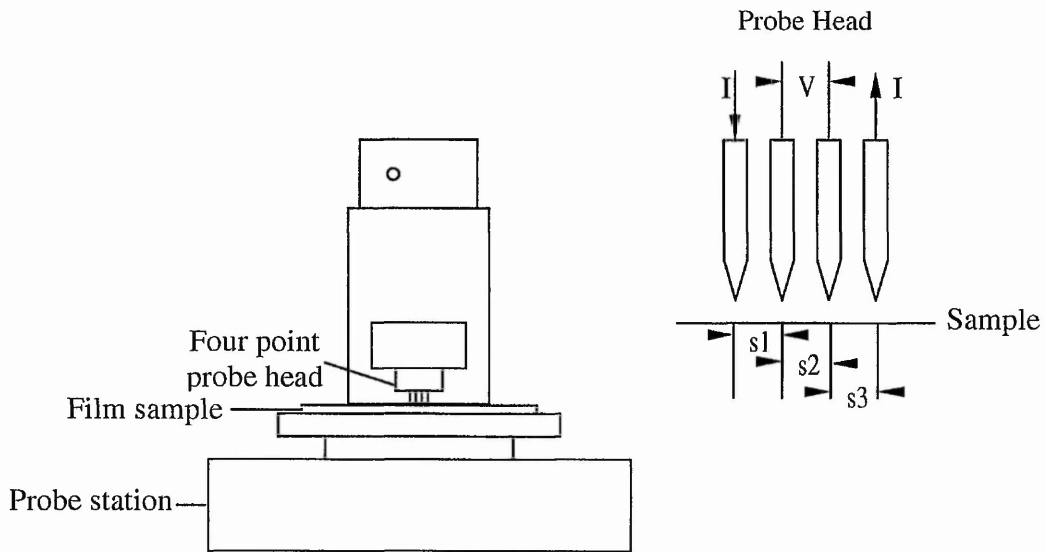


Figure 3-7: Schematic of four point probe

The sheet resistance is determined by the following:

The resistivity of a semi-infinite volume measured using the four point probe is given by:

$$\rho = \frac{v}{I} \frac{2\pi}{1/s1 + 1/s2 - 1/(s1 + s2) - 1/(s2 - s3)} \quad \text{Eq 3-2}$$

where ρ = resistivity (Ωcm), v = measured voltage (V), I = current (A) from the current source and $s1$, $s2$ and $s3$ are the probe point spacings.

So where $s1 = s2 = s3 = s$ then:

$$\rho = \frac{V}{I} 2\pi s \quad \text{Eq 3-3}$$

For an infinitely thin film on an insulating substrate, this equation becomes:

$$\rho = \frac{V}{I} \frac{\pi t}{\ln 2} \quad \text{Eq 3-4}$$

where t = thickness (nm)

$$\text{or since sheet resistance (Rs)} = \frac{\rho}{t} \quad \text{Eq 3-5}$$

$$R_s = 4.53V/I \quad \text{Eq 3-6}$$

For each measurement, a range of currents were used to ensure accuracy. The exact current values varied depending upon the sheet resistance of the sample, higher sheet resistance values used lower current values (typically: 0.2, 0.4, 0.6, 0.8 and 1 μ A). Selected current values were kept low to minimise heating effects and to prevent voltage limiting. The current source was limited for some higher sheet resistance values – the battery powered current source generated a voltage to give the desired current through the sample, if the sheet resistance was too high, the voltage required to generate the desired current was too high and therefore not possible.

References

- [1] Emmanuel Antoine Mastio, "*Materials engineering for high efficiency thin film electroluminescent devices*," Doctoral Thesis, Nottingham Trent University, 1999.
- [2] H. L. Hartnagel, A. L. Dawar, A.K. Jain, C. Jagadish, "*Semiconducting Transparent Thin Films*," Institute of Physics Publishing, 1995.
- [3] Joseph I. Goldstein, Dale E. Newbury, D.C. Joy, Charles E. Lyman, Patrick Echlin, Eric Lifshin, Linda C. Sawyer, J.R. Michael, "*Scanning Electron Microscopy and X-ray Microanalysis*," Kluwer Academic / Plenum Publishers, 3rd Rev Ed edition, 2002.
- [4] David B. Williams, C. Barry Carter, "*Transmission Electron Microscopy: A Textbook for Materials Science*," Kluwer Academic / Plenum Publishers, 1996.
- [5] W. R. Runyan and T. J. Shaffner, "*Semiconductor Measurements & Instrumentation*," McGraw-Hill Professional, 2nd edition, 1998.
- [6] C. Suryanarayana, M.Grant Norton, "*X-ray Diffraction: A Practical Approach*," Kluwer Academic / Plenum Publishers, 1998.
- [7] Powder Diffraction File. Education Indexes: Inorganic and organic phases. International Centre for Diffraction Data, 1996.
- [8] S. Ted Oyama, "*The Chemistry of Transition Metal Carbides and Nitrides*," Kluwer Academic Publishers, 1996
- [9] F. M. Smits, "Measurement of Sheet Resistivities with the Four-Point Probe," *Bell System Technical Journal*, pp. 711, 1958.

4. Electrical and Optical Properties

4.1 Thermal Annealing

Thermal annealing is a well documented method of improving the electrical characteristics of transparent conducting oxide layers[1-3]. Unless otherwise stated, samples discussed in the following chapter were annealed in a Carbolite CWF 12/5 furnace using the thermal anneal ramp profile shown in Appendix A.

4.1.1 Thermal annealing in air of inkjet printed SnO₂:Sb on soda lime glass

An initial investigation was carried out into the effects of thermal annealing on the sheet resistance of printed ATO layers. The initial investigation focussed on a batch of 30 samples which had been inkjet printed onto soda lime glass. The batch had been prepared with three sets of starting powder; all of which had been manufactured in the same way by Keeling & Walker. The precise method of manufacture is proprietary to Keeling & Walker Ltd, however a summary of the process follows: The ink was based on an electrically conductive ATO powder produced from separate chemical precursors of antimony oxide and tin oxide. These precursors were precipitated and chemically combined, pH adjusted and washed to remove impurities. The resulting powder was dried and calcined to form the electrically conductive ATO material. The resultant material, comprising aggregates of nano-sized primary ATO particles, was milled to an agglomerate size of less than 100nm. This was formed into an aqueous dispersion, which was subsequently formulated for ink jet printing. The formulation has been designed to provide stable jetting with good wetting characteristics on a variety of substrates and with minimal Marangoni effect (coffee staining).

Ten samples from each set were printed and the samples were labelled A, B and C. Each sample was a five layer printed film, allowed to dry between successive layers. Half of each of the A, B and C batches were thermally annealed at 400°C for 1 hour in between layers. Table 4-1 shows a summary of the samples used. The printing and annealing process was carried out by PTL Ltd.

Batch A 5 layers on glass	Annealed 400°C 1hr each layer	HA1
		HA2
		HA3
		HA4
		HA5
	Non-Annealed	A1
		A2
		A3
		A4
		A5
Batch B 5 Layers on glass	Annealed 400°C 1hr each layer	HB1
		HB2
		HB3
		HB4
		HB5
	Non-Annealed	B1
		B2
		B3
		B4
		B5
Batch C 5 Layers on glass	Annealed 400°C 1hr each layer	HC1
		HC2
		HC3
		HC4
		HC5
	Non-Annealed	C1
		C2
		C3
		C4
		C5

Table 4-1: Summary of samples used for investigation into consistency of Rs results with different batches of material

The sheet resistance of each sample was measured using the four point probe set-up.

The results are shown in the two graphs in Figure 4-1 and 4-2.

Batch A was consistent prior to annealing with all R_s values falling into the range $1\text{M}\Omega/\text{sq} \pm 10\%$. Post annealing values dropped to $29\text{k}\Omega/\text{sq} \pm 15\%$. This was a significant improvement of approximately two orders of magnitude. XRD and subsequent SEM investigations (detailed and discussed in Chapter 5), show no perceivable improvement in crystallinity. Batches B and C show quite a variation in R_s between samples in both the non-annealed and thermally annealed range.

The variation between non-annealed samples could be because of variations in film thickness of the inkjet printed film or it could be caused by more subtle effects such as oxygen adsorption onto the surface of the films[4]. Subsequent work showed that the samples undergo a process of stabilisation once deposited. Taking approximately two weeks from deposition, all samples as-deposited stabilise to approximately $4.5\text{M}\Omega/\text{sq} \pm 10\%$. This could explain the variation in the R_s results shown in Figure 4-1.

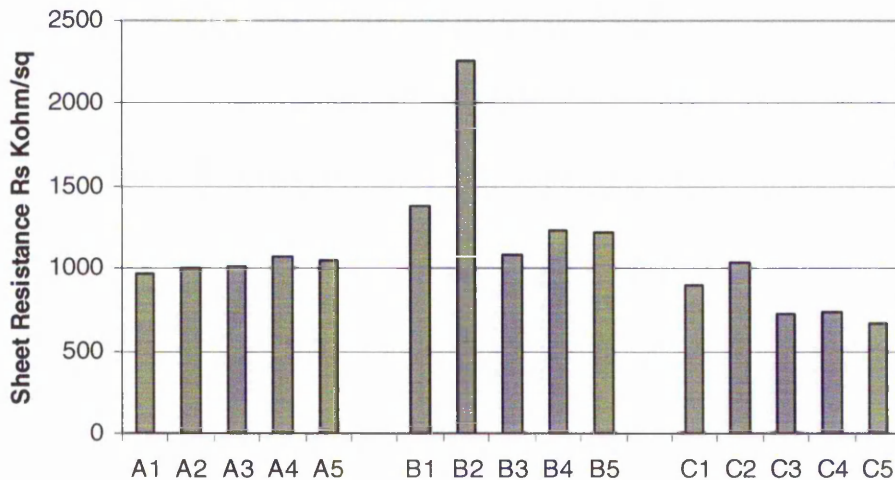


Figure 4-1: Variation in R_s between batches in as-deposited inkjet printed ATO

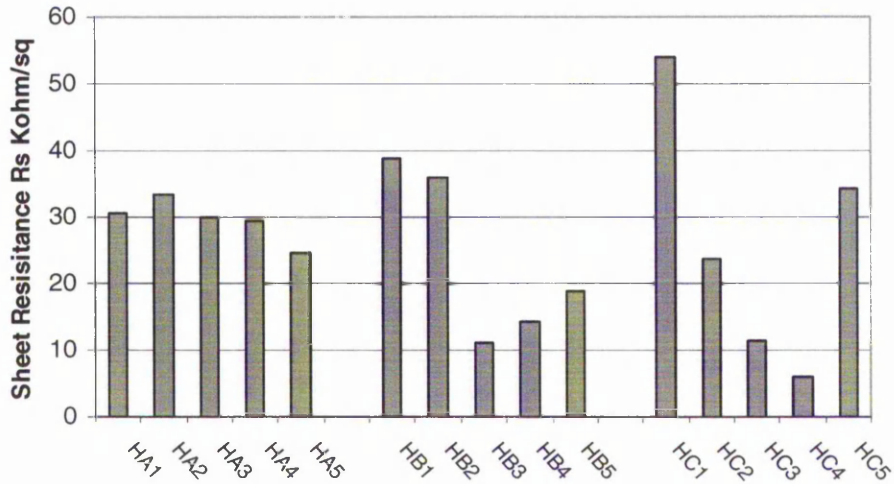


Figure 4-2: Variation in R_s between batches of thermally annealed inkjet printed ATO

The range shown in the thermally annealed C batch between 5 – 55kOhm/sq demonstrates an issue with consistency that is not immediately apparent prior to annealing. It is thought that sodium ion diffusion could have been responsible for the poor consistency following thermal annealing[5]. Initially the variation showed itself as discrepancies between the measurements made at NTU and those made at the project partners, PTL. This was discounted by taking the NTU four point probe to PTL to carry out a direct and immediate comparison. The results demonstrated that R_s values were consistent and a graph of this can be found in the Appendix A.

4.1.1.1 Film Stability

A brief investigation of the stability issue was carried out. Following thermal annealing and laser processing, films left exposed to atmosphere showed an increase in sheet resistance prior to stabilising after, typically, a two-week period. A brief test was carried out by placing a film in a vacuum following laser annealing and monitoring its sheet resistance over a number of days. While there was a small

increase in sheet resistance over time, it was very small in comparison to films left in atmosphere; see Figure 4-3.

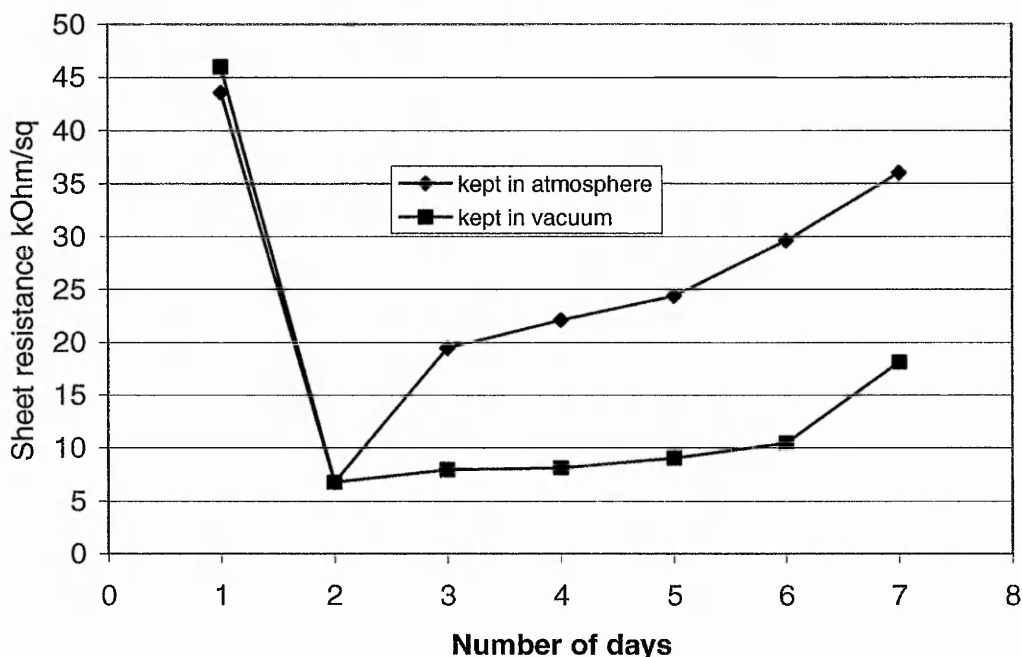


Figure 4-3: Comparison between the change in sheet resistance of inkjet printed SnO₂:Sb left in a vacuum and in atmosphere.

The sample was removed from vacuum for each measurement and this could account for the smaller increase observed in the film kept in a vacuum, however these findings support the idea of oxygen adsorption playing a critical role in the stability of films in atmosphere.

4.1.2 Summary of inkjet printed ATO thermally annealed on soda lime glass

Thermal annealing has been demonstrated to improve the conductivity of inkjet printed ATO on soda lime glass. Typical changes in sheet resistance ranged from 1MOhm/sq as-deposited to 30kOhm/sq following thermal annealing, however stability due to impurity diffusion was an issue. As a result of this investigation, all

further samples were deposited onto borosilicate substrates to minimise this problem.

4.1.3 Thermal annealing in various atmospheres of inkjet printed ATO on borosilicate

As the printing process was refined, samples were printed onto larger borosilicate substrates, approximately 90x70mm, to investigate the consistency of the printed films further. Three samples were deposited and the larger borosilicate substrates allowed the samples to be broken up into quarters. One quarter was kept as a control, one was annealed in atmosphere, one in nitrogen and one in a vacuum. The sample annealed in nitrogen was annealed in the furnace in a crucible with 1.2bar of nitrogen flowing across it. Each of the annealing processes took place over 1 hour at 400°C.

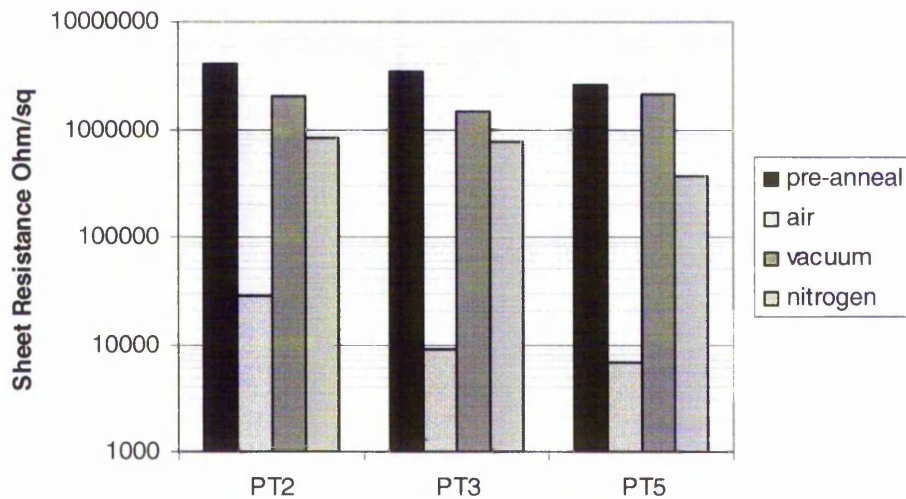


Figure 4-4: Change in R_s with thermal annealing in air, vacuum and nitrogen rich environment

4.1.3.1 Sheet Resistance

The samples were labelled PT2, PT3 and PT5. In all instances of thermal annealing, a decrease in the sheet resistance of the samples was observed, with the greatest decrease occurring with the samples thermally annealed in air. The pre-annealing sheet resistance of the samples measured using the four point probe was about $3\text{M}\Omega/\text{sq}$. The best achieved sheet resistance was $6.8\text{K}\Omega/\text{sq}$ for a sample thermally annealed in air. The samples thermally annealed in nitrogen showed a larger decrease in sheet resistance than the samples annealed in a vacuum. Since the annealing carried out in nitrogen was not an airtight process, the results indicate that the oxygen content of air could be beneficial to the improvement of the conductivity of the film during the thermal anneal process. It has been demonstrated that annealing in an O_2 atmosphere increases carrier concentration, which could therefore account for the decrease in sheet resistance[2].

4.1.3.2 Transmission

The transmission spectrum of the ATO films was measured using the Filmetrics thin film analyser. The results are shown in Figure 4-5, where the effect of the substrate layer has been removed and just the transmission for the ATO film is shown. The fringes observed in the transmission spectra are as a result of interference between incident light and the light reflected by the air-ATO and ATO-substrate interfaces. The change in the fringes in Figure 4-5 possibly indicates a change in thickness, although not necessarily as a result of the processing. Since thickness variation was as much as $\pm 15\%$ (see section 5.2) it is impossible to determine if the change is due to processing.

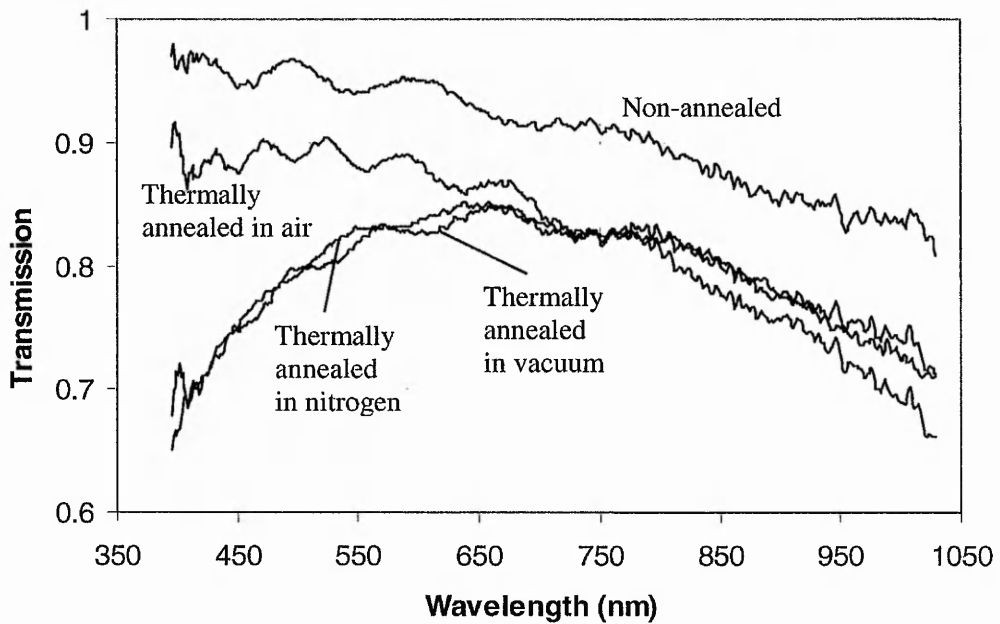


Figure 4-5: Transmission spectra for inkjet printed ATO films; as-deposited and thermally annealed in air, vacuum and nitrogen

The as-deposited films show the best transparency across the wavelength range with a transmission of 94% at 550nm, which steadily decreased to 81% in the short infrared. The film transmission decreases uniformly across the spectrum by approximately 7% for films thermally annealed in air. The reduction in the long visible and near infrared could be an indication of a shift in the plasma wavelength due to an increase in carrier concentration as shown in Figure 2-6[6]. Both the films thermally annealed in nitrogen and in a vacuum showed a considerable reduction in transmission in the long UV and the short-mid visible spectrum with 83% and 82% transmission at 550nm respectively, this could be due to a presence of SnO which has an absorption edge at lower energies than SnO₂[7].

4.1.3.3 Hall Effect

Clover leaf shaped samples were printed and thermally annealed in air to investigate the Hall effect. Contacts were indium soldered to the samples, but no Hall voltage could be measured. A discussion of this is included in the *Discussion* chapter.

4.1.3.4 Summary

Thermal annealing in nitrogen, a vacuum and air reduced the sheet resistance of the inkjet printed ATO on borosilicate, with thermally annealing in air providing up to a 400 fold improvement. The transmission spectra reduced following annealing, with the air annealed samples providing the best results again. Hall effect measurements were unobtainable.

4.1.4 Thermal annealing of SnO₂:Sb on Quartz

To determine the effect of higher temperature annealing, in effect, the gold standard of what may be possible with the inkjet printed material, ATO was dip coated onto quartz substrates (note: during the project, the premises of inkjet partners was destroyed by a gas storage explosion, it was necessary to revert to the use of dip coated samples to continue the project). The dip coating and thermal annealing were carried out at Keeling & Walker Ltd.

Eight samples were produced in two groups, a group of four with one dip coated layer and a second group of four with three dip-coated layers. One sample from each group was thermally annealed at 400°C, a second at 600°C and the third and fourth at 800°C and 1000°C respectively.

4.1.4.1 Sheet Resistance

The R_s of both single dip and three dip coated samples behaved in a similar manner. R_s values fell dramatically with increasing temperature until 800°C, after which R_s was seen to increase. At 800°C the films were showing signs of degradation where ATO was flaking. This increased with the samples annealed at 1000°C, which would account for the increase in sheet resistance above 800°C. The lowest R_s value achieved was 120 Ohm/sq on the three-dip sample thermally annealed at 800°C. The R_s of the one dip coated film at 800°C was 317 Ohm/sq, approximately 3 times that of the 3 dip; as expected with a three fold increase in thickness. Figure 4-6 shows a plot of the change in R_s with increasing temperature.

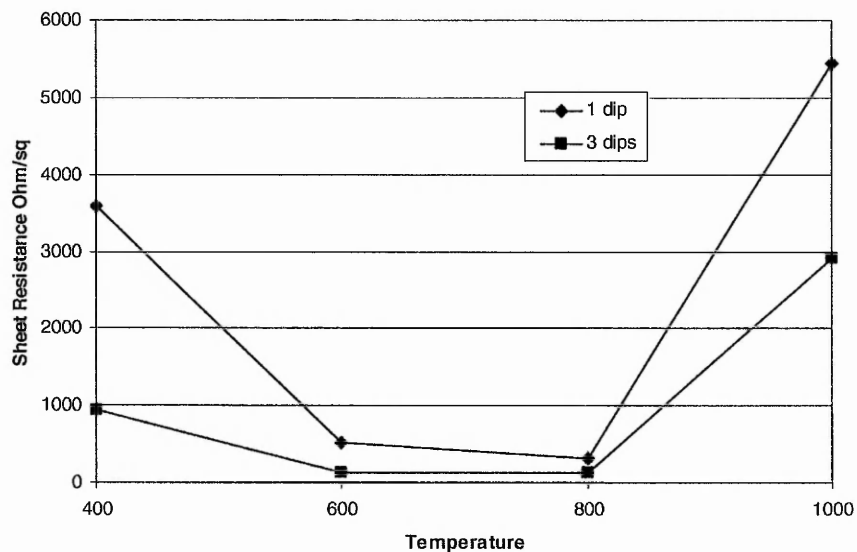


Figure 4-6: Variation in sheet resistance of dip coated ATO on Quartz substrates with temperature of thermal anneal

4.1.4.2 Transmission

The transmission spectrum for each of the 1 dip coated samples was measured with the Filmetrics system and can be seen in Figure 4-7. The thickness of the samples

could not be measured and was unknown since they were dip-coated. The technique previously used to obtain an edge from where to measure the thickness was to remove the film with the laser. However, once thermally annealed, the films became resistant to laser ablation. Since the thickness of the samples was unknown and the thickness directly affects the transmission, it would be inappropriate to comment upon which sample was optically most transparent. However, the increase in transmission in the infrared region indicates a reduction in carrier concentration with increasing annealing temperature; see Figure 2-6 in 2.3.2. This suggests the conductivity is improved by some other means, for example, an increase in mobility. This will be discussed further in the next chapter.

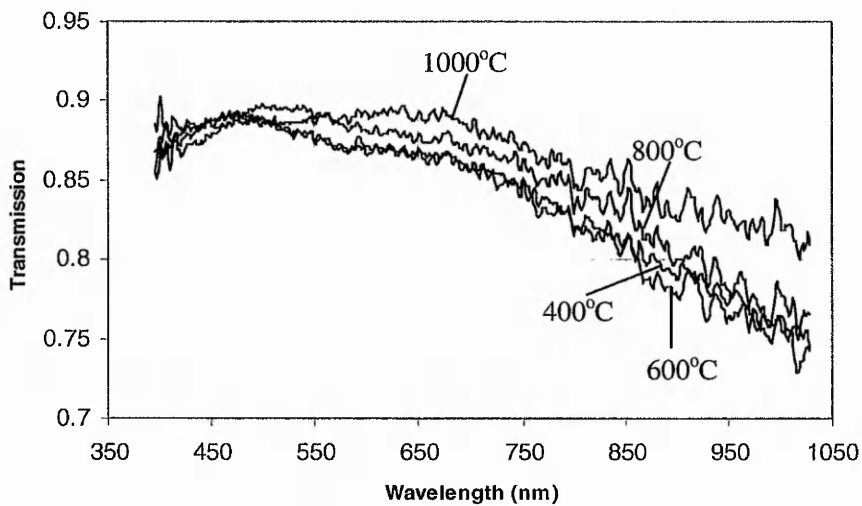


Figure 4-7: Transmission spectra of dip coated ATO on quartz substrates thermally annealed at 400, 600, 800 and 1000°C (thickness unknown)

4.1.4.3 Summary

The sheet resistance of the thermally annealed samples dip-coated onto a quartz substrate decreased with increasing annealing temperature up to 800°C. The sheet resistance increased for temperatures greater than this. The visible transmission

spectra remained constant in terms of shape for each thermal anneal temperature, but was observed to increase in the infrared with increasing anneal temperature, indicating a reduction in carrier concentration.

4.2 Laser Processing

A KrF Excimer laser emitting at 248nm was used to process ATO samples. The raw beam was passed through a homogeniser to create a 10x10mm square beam with a uniform energy profile. The transmission spectrum of as-deposited and laser processed films was measured using the Filmetrics system and the sheet resistance of the films was measured before and after laser processing.

4.2.1 ATO inkjet printed onto borosilicate

Nine samples of inkjet printed ATO were laser processed to determine the effect of the laser processing on the films. Number of pulses and laser fluence were varied as shown in Table 4-2. A five by five array of laser processed areas was created on each sample to give five repeat areas for each annealing condition on each sample and to negate any edge effects. All samples were processed in air at atmospheric pressure. The highest fluence was limited to 70mJcm^{-2} to avoid damage to the film.

Beam Energy	N ^o of Pulses		
	1-10	10-100	100-1000
20mJ/cm ²	Sample 1	Sample 2	Sample 3
40mJ/cm ²	Sample 4	Sample 5	Sample 6
70mJ/cm ²	Sample 7	Sample 8	Sample 9

Table 4-2: Laser processing parameters of ATO inkjet printed onto borosilicate

4.2.1.1 Sheet Resistance

The sheet resistance of each processed area was measured using the four-point probe. The results demonstrated that all laser-processed areas exhibited a decrease in sheet resistance compared with pre-processed values of $4\text{M}\Omega/\text{sq}$. The lowest value of sheet resistance occurred in the areas processed with 1000 pulses. The greatest change in sheet resistance occurred within the first 1-3 pulses with a general decrease to 1000 pulses. Between 10 and 100 pulses, there appears to be little effect. The further increase in number of pulses above 100 shows a continuing decrease in R_s to 1000 pulses. Figure 4-8 shows the change in R_s due to laser processing of a sample with a starting sheet resistance of $4\text{M}\Omega/\text{sq}$.

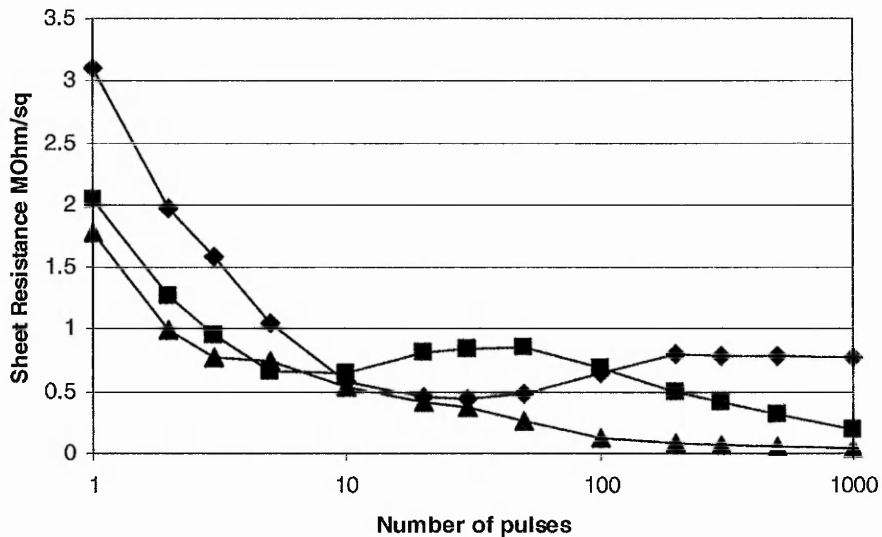


Figure 4-8: The variation in sheet resistance post laser processing as a function of number of pulses and laser energy. ♦ = $20\text{mJ}/\text{cm}^2$, ■ = $40\text{mJ}/\text{cm}^2$, and ▲ = $70\text{mJ}/\text{cm}^2$.

X-ray Diffraction on laser processed samples indicates an increase in crystallinity with laser processing which increases with increasing numbers of laser pulses. This

could explain the observed decrease in sheet resistance and will be discussed fully in Chapter 6.

4.2.1.2 Transmission

The transmission spectra of the samples laser processed with 40mJcm^{-2} were measured and are shown in Figure 4-9. Once again, fringing is observable with a phase shift apparent suggesting differing thickness, although whether due to processing or thickness variation inherent to the inkjet printing deposition method it is not possible to say. The results show a steady reduction in transmission from as-deposited to 1000 pulses. The decrease in the infrared identifies a shift in the plasma wavelength towards the visible and therefore indicates an increase in carrier concentration with increased number of pulses. At 550nm, the transmission for as-deposited, 10 pulses, 100 pulses and 1000 pulses are 93%, 90%, 90% and 86% respectively.

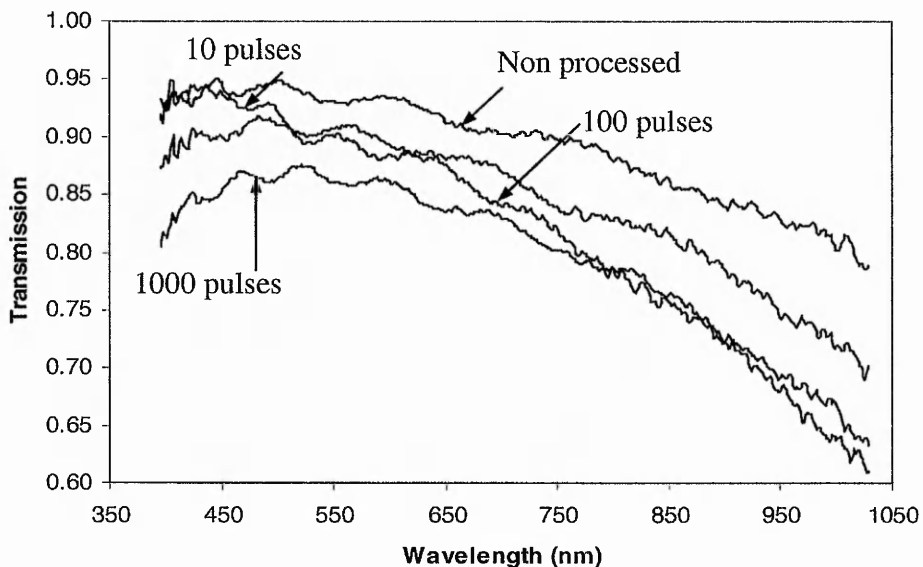


Figure 4-9: Transmission spectra for inkjet printed ATO on borosilicate glass laser processed at 40mJ/cm^2 with 10, 100 and 1000 pulses

4.2.2 Laser Processing in Argon at Pressure

Previous work has shown that laser processing at higher fluences in an inert gas at pressure can result in improved films that would otherwise be damaged or suffer material ejection from the higher fluence values[8]. Since the higher fluence values resulted in film damage for the SnO₂:Sb films, an investigation was carried out to determine the effect of laser processing in a pressurised atmosphere of argon. The sheet resistance was measured prior to laser processing, the films were then processed with two pulses and 99 and 202mJcm⁻² in atmosphere, 50PSI argon and 100 PSI of argon. The results shown in Figure 4-10 indicate that processing in a pressurised argon atmosphere does reduce the sheet resistance, but is not beneficial over processing in air, since the lower sheet resistance values were achieved in air.

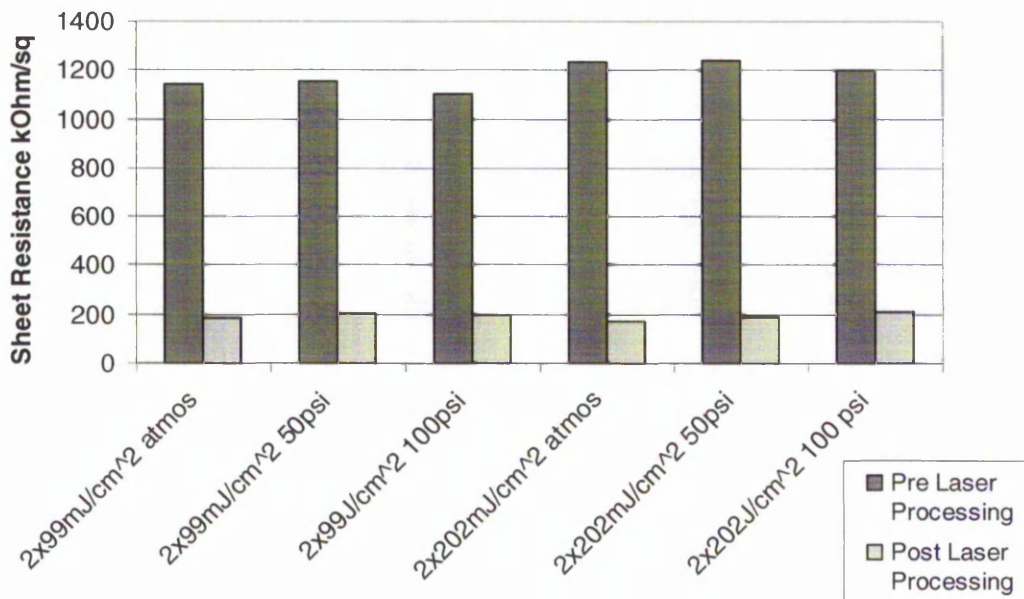


Figure 4-10: Change in sheet resistance following laser processing of inkjet printed SnO₂:Sb in pressurised argon

4.2.3 Thermal Annealing and Laser Processing on Borosilicate

It has been demonstrated that it is possible to reduce the sheet resistance of films of ATO with thermal annealing and also with laser processing. The precise mechanism of this improvement is unknown and so it is not unreasonable to assume that the mechanisms for the two processes may be different. It therefore follows that it may be possible to further reduce the sheet resistance by laser processing a thermally annealed sample.

					Starting Rs
					Post laser Rs
					Improvement factor
817	687	664	606	614	
548	485	492	441	443	
1.49	1.41	1.35	1.37	1.39	
861	725	666	661	665	
570	505	464	478	463	
1.51	1.44	1.43	1.37	1.43	
962	827	719	711	719	
631	570	521	463	484	
1.52	1.45	1.38	1.38	1.49	
1113	945	827	803	796	
744	657	547	532	532	
1.50	1.44	1.51	1.51	1.50	
1343	1110	1019	952	959	
892	719	680	616	631	
1.51	1.54	1.50	1.55	1.52	

Figure 4-11: Change in sheet resistance of a thermally annealed film of inkjet printed SnO₂:Sb laser processed with 100 pulses at 80mJcm⁻²

The thermally annealed samples (for annealing conditions see Section 4.1) proved to be more robust to laser processing and as such it was possible to use higher fluence values, since no visible damage occurred. This observation also supports the theory that the laser is vaporising residual solvents in the ink. An inkjet printed sample thermally annealed by PTL Ltd was laser processed in a 5x5 array with 100 pulses in

each spot at 80mJcm^{-2} . The results are shown in Figure 4-11 which represents the 5×5 laser processed array of inkjet printed $\text{SnO}_2\text{:Sb}$ on borosilicate. The first, second and third numbers in the boxes are the starting sheet resistance (Ohm/sq), post-laser processed sheet resistance(Ohm/sq) and the improvement factor respectively.

It is clear from the results that further improvements can be made to a thermally annealed film with the sheet resistance reducing by a factor of approximately 1.5 for all cases of laser processing. This suggests that improvements observed in laser processed samples arise from different mechanisms compared to thermal annealing.

4.2.3.1 Summary

Laser processing of the inkjet printed layers resulted in a reduction in sheet resistance. In general, for the parameters investigated, the sheet resistance decreased with increasing number of pulses and increasing fluence. Processing in pressurised argon was not beneficial to the sheet resistance. The transmission spectra reduced with increasing number of pulses in the infrared indicating changes to the carrier concentration. It has also been demonstrated that laser processing can be used to further reduce the sheet resistance of a thermally annealed inkjet printed film, suggesting differing mechanisms are at play with laser processing. Discussions on these possibilities are included in the next chapter.

4.2.4 ATO RF magnetron sputtered onto Cronar®

$\text{SnO}_2\text{:Sb}$ was deposited by RF magnetron sputtering onto Cronar® 742 (a biaxially oriented polyester terephthalate (PET) material with a gelatine coating) substrates. Four samples were laser processed at 25, 40, 70 and 100mJ/cm^2 with 10, 100 and 1000 pulses for each fluence condition. The sheet resistance of each of the irradiated

areas was measured before and after laser processing using the four point probe system. A staggered matrix as shown in Figure 4-12 was used on each sample to ensure repeatability and eliminate positional variations.

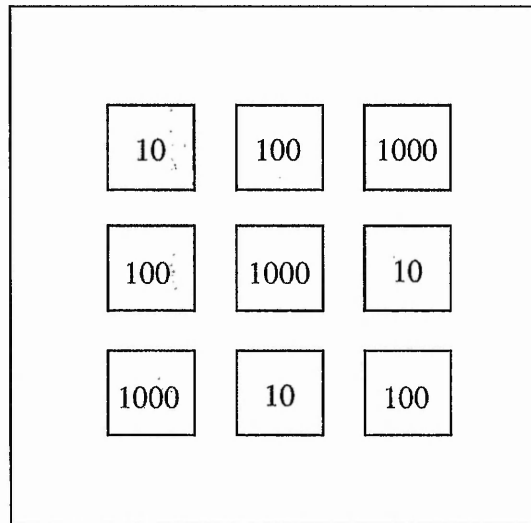


Figure 4-12: Matrix of laser processing parameters; number of pulses at 25, 40, 70 and 100mJcm⁻²

4.2.4.1 Sputter Parameters

Given the temperature sensitive nature of the substrate it was necessary to carry out an initial investigation into the heating effects of sputter deposition at various values of RF power. Temperature sensitive wax dots were placed on glass substrates. The thermally sensitive stickers had an array of wax stickers which permanently changed colour at a particular temperature, so that it was possible to determine that the temperature had reached above 82°C, but below 88°C, for example. Depositions were carried out at 100, 120, 140 and 150W and the results are shown in Table 4-3.

RF Power	Temperature range reached (°C)
100W	66-71
120W	82-88
140W	88-93
150W	99-104

Table 4-3: Temperature at the substrate for various RF magnetron sputtering powers

Since the aim of this part of the investigation was to determine the effect of laser processing on sputter deposited films, a brief rather than a comprehensive optimisation was carried out to determine suitable parameters for sputter deposited films. Based on the temperature results shown above, the power was limited to 140W to prevent overheating of the substrate layer. An experimental design was drawn up by MDSL Ltd who were assisting with the project and is shown with the results in Table 4-4. It was a response surface 3 level factorial quadratic design which required 13 experimental runs including 5 centre points[9]. Difficulties in obtaining conductive films from a commercially produced solid target, meant a switch to a pressed powder target using powder material supplied by Keeling & Walker Ltd. Since powder targets are more susceptible to sputter through, it was decided to limit the maximum power to 120W.

The results were not sufficient to provide meaningful results via the experimental design, it was therefore concluded from these results that a power of 120W and pressure of 3mTorr produced suitable films for the laser processing investigation.

The optimisation process was carried out on display industry glass from Corning; however, once the film was deposited onto the Cronar® substrate considerable cracking appeared in the centre of the sample. It was determined that this was due to stress at the deposition rate. Subsequently, the RF power was reduced and the partial pressure was increased to slow the deposition rate. This resulted in conductive films with no cracking immediately visible. A batch of samples was produced using the parameters and method described in the following section.

Run Order	Power (W)	Pressure (mTorr)	Sheet resistance (Ohm/sq)	Transparency (% at 550nm)
1	50	6.5	2.66M	90.0
2	50	10	>20M	92.4
3	120	10	52.4k	81.0
4	95	6.5	15.3k	76.6
5	95	6.5	25.4k	77.4
6	95	6.5	23k	76.7
7	95	10	152.9k	86.5
8	95	6.5	35.7k	78.9
9	50	3	>20M	78.3
10	95	3	4.3k	73.5
11	95	6.5	26.2k	78.6
12	120	6.5	4.6k	83.6
13	120	3	1.7k	76.9

Table 4-4: Sputter parameters and the resultant sheet resistance and transmission for the simple optimisation process

Films were clipped to a silicon substrate and loaded into the sputtering chamber for deposition. Sputter parameters used were as follows: Power: 95W, Chamber Pressure: 6.5mTorr (Chamber base pressure, typically 1×10^{-7} mbar), Gas: 10% O₂ in Ar. Gas flow was fixed, but not measured, with two turns of a needle valve. The sputter target was a pressed powder SnO₂:Sb target supplied by Keeling & Walker Ltd. Sb concentration was 6wt%. The thickness monitoring equipment was not employed for the growths because the uneven nature of the substrate meant the trace was unreliable. All films were grown over a two hour period.

4.2.4.2 Sheet Resistance

Figure 4-13 shows the change in sheet resistance of the sputter deposited ATO following laser processing.

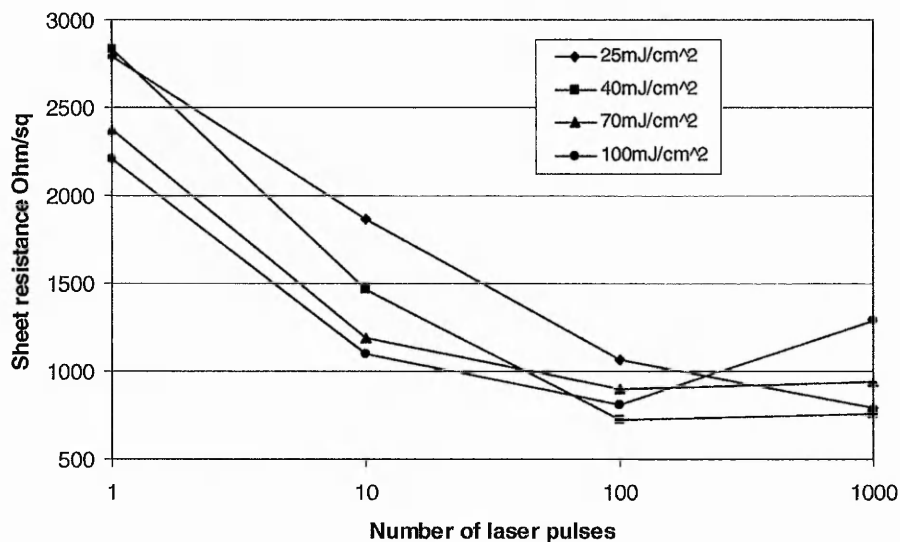


Figure 4-13: Change in sheet resistance of sputter deposited ATO on Cronar® following laser processing at 25, 40, 70 and 100mJcm⁻²

The results shown are an average of the results recorded in each area for a given set of laser parameters and also an average of the pre-laser processing sheet resistance

value which showed positional variation. The nature of the substrate meant it was impossible to methodically clean the substrates prior to deposition, this could account for the small positional variation observed. Typical starting sheet resistance values were $2.5\text{k}\Omega/\text{sq}$. In all cases of laser processing, the sheet resistance of the film was reduced with the greatest reduction to $724\Omega/\text{sq}$ produced with 100 pulses at 40mJcm^{-2} . For 40, 70 and 100mJcm^{-2} energies, the sheet resistance of the films reduced with increasing number of pulses up to 100 pulses. After this, the sheet resistance began to increase again. Cracking in the film was observed for 1000 pulses at the higher energies, which would explain an increase in sheet resistance. For areas processed with 25mJcm^{-2} , the sheet resistance dropped with increasing number of pulses up to and including 1000. This trend was investigated further with 2000, 3000 and 10000 pulses. The results are shown in Figure 4-14.

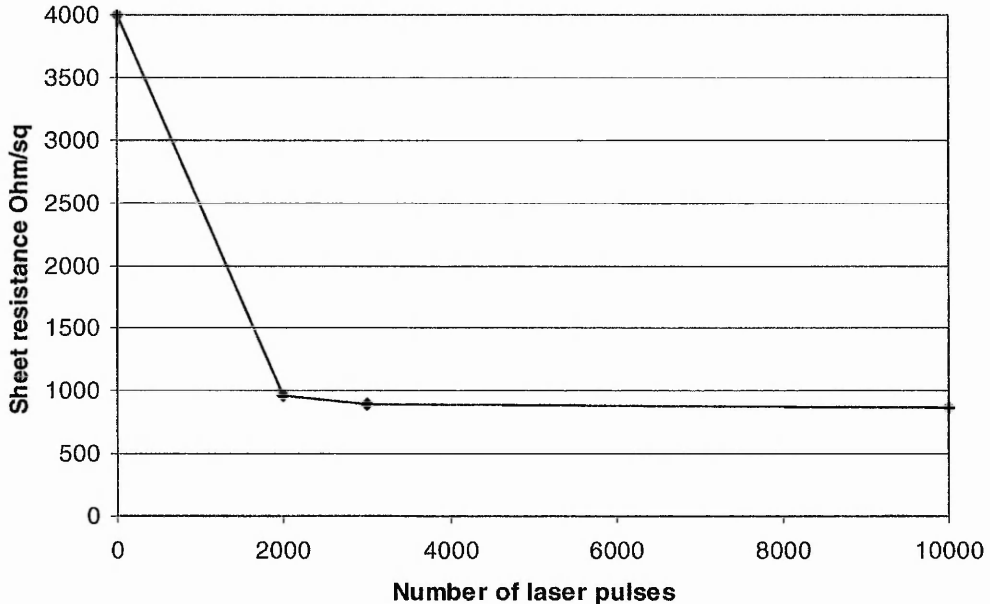


Figure 4-14: Change in sheet resistance of sputter deposited ATO after 2000, 3000 and 10000 pulses at 25mJcm^{-2}

The results show that further pulses at a low fluence further decreases the sheet resistance, but with diminishing returns, so that after 10000 pulses, the sheet resistance had only decreased by $20\Omega/\text{sq}$ from the area processed with 3000 pulses.

4.2.4.3 Transmission

Using the Filmetrics spectrometer the transmission spectra of as-deposited and laser processed areas of sputtered ATO were measured. The spectra are plotted in Figures 4-15 – 4-18 and show that the transparency of the film decreases uniformly across the spectrum with laser processing. Transmission values at 550nm are shown in Table 4-5. Transparency decreases with increasing fluence and increasing number of pulses. As expected with sputter deposited films the thickness of the films, as indicated by the fringes, appears more consistent compared to the inkjet printed films. However a clearly observable shift in the fringes is apparent on the films laser processed at 40mJcm^{-2} . This does not appear on the other laser processed films and the cause is unknown. Further investigations would be necessary to determine repeatability of this effect.

At the lowest fluence investigated, 25mJcm^{-2} , a reduction of 1% in transmission was observed at 550nm after 10 pulses with little or no change after 100 pulses. The decrease in transmission increased to 2% for 1000 pulses. At 40mJcm^{-2} , a 3% decrease in transmission was observed with 10 pulses, reducing to 4% for 100 pulses and a 5% for 1000 pulses. At 70mJcm^{-2} , the reduction in transmission for 10 pulses increases to 5%, with 7% and 10% respectively for 100 and 1000 pulses. Finally at 100mJcm^{-2} , the largest fluence in the investigation, a 3% reduction is observed for 10 pulses, 7% for 100 and 12% for 1000 pulses.

Number of pulses	25mJ/cm ²	40mJ/cm ²	70mJ/cm ²	100mJ/cm ²
As-deposited	70%	74%	72%	70%
10	69%	71%	67%	67%
100	69%	70%	65%	63%
1000	68%	69%	62%	58%

Table 4-5: Transmission at 550nm for as-deposited and laser processed RF magnetron sputtered ATO on Cronar®

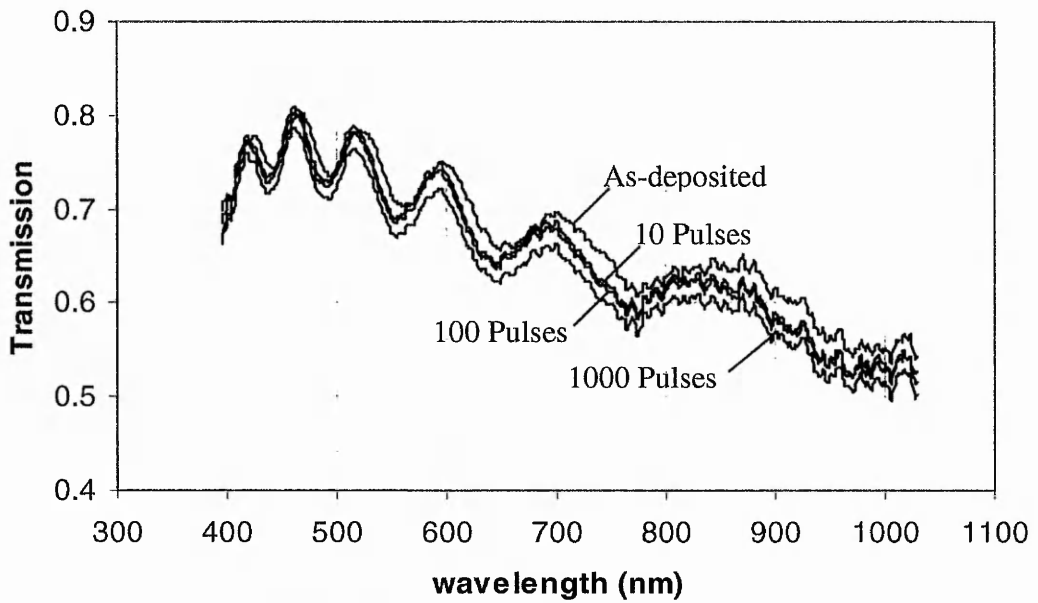


Figure 4-15: Transmission spectra for RF magnetron sputtered ATO on Cronar® laser processed with 25mJ/cm²

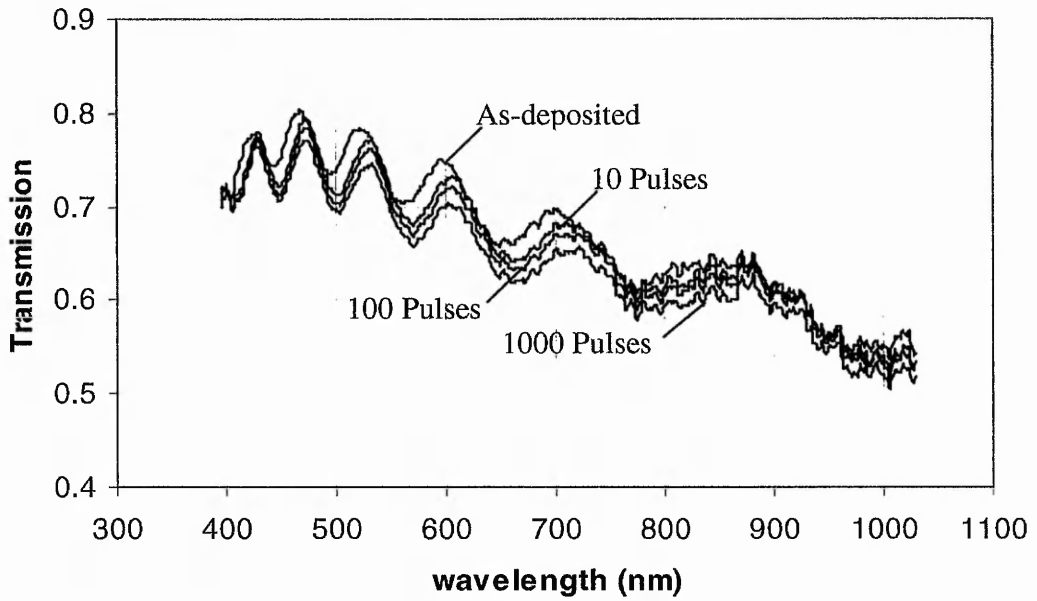


Figure 4-16: Transmission spectra for RF magnetron sputtered ATO laser processed with 40mJ/cm²

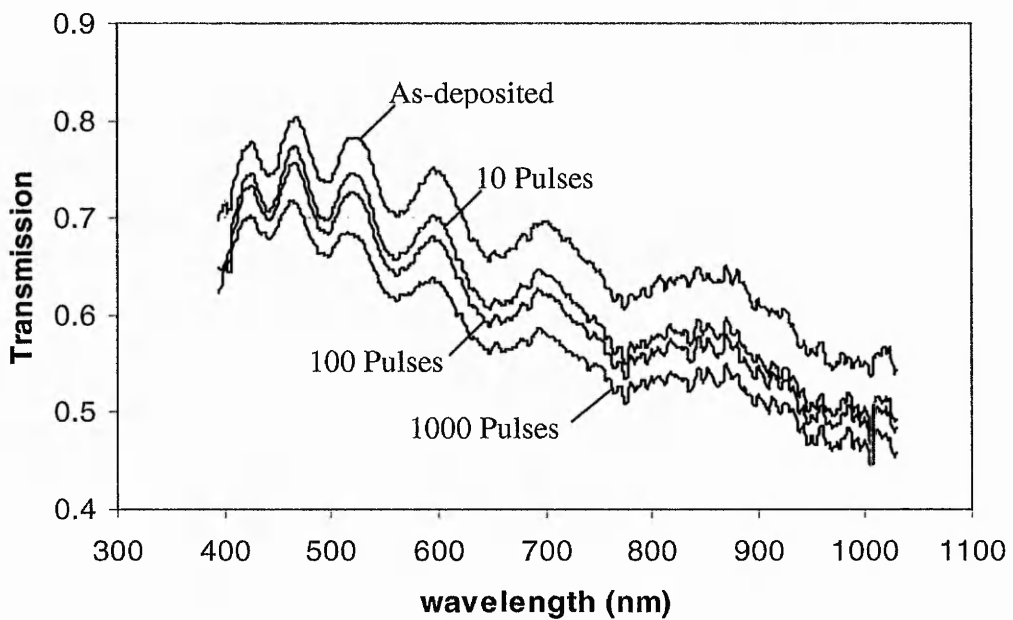


Figure 4-17: Transmission spectra of RF magnetron sputtered ATO laser processed with 70mJ/cm²

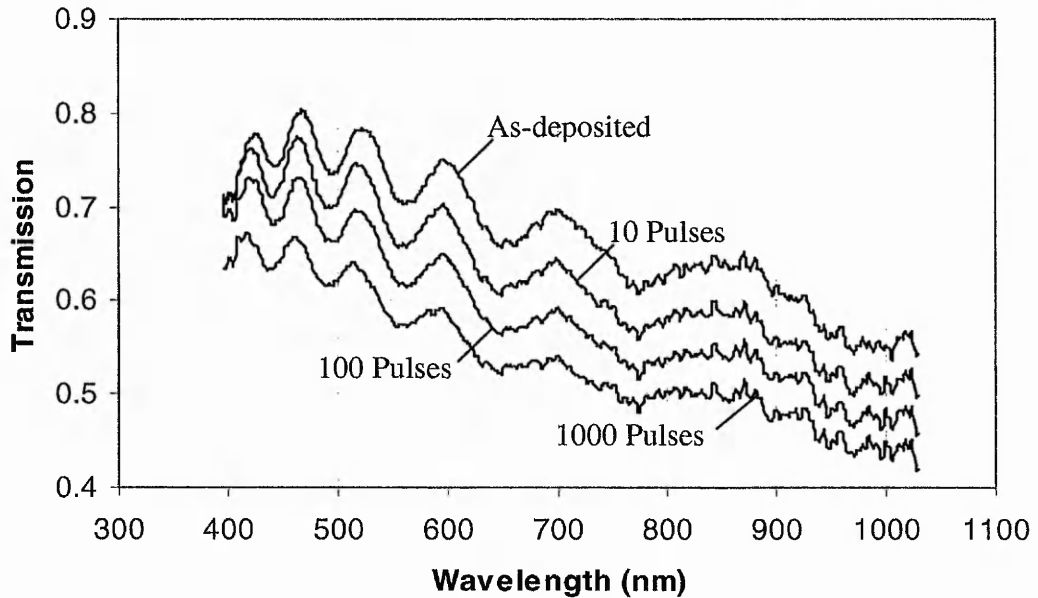


Figure 4-18: Transmission spectra of RF magnetron sputtered ATO laser processed with $100\text{mJ}/\text{cm}^2$

4.2.4.4 Summary

Lower fluences with a high number of pulses produced the best results. Sheet resistance values decreased the most with a minimal decrease in transmission compared to higher fluence values. Further increases in pulse number resulted in minimal further reductions in sheet resistance.

4.3 Summary of Electrical and Optical Properties

The electrical and optical properties of inkjet printed, dip-coated and RF magnetron sputter deposited transparent conducting films of $\text{SnO}_2:\text{Sb}$ have been investigated as a function of thermal annealing and laser processing. A summary of the deposition method, processing, electrical and optical results can be found in Table 4-6. While most of these results fall short of that of state of the art ITO (often less than

50Ohm/sq with 80% transparency), the techniques used are a promising indicator for future work.

It has been demonstrated that both thermal annealing and laser processing reduce film sheet resistance and that thermally annealed films may be further reduced by laser processing. While thermal anneal temperatures of 600-800°C provide the greatest reduction in sheet resistance, thermal anneals have, in the main, been carried out at 400°C due to substrate limitations. This typically resulted in a 400-fold improvement in conductivity. Whilst the precise mechanisms for this reduction in sheet resistance are unknown, the optical properties appear to show a shift in the plasma frequency in the infrared towards higher energies, indicating an increase in carrier concentration. It was also demonstrated that annealing in an O₂ atmosphere provided greater decreases in sheet resistance than annealing in a vacuum or N₂. This could be due to an increased presence of the highly resistive SnO in films annealed in an O₂ free environment.

Laser processing has reduced the sheet resistance of inkjet printed and RF Magnetron sputtered films, both on borosilicate and Cronar®. No apparent heating damage was observed on the Cronar® substrate with laser processing. Higher fluences (>70mJcm⁻²) resulted in damage to the film. Larger numbers of pulses (up to 1000) produced the greatest reduction in sheet resistance. XRD and TEM analysis reported on in the next chapter have revealed both an increase in crystallinity and densification of the films following laser processing. The transmission spectra indicate a shift of the plasma wavelength in the infrared towards higher energy wavelengths, indicating an increase in carrier concentration.

4. Electrical and Optical Properties

Deposition Method	Substrate	Processing Method	Thickness	Pre-Process Rs (Ohm/sq)	Post-Process Rs (Ohm/sq)	Transmission @ 550nm (%)
Inkjet	Soda Lime	Thermal @ 400°C	2500nm	4.5M	5-50k	—
Inkjet	Borosilicate	Thermal @ 400°C in air	1000nm	3M	7-30k	88
Inkjet	Borosilicate	Thermal @ 400°C in vacuum	1000nm	3M	1.5-2M	82
Inkjet	Borosilicate	Thermal @ 400°C in nitrogen	1000nm	3M	400-850k	83
1 dip dip-coat	Quartz	Thermal @ 400°C	—	—	3600	87.5
1 dip dip-coat	Quartz	Thermal @ 600°C	—	—	570	87.5
1 dip dip-coat	Quartz	Thermal @ 800°C	—	—	320	88
1 dip dip-coat	Quartz	Thermal @ 1000°C	—	—	5400	88
3 dip dip-coat	Quartz	Thermal @ 400°C	—	—	900	—
3 dip dip-coat	Quartz	Thermal @ 600°C	—	—	130	—
3 dip dip-coat	Quartz	Thermal @ 800°C	—	—	120	—
3 dip dip-coat	Quartz	Thermal @ 1000°C	—	—	2900	—
Inkjet	Borosilicate	Laser 10@40mJcm ⁻²	1000nm	4M	650k	90
Inkjet	Borosilicate	Laser 100@40mJcm ⁻²	1000nm	4M	700k	90
Inkjet	Borosilicate	Laser 1000@40mJcm ⁻²	1000nm	4M	200k	86
Inkjet	Borosilicate	Laser in 50PSI argon 2@99mJcm ⁻²	1000nm	1.2M	200k	—
Inkjet	Borosilicate	Laser in 100PSI argon 2@99mJcm ⁻²	1000nm	1.1M	200k	—
Inkjet	Borosilicate	Laser in 50 PSI argon 2@202mJcm ⁻²	1000nm	1.2M	200k	—
Inkjet	Borosilicate	Laser in 100PSI argon 2@202mJcm ⁻²	1000nm	1.2M	200k	—

Cont.

Deposition Method	Substrate	Processing Method	Thickness	Pre-Process Rs (Ohm/sq)	Post-Process Rs (Ohm/sq)	Transmission @ 550nm (%)
RF magnetron sputtering	Cronar®	Laser 10@25mJcm ⁻²	800nm	2500	1900	69
RF magnetron sputtering	Cronar®	Laser 10@40mJcm ⁻²	800nm	2500	1500	71
RF magnetron sputtering	Cronar®	Laser 10@70mJcm ⁻²	800nm	2500	1200	67
RF magnetron sputtering	Cronar®	Laser 10@100mJcm ⁻²	800nm	2500	1100	67
RF magnetron sputtering	Cronar®	Laser 100@25mJcm ⁻²	800nm	2500	1100	69
RF magnetron sputtering	Cronar®	Laser 100@40mJcm ⁻²	800nm	2500	700	70
RF magnetron sputtering	Cronar®	Laser 100@70mJcm ⁻²	800nm	2500	800	65
RF magnetron sputtering	Cronar®	Laser 100@100mJcm ⁻²	800nm	2500	800	63
RF magnetron sputtering	Cronar®	Laser 1000@25mJcm ⁻²	800nm	2500	800	68
RF magnetron sputtering	Cronar®	Laser 1000@40mJcm ⁻²	800nm	2500	750	69
RF magnetron sputtering	Cronar®	Laser 1000@70mJcm ⁻²	800nm	2500	950	62
RF magnetron sputtering	Cronar®	Laser 1000@100mJcm ⁻²	800nm	2500	1300	58

Table 4-6: Summary of results for electrical and optical properties

References

- [1] M. A. Aegerter, A. Reich, D. Ganz, G. Gasparro, J. Putz, and T. Krajewski, "Comparative study of SnO₂:Sb transparent conducting films produced by various coating and heat treatment techniques," *Journal of Non-Crystalline Solids*, vol. 218, pp. 123, 1997.
- [2] J. L. Huang, Y. Pan, J. Y. Chang, and B.-S. Yau, "Annealing effects on properties of antimony tin oxide thin films deposited by RF reactive magnetron sputtering," *Surface and Coatings Technology*, vol. 184, pp. 188, 2004.
- [3] T. Boudiar, C. S. Sandu, B. Canut, M. G. Blanchin, V. S. Teodorescu, and J. A. Roger, "Interest of Rapid Thermal Annealing (RTA) for the Elaboration of SnO₂:Sb Transparent Conducting Oxide by the Sol-Gel Technique," *Journal of Sol-Gel Science and Technology*, vol. 26, pp. 1067, 2003.
- [4] P. Y. Liu, J. F. Chen, and W. D. Sun, "Characterizations of SnO₂ and SnO₂:Sb thin films prepared by PECVD," *Vacuum*, vol. 76, pp. 7, 2004.
- [5] M. Mizuhashi, "Electrical properties of SnO₂ films on various glass substrates," *Journal of Non-Crystalline Solids*, vol. 38-39, pp. 329, 1980.
- [6] R. P. Howson, M. I. Ridge, and C. A. Bishop, "Production of transparent electrically conducting films by ion plating," *Thin Solid Films*, vol. 80, pp. 137, 1981.
- [7] K. Suzuki and M. Mizuhashi, "Structural, electrical and optical properties of r.f.-magnetron-sputtered SnO₂:Sb film," *Thin Solid Films*, vol. 97, pp. 119, 1982.

- [8] D. C. Koutsogeorgis, E. A. Mastio, W. M. Cranton, and C. B. Thomas, "Pulsed KrF laser annealing of ZnS:Mn laterally emitting thin film electroluminescent displays," *Thin Solid Films*, vol. 383, pp. 31, 2001.
- [9] S. Speakman, MDSL Ltd; Personal conversation; 2006.

5. Analysis of Structure

5.1 Introduction

A morphological examination is essential to determine the effects of thermal and laser processing on the films. By XRD, SEM and TEM analysis, crucial information regarding the crystalline structure and phase, including size and orientation, can be determined. Also of particular importance for this body of work is an inspection of the grain layout throughout the depth of the film, since laser processing is anticipated to affect only the uppermost surface. Each of these techniques has been applied to the inkjet printed films which have been thermally annealed and laser processed. In addition, XRD and TEM have also been applied to the RF magnetron sputtered films on Cronar® substrates. In addition a study of the thickness of the films has been carried out.

5.2 Film Thickness Measurements

Unless otherwise stated, the inkjet printed films investigated in this work were deposited as two wet layers. Film thickness measurements were carried out on inkjet printed SnO₂:Sb on borosilicate using an optical profiler following film ablation using the KrF laser at higher fluences. Typically, 10-15 pulses at 130-150mJcm⁻² were required to provide a suitable edge for thickness measurement, although results were varied with some areas not cleanly ablating. These areas were avoided during measurement and 'clear' areas were checked using the Filmetrics spectrometer.

Two samples were prepared for step height measurement and 18 measurements were carried out across each sample. The results are shown in Table 5-1 and that typical

film thickness is 1.05-1.1 μm with a standard deviation of approximately 150nm.

Figure 5-1 shows a typical step profile measured using a Dektak 6M stylus profiler.

Table of ATO thickness (nm)		
Position	Sample 1 thickness (nm)	Sample 2 thickness (nm)
1	809.2	no reading
2	874.1	955.0
3	1045.1	1054.3
4	1245.2	1289.5
5	1127.8	1402.9
6	1053.3	1271.7
7	1299.4	1264.9
8	1087.6	1075.7
9	849.6	934.7
10	850.5	no reading
11	928.2	1012.3
12	923.5	974.5
13	1200.0	1219.3
14	1231.3	1265.6
15	1138.4	1088.2
16	1268.2	1031.1
17	1124.5	906.7
18	924.1	934.8
Average	1054.4	1105.0
StdDev	160.8	157

Table 5-1: Thickness variation of inkjet printed SnO₂:Sb on borosilicate substrate

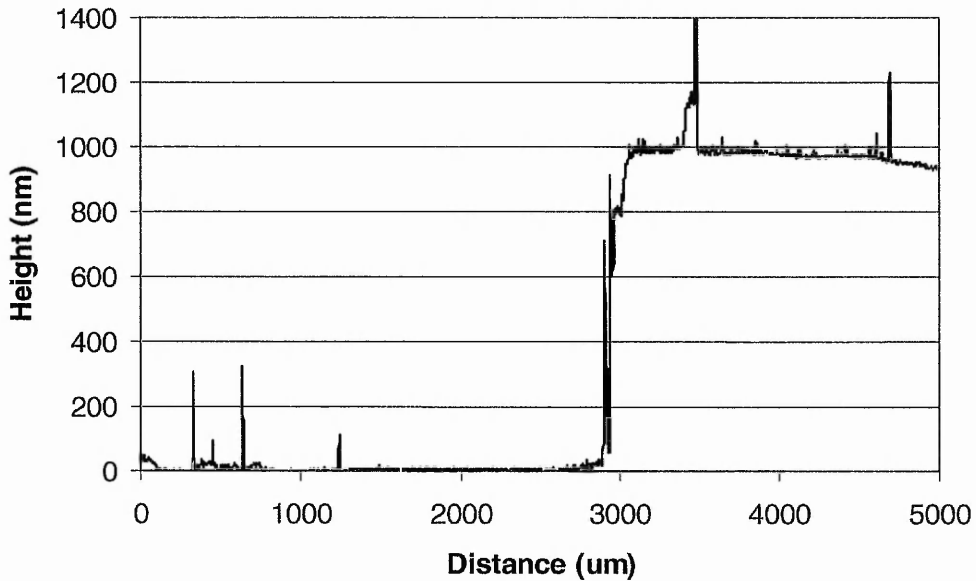


Figure 5-1: Typical step height of ablated inkjet printed SnO₂:Sb

5.3 The Effect of Thermal Annealing on the Morphology of Inkjet Printed SnO₂:Sb

5.3.1 SEM

A Jeol JSM 840A scanning electron microscope was used to investigate the surface and cross section of an as-deposited and a thermally annealed inkjet printed SnO₂:Sb on borosilicate. The samples were prepared by breaking off small sections of the films on the substrate. These were attached to a stub using a sticky pad and silver daub was used to electrically connect the SnO₂:Sb layer to the stub. All films were then coated with a thin layer of gold, a few nm in thickness, using sputter deposition.

Figure 5-2 shows the uppermost surfaces of the as-deposited and thermally annealed inkjet printed SnO₂:Sb on borosilicate obtained by SEM. Both the as-deposited and thermally annealed films appear to be uniform layers with no apparent signs of

cracking. With thermal annealing there appears to be no observable change in grain size or any obvious signs of densification, although there is a reduction in sheet resistance in the region of two orders of magnitude.

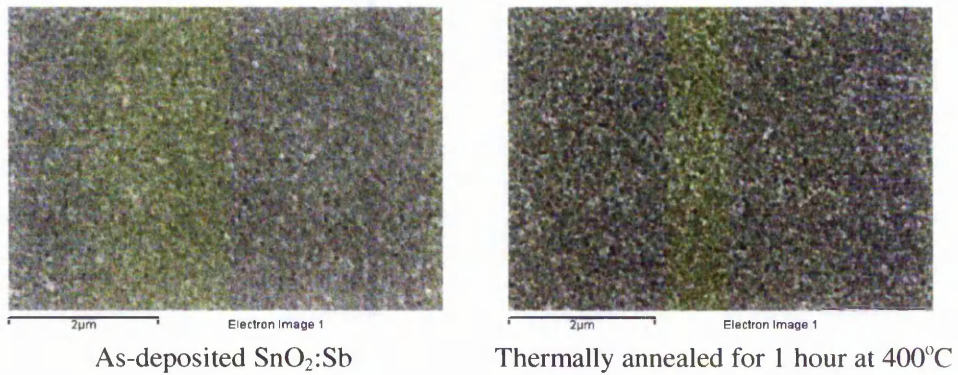


Figure 5-2: SEM images of the top surface of as-deposited and thermally annealed inkjet printed SnO₂:Sb

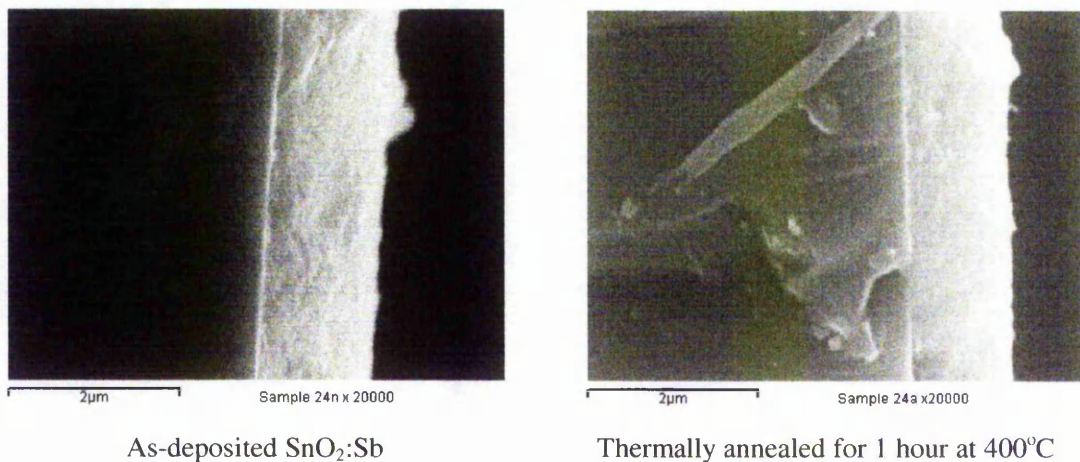


Figure 5-3: Cross section of as-deposited and thermally annealed inkjet printed SnO₂:Sb showing a film approximately 1µm thick

Figure 5-3 shows SEM images of the cross section of the as-deposited and thermally annealed inkjet printed films. Once again both the films appear to be uniform

throughout and also show no observable change in grain size or densification with thermal annealing.

5.3.2 TEM

A Jeol JEM 2010A TEM system was used to further investigate as-deposited and laser processed inkjet printed ATO films. The films were deposited onto a flexible substrate before being microtomed to a thickness of between 10-100nm. Figure 5-4 shows the cross section of an as-deposited film. It also shows a typical film thickness of 1µm and a uniform distribution of grains. This is in good agreement with the thickness measurements obtained using the optical profilometer and shows good consistency between samples.

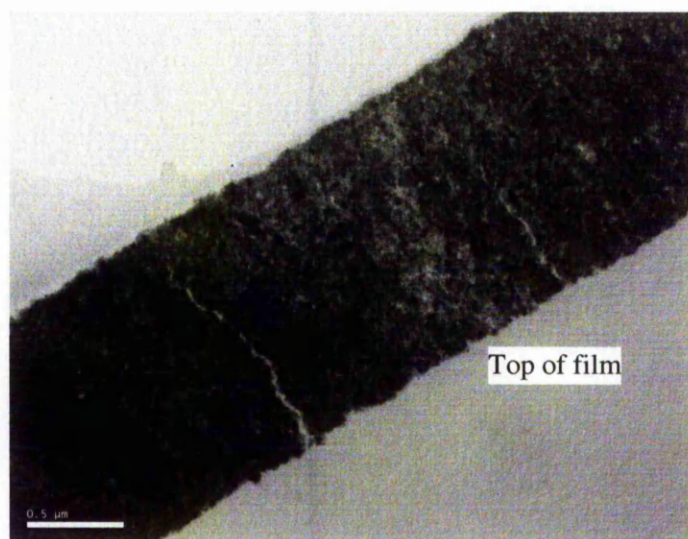


Figure 5-4: TEM cross section of as-deposited and thermally annealed inkjet printed SnO₂:Sb showing a film approximately 1µm thick

5.3.3 XRD

X-ray diffraction was carried out on the powder material used to make the ink and sputter target and on as-deposited and thermally annealed inkjet printed ATO layers.

A summary table of the results, including FWHM and particles sizes, can be found in Section 5.6. The X-ray diffraction system used was a Philips PW 1049/10 XRD system using a $\text{CrK}\alpha$ Source ($\lambda = 2.229\text{\AA}$). Experimental conditions were 40kV, 25mA, with diffraction intensity examined over an angular range of $2\theta = 5^\circ - 65^\circ$, incremented in 0.01° steps. Figure 5-5 shows the diffraction patterns from the SnO_2 and Sb_2O_3 powder prior to processing into an ink.

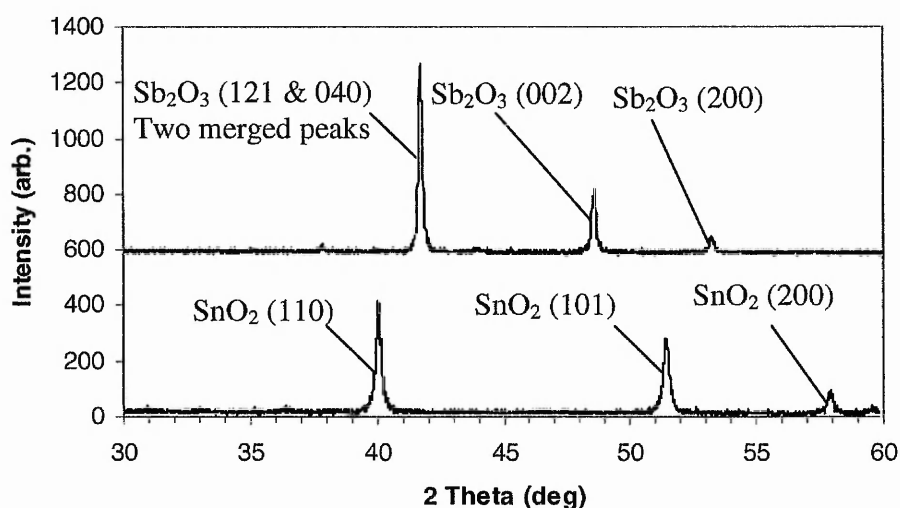


Figure 5-5: X-ray diffraction pattern from powdered SnO_2 and Sb_2O_3 used to produce the SnO_2 :Sb ink

Sb_2O_3 can occur in two forms, valentinite (orthorhombic) and senarmonite (cubic). The XRD diffraction pattern indicates the presence of the former primarily in the (121), (040) and (002) orientation, the first two of which produce XRD peaks at 41° and 48° respectively and the latter at 53° . The peaks correspond to d-spacings of 3.142\AA (121), 3.118\AA (040), 2.712\AA (002) and 2.456\AA (200).

The diffraction spectra for the powder SnO_2 are consistent with the tetragonal cassiterite phase of SnO_2 and primarily show the presence of the (110), (101) and

(200) orientation with peaks occurring at 40° , 51° and 58° respectively. These peaks correspond to d-spacings of 3.347\AA , 2.643\AA and 2.369\AA respectively. Using the Debye-Scherrer equation (see Chapter 3, section 3.2.5.1), the particle sizes of the SnO_2 and Sb_2O_3 powder appears to be approximately 50nm and 65nm respectively (see summary Table 5-3).

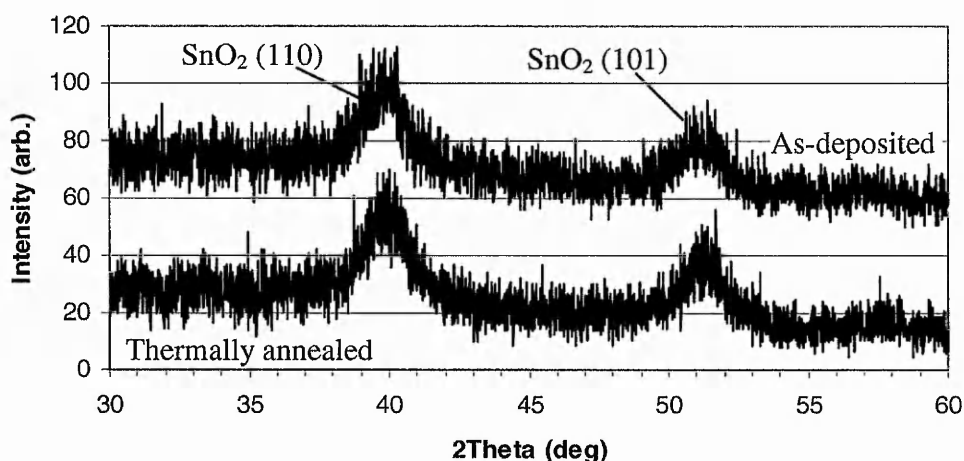


Figure 5-6: XRD of as-deposited and thermally annealed inkjet printed $\text{SnO}_2:\text{Sb}$

X-ray diffraction patterns of as-deposited and thermally annealed inkjet printed thin films of $\text{SnO}_2:\text{Sb}$ are shown in Figure 5-6. They indicate that the process of developing the ink and the printing has reduced crystallinity and particle size. The (110) and (101) peaks of SnO_2 are still visible, but (200) is no longer present. No Sb_2O_3 peaks are present since the quantity of doping is so small. The average particle size estimated using the Debye-Scherrer equation is approximately 8nm . This is supported by the $\times 300\,000$ magnification TEM image shown in Figure 5-7, where individual grains can be identified. Further magnification was not possible with the equipment and samples available.

The XRD on as-deposited and thermally annealed films also indicate that the annealing process does not alter the film's morphology since there is negligible difference between the as-deposited and thermally annealed film. This suggests the reduction in sheet resistance observed with thermally annealed is more likely to be due to increases in the carrier concentration or defect reduction rather than an increase in mobility due to sintering.

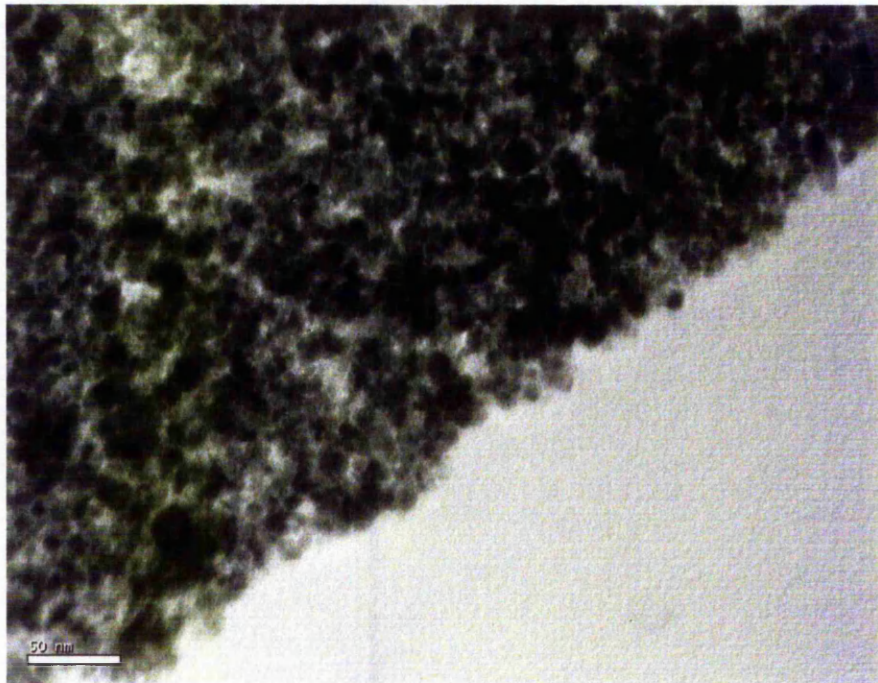


Figure 5-7: 300k magnification of uppermost surface of inkjet printed SnO₂:Sb

5.4 The Effect of Laser Processing on the Morphology of Inkjet Printed SnO₂:Sb

5.4.1 The Thermal Model

As mentioned in Chapter 3, a thermal model was used early in the project to indicate possible surface temperatures immediately following laser processing. The thermal model relies upon material specific values such as absorption coefficient, thermal

conductivity and specific heat capacity. There was not sufficient time to measure these on our material so approximate values, based on published work for SnO_2 , were used and were as follows: Specific heat (C_p) = $1.016\text{Jg}^{-1}\text{K}^{-1}$ [1], Absorption coefficient (α) = $3 \times 10^5\text{cm}^{-1}$ [2], Thermal conductivity (K) $\approx 40\text{Wm}^{-1}\text{K}^{-1}$ [3].

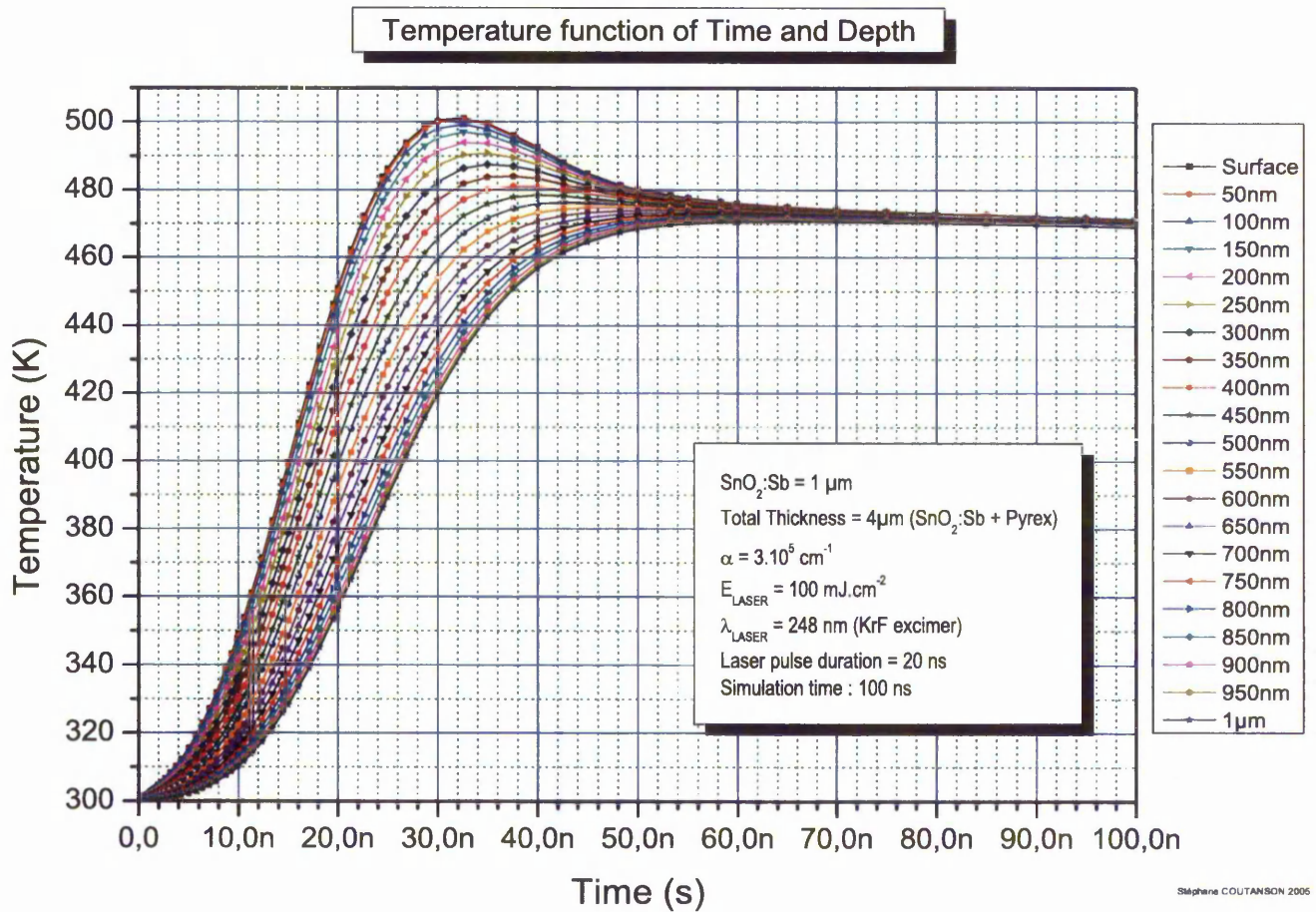


Figure 5-8: A modelled temperature and depth profile of SnO_2 following laser processing

Other parameters that were applied to the model were film thickness ($1\mu\text{m}$), laser wavelength (248nm), laser fluence (100mJcm^{-2}) and pulse duration (20ns). For an in depth analysis of the thermal model see in the doctoral thesis by Emmanuel Antoine Mastio[4].

While a range of analyses were undertaken, Figure 5-8 shows temperatures for a depth profile of $1\mu\text{m}$ over the first 100ns following laser processing. Since results are only indicative due to the lack of accurate values for certain parameters, further results are not shown, but can be found in Appendix D.

The results show a peak temperature of a little over 500°K approximately 30 seconds after the pulse is incident. This is nowhere near the melting point of tin oxide which is usually in excess of 1000°C and so it is thought that no melting occurs with the laser processing and the SEM and TEM images that follow appear in agreement with this.

5.4.2 SEM

Films of inkjet printed $\text{SnO}_2:\text{Sb}$ on borosilicate were laser processed to investigate the effect on their electrical and optical properties. Figure 5-9 shows SEM images of the surfaces of inkjet printed $\text{SnO}_2:\text{Sb}$ following laser processing.

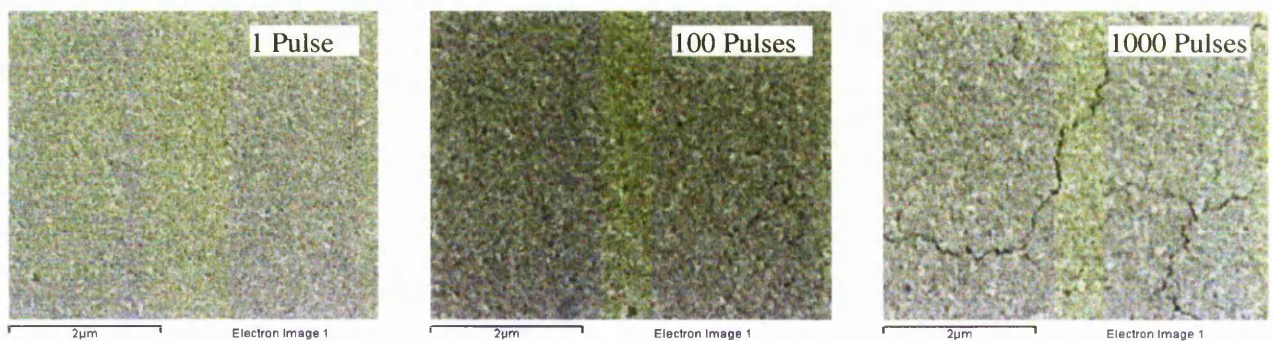


Figure 5-9: SEM images of laser processed inkjet printed $\text{SnO}_2:\text{Sb}$

From left to right, the samples were processed with 1, 100 and 1000 pulses at 40mJcm^{-2} . While the 1 pulse and 100 pulse samples show little, if any change from as-deposited samples, the sample processed with 1000 pulses shows signs of crack formation typical of laser processed materials[5]. The cracking is likely to be, at least

in part, responsible for the increases in sheet resistance observed with higher fluences and higher number of pulse.

5.4.3 TEM

An identical sample was laser processed with 1000 pulses at 70mJcm^{-2} and prepared for TEM analysis. Figure 5-10 shows the cross section of the laser processed sample showing a clear area of densification approximately 200nm thick on the upper surface, which is consistent with the expected depth of penetration with a 248nm laser on this material. Interestingly, there is no indication of grain growth.

The densification shown in the upper most surface in the TEM images could account for the reduction in sheet resistance observed in laser processed films since it would lead to a reduction in the grain boundary potential and therefore an increase in the carrier mobility.

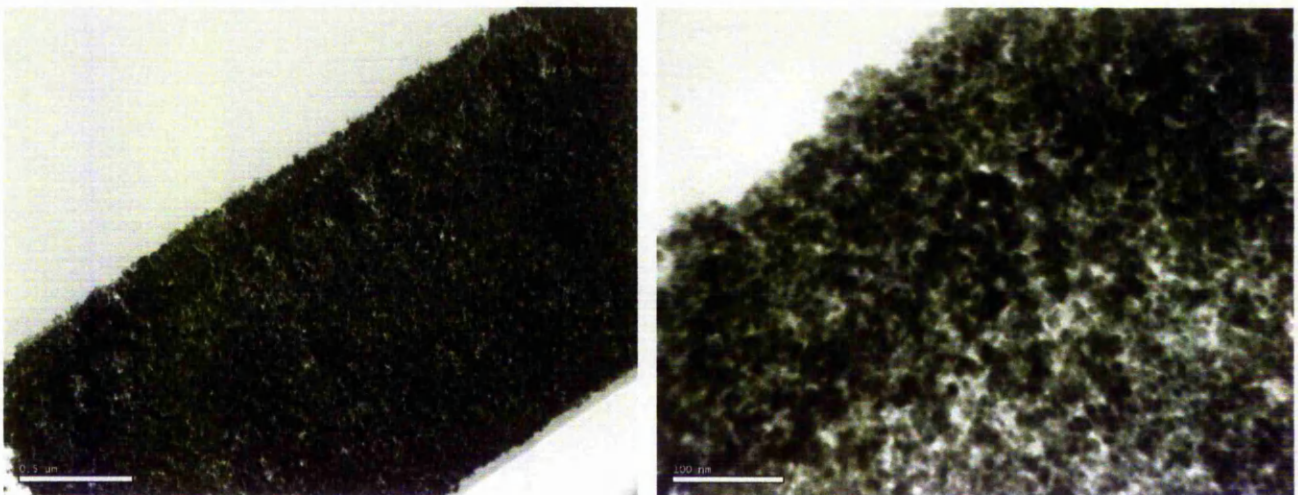


Figure 5-10: Cross sectional TEM of $\text{SnO}_2\text{:Sb}$ laser processed with 1000 pulses at 70mJcm^{-2} (x50000 magnification left, x100000 magnification right)

5.4.4 XRD

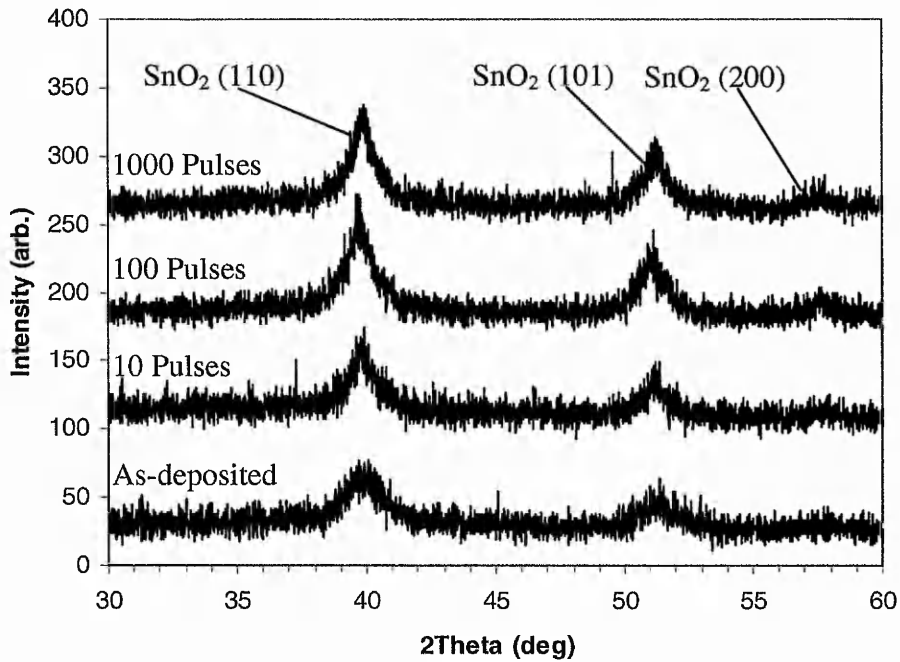


Figure 5-11: XRD of laser processed SnO₂:Sb inkjet printed onto borosilicate

Further inkjet printed films of SnO₂:Sb were laser processed with 10, 100 and 1000 pulses at 100mJcm⁻². The XRD results are shown in Figure 5-11, with a summary of FWHM and particle sizes included in Table 5-3 in Section 5.6. The results also show the presence of the 110 and 101 orientation of SnO₂ which produce XRD peaks at 40° and 51°. The peak intensity increases following laser processing, with increasing number of laser pulses indicating an increase in the crystallinity of the films with laser processing. The SnO₂(200) phase is also beginning to show on the film processed with 1000 pulses. However, no change is observed in the full width at half maximum height (FWHM), suggesting there is no change in the grain size with laser processing, which confirms the observed results from TEM analysis. Using the Debye-Scherrer equation, the particle size is estimated to be 10nm. It is expected that an increase in crystallinity would lead to a decrease in sheet resistance; however

this may be offset by the appearance of cracking at higher fluences and higher number of pulses as shown in Figure 5-9.

5.5 The Effect of Laser Processing on the Morphology of RF Magnetron Sputtered SnO₂:Sb on a Cronar® Substrate

RF Magnetron sputter deposited SnO₂:Sb on Cronar was laser processed for investigation by x-ray diffraction and TEM analysis. The films were analysed with a Philips X'pert Pro X-ray diffraction system with a CuK α 1 source and by Begbroke Nano in Oxfordshire using a JEOL 2010 analytical TEM. As-deposited and laser processed samples were investigated.

5.5.1 TEM

Figure 5-12 shows the as-deposited film with the uppermost layer on the left hand side. The image shows a uniform layer approximately 1000nm thick with columnar growth perpendicular to the substrate; an often typical characteristic of a sputter deposited film.

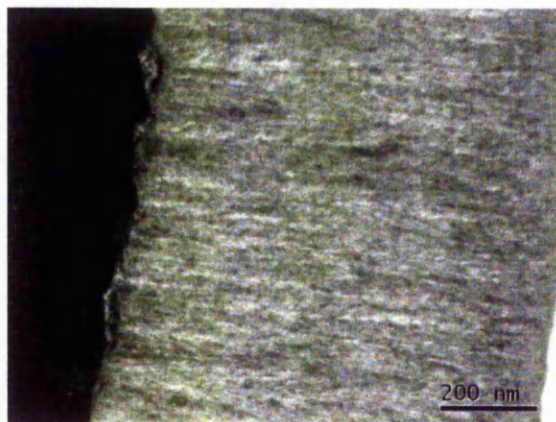


Figure 5-12: TEM cross-sectional image of as-deposited RF magnetron sputtered SnO₂:Sb

Films analysed with TEM were laser processed at 40mJcm^{-2} with 10, 100 and 1000 pulses. Figure 5-13 shows cross sections of the films following laser processing with 10, 100 and 1000 pulses. The columnar structure appears unchanged, even on the uppermost surface with no evidence of grain growth or sintering. However compared to the as-deposited film the surface roughness appears to have improved with laser processing.

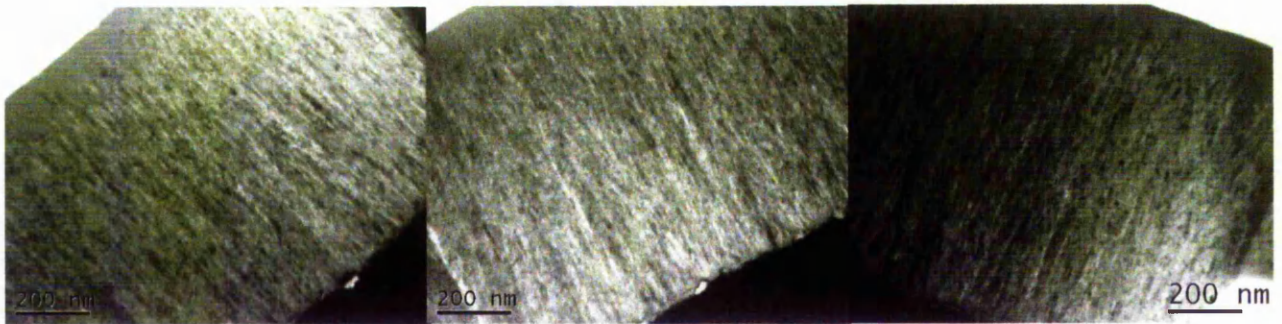


Figure 5-13: TEM cross sectional images of laser processed RF Magnetron sputtered $\text{SnO}_2\text{:Sb}$ processed with (L to R) 10, 100 and 1000 pulses at 40mJcm^{-2}

At the intersection with the substrate, an apparently amorphous area is visible on the laser processed films that is not present on the as-deposited sample. The origin of this is unknown, but could be as a result of heating of the gelatine coating present on Cronar®.

Figure 5-14 shows a higher magnification image of the sample laser processed with 1000 pulses with individual grains approximately 8-10nm in size apparent.



Figure 5-14: A higher magnification TEM cross-sectional image of the grain structure of RF magnetron sputtered SnO₂:Sb

5.5.2 XRD

XRD was carried out on as-deposited films and laser processed films RF magnetron sputtered SnO₂:Sb using a PANalytical X'Pert PRO diffraction system with CuK α 1 source (wavelength = 1.54056Å). The substrate layer was however crystalline as explained in Basic Principles of Organic Chemistry[6]. The strong peaks made analysis difficult. Figure 5-15 shows the XRD spectra for Cronar®, as-deposited SnO₂:Sb and SnO₂:Sb laser processed at 120mJcm⁻² with 100 pulses. Since a different source was used compared to that used on the inkjet printed films, the SnO₂ peaks appear at different angles. Table 5-2 shows the peak equivalents for each source for each of the main peaks that appear in the inkjet printed films for easy comparison.

SnO ₂ Phase	Angle of peak(°) CrKα1 Source (λ = 2.229Å)	Angle of peak(°) CuKα1 Source (λ = 1.541Å)
(110)	39.0	26.6
(101)	49.9	33.9
(200)	56.36	38.1

Table 5-2: Comparison of phase peaks for different XRD sources

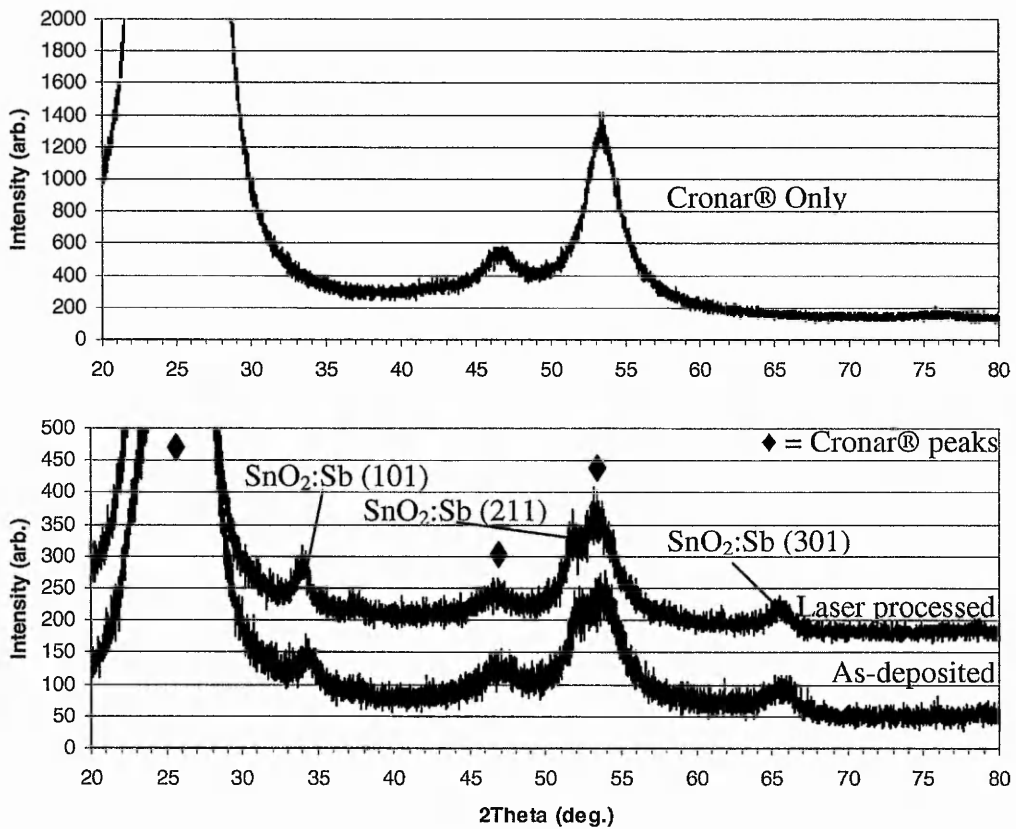


Figure 5-15: XRD of as-deposited and laser processed (100 pulses@120mJcm⁻²) SnO₂:Sb RF magnetron sputtered onto Cronar® (bottom) and Cronar® only (top)

The SnO₂(110) peak is likely to be present, but it is hidden by the strong Cronar® peak at 25°. The SnO₂(101) peak can be identified at 33.9°, while the peak indicating the presence of SnO₂(211) is partially obscured by a Cronar® peak at 54°. A further

peak is identifiable at 66° indicating the presence of the (301) phase of SnO_2 . The (211) and (301) peaks correspond to d-spacings of 1.75\AA and 1.41\AA respectively.

By comparing the laser processed and as-deposited diffraction peaks, it is evident that there is little or no change in the peak heights or widths suggesting that the laser irradiation is not increasing the crystallinity nor grain size of RF magnetron sputtered $\text{SnO}_2\text{:Sb}$. This is in agreement with the images obtained by TEM where there is also no evidence of morphological change following laser processing.

5.6 Summary

The morphology of inkjet printed deposited transparent conducting films of $\text{SnO}_2\text{:Sb}$ has been investigated for as-deposited, thermally annealed and laser processed samples using SEM, TEM and XRD. As-deposited and laser processed RF magnetron sputtered films were also investigated using TEM and XRD.

It has been found that as-deposited inkjet printed films are uniform layers with grain sizes of approximately 8-10nm. The (110) phase of SnO_2 was identified as the preferred orientation using XRD and it was found that neither the grain size, nor film crystallinity changed with thermal annealing. TEM images confirmed these results and also showed that no obvious sintering was occurring. Table 5-3 shows a summary of the XRD findings with FWHM and particles sizes obtained from the Debye-Scherrer equation.

Description	Phase	Orientation	2 θ ($^{\circ}$)	FWHM	Grain Size (nm)
Powder SnO ₂	Tetragonal cassiterite SnO ₂	110	40	0.21	58
		101	51	0.26	49
		200	58	0.27	49
Powder Sb ₂ O ₃	Valentinite Sb ₂ O ₃	002	48	0.19	66
Inkjet printed SnO ₂ :Sb As-deposited	Tetragonal cassiterite SnO ₂	110	40	1.53	8
		101	51	1.41	9
	Tetragonal cassiterite SnO ₂	110	40	1.53	8
		101	51	1.59	8
Inkjet printed SnO ₂ :Sb Laser processed 100 pulses @ 100mJcm ⁻²	Tetragonal cassiterite SnO ₂	110	40	1.22	10
		101	51	1.27	10

Table 5-3: Summary of XRD findings including FWHM and particle size

Laser processed films of inkjet printed SnO₂:Sb began to show signs of cracking at higher fluences or after a large number of pulses. The preferred orientation remained the same as for as-deposited films following laser processing; however XRD indicated an increase in crystallinity with increasing number of pulses and the (200) phase of SnO₂ also became apparent. The TEM images showed an apparent densification of the uppermost 200nm of the laser processed films which is not present on as-deposited layers.

TEM images of the RF magnetron sputtered films on Cronar® substrates showed that they grew in a columnar structure perpendicular to the substrate and identified

the grain size to be approximately 10nm. Diffraction peaks from XRD were obscured by peaks from the substrate layer, however the (101), (211) and (301) peaks were identifiable. No change was apparent in the diffraction spectra from as-deposited to laser processed films, indicating no grain growth and no change in crystallinity.

References

- [1] K. N. Yu, Yong-Hong Xiong, Cao-Shui Xiong, Yi-Tai Qian, Y. Hu, "Investigation of microstructural and optical properties in SnO₂ nanocluster-assembled solids," *Nanostructured Materials*, vol. 5, pp. 819-828, 1995.
- [2] S. Shanthi, C Subramanian, P Ramasamy, "Investigations on the Optical Properties of undoped, Fluorine Doped and Antimony Doped Tin Oxide Films" *Cryst. Res. Technol.*, Vol. 34, pp. 1037-1046, 1999.
- [3] C. Poulhier, D. S. Smith, J. Absi, "Thermal conductivity of pressed powder compacts: Tin oxide and alumina," *Journal of European Ceramic Society*, vol. 27, pp. 475-478, 2007.
- [4] Emmanuel Antoine Mastio, "*Materials engineering for high efficiency thin film electroluminescent devices*," Doctoral Thesis, Nottingham Trent University, 1999.
- [5] O. Baldus and R. Waser, "Laser crystallization studies of barium strontium titanate thin films," *Journal of the European Ceramic Society*, vol. 24, pp. 3013, 2004.
- [6] Roberts, John D. and Caserio, Marjorie C, "*Basic Principles of Organic Chemistry*," second edition, W. A. Benjamin, Inc., Menlo Park, CA. 1977.

6. Discussion

6.1 Introduction

In total, over 200 samples have been produced by inkjet printing and RF magnetron sputtering to investigate the effects of laser processing on SnO₂:Sb. Substrate materials have included soda lime glass, borosilicate, quartz and Cronar®. Samples have been investigated for changes in sheet resistance, transmission spectra, crystallinity and morphology. It should be noted however, that progress was considerably hindered following the destruction of the premises of the inkjet printing company PTL Ltd in the Buncefield gas explosion in December 2005. The destruction of the property and equipment lead to difficulties in obtaining a consistent supply of samples on which to carry out the research and make direct comparisons.

The following chapter contains a discussion of the results, including comparisons with other deposition and post-processing techniques. There is also a comparison made between the effect of laser processing on the properties of inkjet printed and RF magnetron sputtered samples from this investigation.

6.2 Thermal Annealing

6.2.1 Inkjet Printed SnO₂:Sb on Soda Lime Glass

The sheet resistance of a range of inkjet printed samples on soda lime glass was investigated. The samples were thermally annealed and the sheet resistance was measured again. A variation in sheet resistance between samples was observed for as-deposited films and it was subsequently discovered that the films would undergo

a process of stabilisation in the days following deposition. The stabilised sheet resistance is of the order of 4M Ω /sq. The stabilisation process could possibly be explained by the presence of impurities on the surface of the substrate prior to film deposition since the substrates were not subject to a rigorous cleaning procedure. The impurities could diffuse into the SnO₂:Sb layer therefore increasing impurity scattering, which would decrease carrier mobility and therefore increase the sheet resistance[1]. It is well known that SnO₂ in its stoichiometric state is an insulator[2], so an alternative explanation to the stabilisation process could be oxygen from the atmosphere being adsorbed onto the surface of the film eventually becoming chemisorbed and reducing the number of oxygen vacancies. This would result in a reduction in the carrier concentration and therefore an increase in sheet resistance[3]. Samples at different stages of stabilisation could account for the range in as-deposited sheet resistance together with variations in film thickness.

Upon thermal annealing, a reduction in sheet resistance was observed with all samples to typical values of 30k Ω /sq. Once again, considerable variation was observed in the sheet resistance between samples, indeed this variation was particularly noticeable in sample C, where pre-annealing sheet resistance values had been quite consistent. It is likely that this variation is caused by Na ions from the substrate layer diffusing into the SnO₂:Sb layer[4]. To prevent the need for a barrier layer such as SiO₂ and to avoid further discrepancies, all future samples were deposited onto borosilicate glass.

With the substrate issue as an aside, it is evident that thermal annealing of the inkjet printed SnO₂:Sb layer reduces its sheet resistance. There are many possible

explanations for this reduction including increases in crystallinity[5], a reduction in the grain boundary potential[6], an increase in the carrier concentration due to desorption of oxygen[7], or reduction in carrier defects[8]. XRD analysis of thermally annealed samples showed no increase in crystallinity, indicating that annealing is not strongly influencing the crystallinity of the particles or grain size. SEM images were in agreement with the XRD and also showed no obvious signs of densification. This would suggest that a process of the removal of defect regions could be one of the main mechanisms for reducing resistance or possibly incorporation of the Sb into the lattice.

With sheet resistance values in the tens of kOhm range, it was also not possible to carry out Hall voltage measurement to determine carrier concentrations or mobility (See Section 6.2.2.1). Further investigations carried out on inkjet printed SnO₂:Sb films on borosilicate are discussed in the next section with optical properties and annealing environments also investigated.

6.2.2 Inkjet Printed SnO₂:Sb on borosilicate thermally annealed in various atmospheres

Inkjet printed SnO₂:Sb was thermally annealed in air, a vacuum and nitrogen to determine the effect of the annealing atmosphere on the film sheet resistance and optical properties. The results, shown in Figure 4-4, showed that air was the preferred atmosphere both for reducing sheet resistance and for maintaining good optical transmission in the visible region. This finding suggests that oxygen plays an important part in the improvement process which appears to be contrary to some

other research findings[7, 9] where it has been found that annealing in oxygen is detrimental to the film conductivity. Other authors have discovered improvements with annealing in an atmosphere containing oxygen, but smaller improvements than those annealed in nitrogen[5], however this was with RF reactive sputtered films and deposition method appears to play a significant part in the effect of thermal annealing. Lin et al[10] found little change to the film's sheet resistance with thermal annealing, although increases in crystallinity were observed, suggesting the mobility or carrier concentration are detrimentally effected.

The transmission curves shown in Figure 4-5 show a shift in the absorption spectra in the UV towards the visible for films annealed without oxygen. They also seem to indicate a shift in the plasma wavelength towards the shorter wavelengths for all thermally annealed films compared to as-deposited films. It has previously been reported[11] that films grown in an oxygen free environment have higher levels of the SnO phase present. It is also noted that the absorption edge of SnO is at lower energies than that of SnO₂. It is therefore suggested that the shift in the absorption edge in the films annealed without oxygen could indicate the presence of SnO. SnO is also much more resistive compared to SnO₂[11] so this could also explain the comparatively high sheet resistance compared against the air annealed film. The slightly better sheet resistance reduction for films annealed in nitrogen compared to a vacuum could be due to oxygen leaking into the system during annealing since the process was not carried out in an air-tight environment.

The fringing observable in the Figure 4-5 appears to change with processing, indicating a change in films thickness. However, since an analysis of the thickness of

the two-wet-pass inkjet printed films (see Table 5-1) shows a $\pm 20\%$ variation in thickness, a meaningful interpretation could not be made. Similarly, without more precise thickness control it was not possible to use the fringing to determine n .

All of the annealed films show the same reduction in transmission in the infrared indicating a move in the plasma wavelength towards the visible. Since the plasma wavelength is given by $\omega_p = (4\pi N e^2 / \epsilon_0 \epsilon_\infty m_e)^{1/2}$ where N is the carrier concentration, ϵ_0 , ϵ_∞ , are permittivity of free space and the medium respectively and m_e is the effective mass of the electrons in the medium, it is suggested that this shift is due to an increase in the carrier concentration for all films. Furthermore, since lack of oxygen has been seen to increase the sheet resistance, it is unlikely that the increase in carrier concentration comes from an increase in oxygen vacancies, it is therefore suggested that the increase in carrier concentration and subsequent reduction in sheet resistance is due to incorporation of the Sb dopant into the lattice.

6.2.2.1 Hall effect

Attempts were made to further quantify the annealing results by obtaining the carrier concentration and mobility by Hall voltage measurements. Upon investigation, the voltage was not sufficiently stable to obtain reliable results. A quick analysis with estimated figures for mobility indicates that the resistivity was too high for the sensitivity of the equipment available.

Given an estimated mobility of $1\text{cm}^2\text{V}^{-1}\text{s}^{-1}$ (very modest, but taking account of the relatively high sheet resistance), a measured sheet resistance of $7\text{k}\Omega/\text{sq}$ from the films thermally annealed in air and a thickness of $1\mu\text{m}$, the variation in Hall voltage

with change in magnetic field from 0.1 – 0.5T would be of the order of tens of mV. The measured signal was seen to vary by amounts greater than this, possibly due to heating effects or charge trapping, it was therefore not possible to investigate carrier concentrations and mobility by this method. Better quality films with higher mobility values would permit re-measurement and this will be discussed in the further work section in Chapter 7.

6.2.3 Dip-coated SnO₂:Sb on quartz substrates thermally annealed at various temperatures

Dip-coated samples were created and thermally annealed at 400, 600, 800 and 1000°C in air to determine the effect of thermal annealing temperature. Sheet resistance values dropped with increasing annealing temperature up to 800°C, however the appearance of the film annealed at 800°C had begun to deteriorate, with signs of cracking and flaking in the film. At 1000°C, the sheet resistance was observed to increase and the appearance of the film had deteriorated further with much of the film flaking. Very similar results have been reported by Van Bommel et al[6] with physical vapour deposited ATO.

While it is suggested that, for annealing temperatures up to 400°C, the primary cause for reductions observed in sheet resistance is due to Sb incorporation in the lattice causing a subsequent increase in the carrier concentration, above this temperature other mechanisms appear to dominate. The transmission spectra of the films were measured with little change observed in the UV and visible region. In the infrared the films annealed up to and including 800°C showed little change from one another suggesting that the decrease in sheet resistance observed with increasing annealing

temperature is attributable to an increase in mobility rather than an increase in carrier concentration. Since crystalline growth has not been observed in the thermally annealed films it is likely that the decrease in sheet resistance comes from a reduction in defect states and perhaps a sintering effect that is too subtle to be picked up from TEM images, causing a reduction in grain boundary scattering as described in Section 2.2.5.3.

The transmission spectra in the infrared of the sample thermally annealed at 1000°C showed signs of a shift in plasma wavelength away from the visible, indicating a reduction in the carrier concentration. It is possible that at the higher temperature increased oxygen chemisorption leads to a reduction in oxygen vacancies. The increase in sheet resistance at 1000°C is however quite dramatic and it is likely that the flaking has a greater part to play in its increase.

6.3 Laser Processing

6.3.1 Laser Processed Inkjet Printed SnO₂:Sb on Borosilicate

Inkjet printed samples of SnO₂:Sb were laser processed at 20, 40 and 70mJcm⁻² with 1, 10, 100 and 1000 pulses. The sheet resistance of the films was observed to reduce with increasing number of pulses and increasing fluence, although the film was showing signs of damage following processing with high numbers of pulses at 70mJcm⁻². The transmission spectra reduced across the spectrum with all laser processing parameters, with 100 and 1000 pulses showing a notable reduction in the infrared, indicating an increase in carrier concentration by a shift in the plasma frequency towards the visible region. X-ray diffraction of the films laser processed with 100mJcm⁻² identified an increase in crystallinity with increasing number of

laser pulses, although grain size was not observed to increase. Furthermore, cross sectional TEM analysis appears to show densification of the uppermost surface of laser processed films to a depth of approximately 150nm. This depth correlates with the depth of penetration expected for 248nm wavelength light in this material[12].

From the analysis it would appear that the laser is reducing the sheet resistance through a number of mechanisms. An increase in crystallinity would provide a decrease in sheet resistance by causing a subsequent increase in mobility. The densification observed in the TEM images would suggest a reduction in the potential barrier at the grain boundaries, therefore also increasing mobility by reducing grain boundary scattering. An increase in carrier concentration, indicated by the transmission spectra, would also account for the decrease in sheet resistance. This is likely to be from better incorporation of the Sb dopant into the SnO₂ lattice rather than oxygen desorption since oxygen was present during the processing. The shift in fringing observed in the transmission spectra between the differently laser processed films is more likely to be as a result of the variation in thickness from the deposition process than a variation in thickness due to processing. This can more easily be appreciated by comparing the consistency of the transmission spectra of inkjet printed films to those later in Chapter 4 produced by RF Magnetron sputtering where thickness is more consistent.

Other authors have used a range of lasers to process various oxide materials[13-18] including ArF (193nm), XeCl (308nm), Nd:YAG (1064nm) and CO₂ (10.6µm). Infrared lasers are used as an alternative source of heat and the CO₂ laser was observed to reduce the resistivity of SnO₂:Sb sol-gel films by a greater amount

compared to conventional furnace annealing[15] with increases in crystallinity measured. Of course, the use of an infrared laser is not compatible with temperature sensitive substrates with surface temperatures reaching up to 1000°C[13], so UV lasers have been the subject of more recent investigations with an eye to the flexible electronics market.

Sandu et al[12, 19] have investigated the effects of KrF and ArF laser processing on Sol-Gel elaborated SnO₂:Sb films. They found the KrF laser more effective at reducing sheet resistance since its penetration depth was greater and more of the material could be processed. In concurrence with the findings here, they found that relatively low fluences induced the greatest reduction in sheet resistance, with 1000 pulses from the KrF laser at 78mJcm⁻² producing their minimum sheet resistance of approximately 20kOhm/sq. However, the reasons for the improvements in the film's electrical characteristics were attributed to an increase in grain size which was clearly visible in XTEM images. No such grain growth was evident with the inkjet printed films so it would appear that the deposition method is critical in determining the effect of the laser processing.

Similar findings to those reported here have been reported by Chung et al[17]. They deposited ITO onto glass substrates by DC magnetron sputtering at room temperature and laser processed the films with a XeCl laser. Fluence values for this study were also kept relatively low, no higher than 175mJcm⁻², to prevent film damage. They observed an increase in crystallinity with increasing fluence, however there was no available data on the effect of an increase in the number of pulses. A reduction in sheet resistance was reported up to 150mJcm⁻² and this corresponded to

an increase in both the mobility and carrier concentration and was attributed to an increase in substitutional Sn and increased crystallinity.

6.3.2 Laser Processing in Argon at Pressure

Inkjet printed films of SnO₂:Sb on borosilicate were laser processed in a pressurised argon atmosphere to determine if the films were more robust to higher fluences under pressure. The results showed a reduction in sheet resistance with laser processing, however not as great as observed in air. Higher fluence values were used, but showed no further improvement. Given the improvements shown with oxygen environments at the time of processing, it would be interesting to repeat this investigation with a 20% oxygen 80% Nitrogen gas mix to simulate atmosphere. This will be discussed in future work in the following chapter. The author has been unable to identify any published research attempting similar investigations and so is unable to make any comparisons.

6.4 Thermal Annealing and Laser Processing

It seems that thermal annealing and laser processing act to elicit a change in the material properties of inkjet printed SnO₂:Sb in different ways. To examine this further, a thermally annealed sample was laser processed to determine if further changes to the sheet resistance could be achieved. Since thermal annealing has always achieved lower sheet resistance values than laser processing by a factor of 10, it was not possible to determine if laser processing followed by thermal annealing was beneficial. Laser processing following thermal annealing provided a further reduction in the sheet resistance of the films; improving conductivity by a factor of 1.5. This improvement is not as great as that achieved on as-deposited films and it should be noted that the film already had the lowest sheet resistance of all the inkjet

printed films. There is a clear trend that the greater the starting sheet resistance, the greater the improvement that can be made and vice versa. The results therefore suggest that the mechanisms for improvement by laser processing are different in part, if not exclusively.

It was interesting to note that following thermal annealing the films were more robust to higher fluences. It is thought that the damage caused at higher fluences is possibly due to vaporisation of solvents remaining in the film effectively blasting the material away from the substrate. It would follow that if this is driven off by a thermal anneal, then the film would become more robust to higher fluences. This theory was tested by placing one film in water for 30 minutes and then using the same parameters to attempt to ablate this film as an identical film which had not been soaked. The material in the soaked film was cleanly removed after no more than 10 pulses at 150mJcm^{-2} , whilst it was generally not possible to remove all the material from the non-soaked film. An image of the two films can be seen in Appendix C.

6.5 RF Magnetron Sputtered SnO₂:Sb

Films of SnO₂:Sb were deposited onto Cronar substrates and laser processed to determine the effect on the material. The films were processed at 25, 40, 70 and 100mJcm^{-2} with 10, 100 and 1000 pulses. The sheet resistance of the laser processed areas was measured prior to processing. There was evidence of positional variation in the as-deposited sheet resistance which was on average $2.5\text{k}\Omega/\text{sq}$. The lowest sheet resistance achieved was $1.5\text{k}\Omega/\text{sq}$ which bearing in mind the process was not fully optimised is comparable for the deposition temperature with that achieved by

Ma et al[20] on polyimide The positional variation, although still present, was least pronounced in the central areas of the samples. It is therefore likely that the variation is caused by both edge effects in taking sheet resistance measurements and also in impurities present on the surface of the substrate prior to deposition. The nature of the substrate was such that a rigorous cleaning procedure could not be undertaken. To minimise the positional variation and ensure repeatability a matrix of repeated parameters was used as detailed in the results chapter. Sheet resistance and transmission values were averaged from the three measurements.

The results showed a decrease in sheet resistance with increasing number of pulses up to and including 100 pulses. Following 1000 pulses, the films processed with 40, 70 and 100mJcm⁻² all showed an increase in sheet resistance. At these values, cracks were apparent in the films as shown in Figure 6-1. The cracks would almost certainly cause an increase in the sheet resistance of the film. However with 1000 pulses at 25mJcm⁻², the sheet resistance continues to drop suggesting that while the fluence is sufficiently high to continue to improve the film, it is not so high as to create damage through stress or shrinkage. To investigate the effect of further pulses, a separate area was laser processed with 2000, 3000 and 10000 pulses. This resulted in further reductions in the sheet resistance, but by very small amounts such that between 3000 and 10000 pulses a reduction of 20Ω/sq was observed. This suggests that the improvements made by the laser are at their limit. The lowest sheet resistance of 580Ω/sq (approximately 4.6x10⁻²Ω.cm based on a thickness of 800nm) was achieved with 1000 pulses at 40mJcm⁻² with the processed sheet resistance being dependent upon the pre-processed sheet resistance. With further optimisation

of the deposition process, it should be possible to further reduce the sheet resistance of the films.

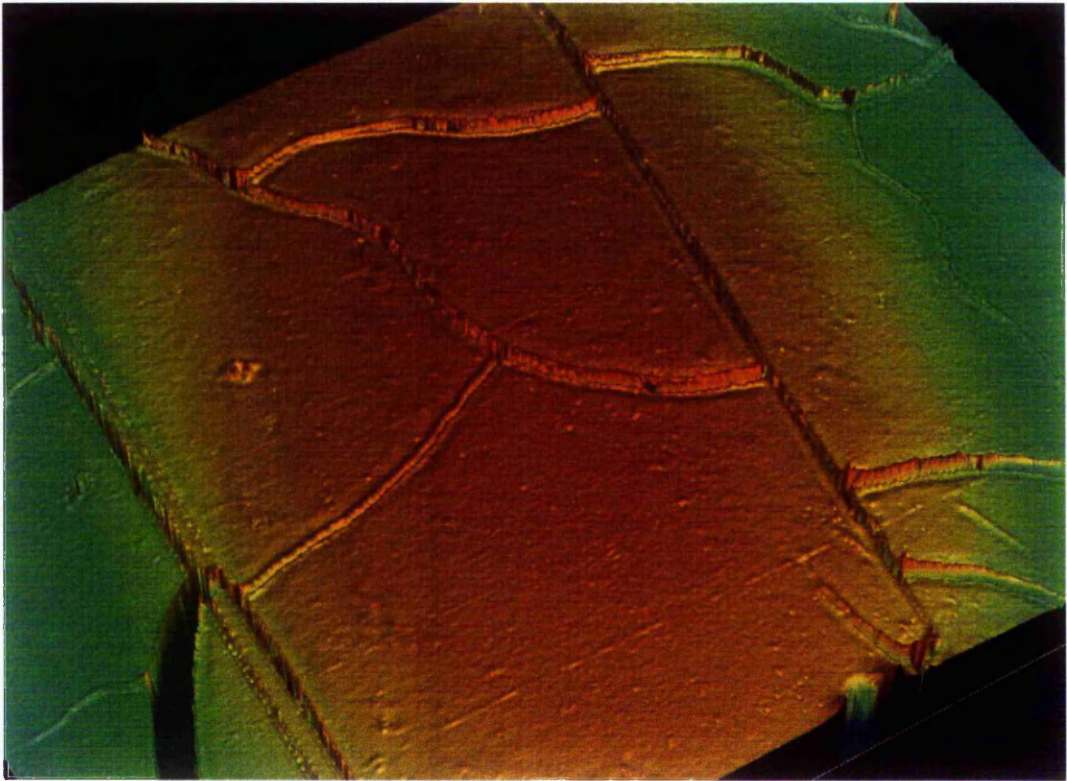


Figure 6-1: Surface Profiler image of RF Magnetron Sputtered SnO₂:Sb following laser processing with 1000 pulses at 100mJcm⁻²

The exact nature of the mechanisms for improvement are still unknown. X-ray diffraction on the samples showed no change in crystallinity with laser processing, unlike that observed with laser processed inkjet printed films on borosilicate. TEM images appear to confirm the findings from XRD since there is no obvious change in grain size and no apparent densification. The transmission spectra shown in Figures 4-14 to 4-17 shows no sign of an increase in carrier concentration since there is no shift in the infrared region. It is therefore likely that the improvements observed with laser processing come primarily from an increase in mobility possibly due to a reduction in defects. There may also be a subtle sintering effect that cannot be

detected with TEM. Curiously, there appears to be a consistent phase shift in the fringing observed on the film processed with 40mJcm^{-2} for all number of pulses that does not appear for any other fluence value. The reason for this is unknown and is a potential area for further work. It was not been possible to determine the value of n of the film from the fringes because the value of n for the substrate is not published and could not be measured.

Interestingly, the transmission spectra show a greater reduction in transmission for films processed with higher fluences so that in terms of transmission, lower fluences are better because they are more transparent across the spectra. While the transmission at 550nm for 1000 pulses at 25mJcm^{-2} is 68%, this reduces a further 10% to 58% for those processed with the same number of pulses at 100mJcm^{-2} . This is likely to be due to damage to the film surface making a rougher more opaque appearance.

6.6 Summary

Inkjet printed $\text{SnO}_2\text{:Sb}$ has been thermally annealed and laser processed to improve its material properties. Laser processing is suggested as an alternative to thermal annealing since the move towards flexible electronics means using temperature sensitive substrates. It has been demonstrated that thermal annealing of the inkjet printed $\text{SnO}_2\text{:Sb}$ film improves its conductivity and it is thought this is due to an increase in carrier concentration due to better incorporation of the Sb dopant for temperatures up to 400°C . Above this temperature and up to 800°C the mobility of the films seems to improve and it is suggested that this is due to reduction in defect

states and perhaps sintering effects. Above 800°C the film deteriorates with flaking and cracking evident.

The effect of laser processing on SnO₂:Sb films is highly dependent upon the deposition method as illustrated in the summary of findings in Table 6-1.

Summary of Laser Processing of SnO₂:Sb	
Inkjet Printed on borosilicate	RF Magnetron Sputtered on Cronar®
Improvements with fluences up to 70mJcm ⁻²	Improvements with fluences up to 100mJcm ⁻²
Increase in carrier concentration observed with Tx spectra	No increase in carrier concentration observed with Tx spectra
Increase in crystallinity with increasing number of pulses	No increase in crystallinity with laser processing observed
Densification observed	No densification observed
Improvements in conductivity likely to be from: <ul style="list-style-type: none"> • Sb incorporation • Reduction in grain boundary potential • More crystalline material 	Improvements in conductivity likely to be from: <ul style="list-style-type: none"> • Increase in mobility by reduction in defects

Table 6-1: Comparison of the effect of laser processing on inkjet printed and RF magnetron sputtered SnO₂:Sb

References

- [1] D. Zhang, L. Tao, Z. Deng, J. Zhang, and L. Chen, "Surface morphologies and properties of pure and antimony-doped tin oxide films derived by sol-gel dip-coating processing," *Materials Chemistry and Physics*, vol. 100, pp. 275, 2006.
- [2] A. L. D. Hartnagel H, A.K. Jain, C. Jagadish, "Semiconducting Transparent Thin Films," 1995.
- [3] P. Y. Liu, J. F. Chen, and W. D. Sun, "Characterizations of SnO₂ and SnO₂:Sb thin films prepared by PECVD," *Vacuum*, vol. 76, pp. 7, 2004.
- [4] P. K. Biswas, A. De, L. K. Dua, and L. Chkoda, "Surface Characterization of sol-gel derived indium tin oxide films on glass," *Bulletin of Materials Science*, vol. 29, pp. 323-330, 2006.
- [5] J. L. Huang, Y. Pan, J. Y. Chang, and B.S. Yau, "Annealing effects on properties of antimony tin oxide thin films deposited by RF reactive magnetron sputtering," *Surface and Coatings Technology*, vol. 184, pp. 188, 2004.
- [6] M. J. Van Bommel, W. A. Groen, H. A. M. Van Hal, W. C. Keur, and T. N. M. Bernards, "The electrical and optical properties of thin layers of nano-sized antimony doped tin oxide particles," *Journal of Materials Science*, vol. 34, pp. 4803, 1999.
- [7] E. Shanthi, A. Banerjee, V. Dutta, and K. L. Chopra, "Annealing characteristics of tin oxide films prepared by spray pyrolysis," *Thin Solid Films*, vol. 71, pp. 237, 1980.
- [8] A. G. Sabnis, "Two-step process for thin films of tin oxide," *Journal of Vacuum Science & Technology*, vol. 15, pp. 1565-1567, 1978.

- [9] G. Beensh-Marchwicka, L. Krol-Stepniewska, and A. Misiuk, "Influence of annealing on the phase composition, transmission and resistivity of SnO_x thin films," *Thin Solid Films*, vol. 113, pp. 215, 1984.
- [10] Y. J. Lin and C. J. Wu, "The properties of antimony-doped tin oxide thin films from the sol-gel process," *Surface and Coatings Technology*, vol. 88, pp. 239, 1997.
- [11] K. Suzuki and M. Mizuhashi, "Structural, electrical and optical properties of r.f.-magnetron-sputtered SnO₂:Sb film," *Thin Solid Films*, vol. 97, pp. 119, 1982.
- [12] C. S. Sandu, V. S. Teodorescu, C. Ghica, B. Canut, M. G. Blanchin, J. A. Roger, A. Brioude, T. Bret, P. Hoffmann, and C. Garapon, "Densification and crystallization of SnO₂:Sb sol-gel films using excimer laser annealing," *Applied Surface Science*, vol. 208-209, pp. 382, 2003.
- [13] K. Steiner, G. Sulz, E. Neske, and E. Wagner, "Laser annealing of SnO₂ thin-film gas sensors in single chip packages," *Sensors and Actuators B: Chemical*, vol. 26, pp. 64, 1995.
- [14] N. Asakuma, T. Fukui, M. Aizawa, M. Toki, H. Imai, and H. Hirashima, "Ultraviolet-Laser-Induced Crystallization of Sol-Gel Derived Inorganic Oxide Films," *Journal of Sol-Gel Science and Technology*, vol. 19, pp. 333, 2000.
- [15] D. Ganz, G. Gasparro, J. Otto, A. Reich, N. J. Arfsten, and M. A. Aegerter, "Fast CO₂ laser firing of sol-gel SnO₂:Sb coatings," *Journal of Materials Science Letters*, vol. 16, pp. 1233, 1997.

- [16] T. Nagase, T. Ooie, and J. Sakakibara, "A novel approach to prepare zinc oxide films: excimer laser irradiation of sol-gel derived precursor films," *Thin Solid Films*, vol. 357, pp. 151, 1999.
- [17] W. Chung, M. O. Thompson, P. Wickboldt, D. Toet, and P. G. Carey, "Room temperature indium tin oxide by XeCl excimer laser annealing for flexible display," *Thin Solid Films*, vol. 460, pp. 291, 2004.
- [18] H. Imai, A. Tominaga, H. Hirashima, M. Toki, and M. Aizawa, "Ultraviolet-Laser-Induced Crystallization of Sol-Gel Derived Indium Oxide Films," *Journal of Sol-Gel Science and Technology*, vol. 13, pp. 991, 1998.
- [19] C. S. Sandu, V. S. Teodorescu, C. Ghica, P. Hoffmann, T. Bret, A. Brioude, M. G. Blanchin, J. A. Roger, B. Canut, and M. Croitoru, "Excimer Laser Crystallization of SnO₂:Sb Sol-Gel Films," *Journal of Sol-Gel Science and Technology*, vol. 28, pp. 227, 2003.
- [20] J. Ma, X. Hao, S. Huang, J. Huang, Y. Yang, and H. Ma, "Comparison of the electrical and optical properties for SnO₂:Sb films deposited on polyimide and glass substrates," *Applied Surface Science*, vol. 214, pp. 208, 2003.

7. Conclusions and Further Work

7.1 Conclusions

The feasibility of using inkjet printing for the fabrication of functional transparent conducting thin films has been investigated via a detailed study of the properties of inkjet printed SnO₂:Sb as a function of post deposition processing. Specifically, for the first time, a study of as-deposited, thermally annealed and laser processed inkjet printed films has been undertaken as part of a collaborative research project with industrial partners who are currently exploring the commercial potential of this technique. The work undertaken for this thesis was primarily concerned with the feasibility of using excimer laser processing as a method to realise functional thin films on low temperature, plastic substrates. In addition, comparative studies of RF magnetron sputtered films of SnO₂:Sb were also investigated.

The collaboration has successfully developed an inkjet printing process to direct write SnO₂:Sb by inkjet printing and has underpinned a new 'business to business' DTI supported exploitation collaboration between the two industrial partners. The work presented here demonstrates that the electrical properties of the films have been improved following a study of the effects of both thermal annealing and laser processing. Extensive analysis of the electrical, optical and morphological properties has indicated physical changes have taken place following processing. Based on these findings a tentative model for the mechanisms affecting these changes has been proposed.

The following is a summary of the research findings:

- Inkjet printed films of SnO₂:Sb have been successfully deposited onto borosilicate glass by inkjet printing with a transparency of 94% at 550nm. Films are approximately 1μm in thickness and have a stabilised sheet resistance of 4MΩ/sq. It is thought the high sheet resistance is from a low mobility caused by large numbers of defects trapping free carriers and also a high barrier potential associated with grain boundaries.
- Thermal annealing has been demonstrated to decrease the sheet resistance of inkjet printed SnO₂:Sb, with the lowest sheet resistance achieved of the order of 1kΩ/sq. It is suggested that the decrease, observed in samples annealed up to and including 800°C, is due to a sintering effect reducing grain boundary potential and a reduction in defect regions concomitantly increasing the carrier mobility. Film transparency at 550nm in thermally annealed films increases with increasing temperature and lies between 88 and 90%. No change in crystallinity is observed with thermal annealing.
- Laser processing of inkjet printed SnO₂:Sb with a 248nm KrF excimer laser has been demonstrated to reduce the sheet resistance of the inkjet printed films. The lowest values achieved were with 1000 pulses at fluence of 70mJcm⁻² where the film's sheet resistance was reduced to approximately 40kΩ/sq. The transparency at 550nm of laser processed films reduces with increasing number of laser pulses to a minimum value of 86%. It was shown through XRD that laser processing improved the film's crystallinity while TEM showed a layer of densification, associated with the expected absorption depth of the 248nm laser irradiation. The improvements are thought to be as a result of an increased mobility due to the increase in crystallinity and due to a reduction in the grain boundary potential caused by

the sintering. It is also thought that the carrier concentration of the films may be increasing due to better incorporation of the Sb dopant into the lattice. However, there is no direct evidence for this, since *Hall Effect* studies were inconclusive. This will consequently form a basis for future analysis.

- The electrical characteristics of thermally annealed inkjet printed films of SnO₂:Sb on borosilicate have been further improved by a subsequent laser process. Given that the mechanisms for improving conductivity with thermal annealing and laser processing are different this is perhaps not surprising. It would appear that the mobility is improved with a reduction in grain boundary potential and a decrease in defect regions with thermal annealing and that this is compounded by an increase in crystallinity and densification and increases in the carrier concentration with diffusion of the Sb dopant into the lattice with laser processing.
- Conductive films of SnO₂:Sb were produced on Cronar® substrates by RF magnetron sputtering with average sheet resistance values of 3kOhm/sq and transparency at 550nm of approximately 75%. Laser processing of these films reduced their sheet resistance, with 100 pulses at 40mJcm⁻² producing the lowest sheet resistance of 724Ohm/sq. XRD revealed that laser processing did not produce any changes in crystallinity nor in grain size, while TEM analysis appeared to confirm this. TEM also showed no apparent signs of densification. The improvements in sheet resistance are therefore attributed to a reduction in defects causing an increase in the carrier mobility.

Hence, in summary, Laser processing has been demonstrated to improve the properties of both inkjet printed and RF magnetron sputtered SnO₂:Sb films. Upon

analysis, the effect of the laser processing appears to be quite different for each deposition method. While increases in crystallinity, densification and carrier concentration are observable in inkjet printed films and all of which would account for improvements in the film's conductivity, none of these changes were detected with RF magnetron sputtered films, the improvements in which are attributed to a reduction in defect regions within the film. Clearly, further studies are necessary to fully determine the effects and to begin to understand the mechanisms of the laser and what affects them; directions for further studies are discussed in the next section.

7.2 Further Work

A major hindrance to the analysis of the inkjet printed films was the destruction of the premises and therefore equipment of the project partner's PTL Ltd in the Buncefield explosion in December 2005. As a result of this a supply of optimised and consistent samples was unavailable. Much of the further work that follows is as a direct result of this.

Further work from this study takes two obvious routes, the first being the use of further investigative technologies on the samples available and the second being a study of alternative deposition methods and alternative UV light sources.

7.2.1 Further Analytical Work

Although Hall measurements are extremely useful for determining the properties of semiconductor materials, it has not been possible to obtain any meaningful results with the samples used throughout this project. It is likely that this is both because the sheet resistance of the films is too high and the experimental set-up used was too crude. Time spent optimising the quality of both the inkjet printed and sputtered

films would improve the chances of obtaining useful results. There was also insufficient time to make significant amendments (such as interference screening and development of a method of ensuring good Ohmic contacts to the samples) to the experimental set-up for the Hall measurements and time spent on this could extract interesting results from the films. Assuming this could be achieved, it would be interesting to carry out further investigations using the Hall effect to determine if there is a change in carrier concentration and mobility with time for freshly deposited inkjet printed layers. This would help determine if indeed oxygen chemisorption was responsible for the stabilisation process observed in as-deposited samples. A study of the changes with films cleanly deposited onto quartz would help to determine if impurity diffusion is also partly responsible.

Further work to measure the Hall voltage would be useful with the thermally annealed samples, since morphological changes could not be detected and many authors have reported changes in carrier concentration and mobility with thermal annealing. Also useful on thermally annealed samples would be specific surface area measurements by the adsorption method using the BET isotherm to determine whether or not sintering is occurring.

For laser processed samples further Hall voltage measurements would also help to verify the increase in carrier concentration indicated by the shifts in the plasma frequency towards the visible. Another interesting study would be to investigate the changes in carrier concentration from as-deposited, to thermally annealed, to thermally annealed and laser processed. This method could also be applied with laser then thermal annealing to attempt to distinguish between the processing effects.

Rutherford backscattering would be a useful technique to use on the laser processed samples since the changes caused by the laser will only be observed to a certain depth. Since the radiation from the laser would pass through only the uppermost 150nm changes in elemental concentration due to laser processing could be detected indicating densification or Sb diffusion.

Since oxygen was beneficial to the thermal annealing process, there may be some benefit to laser processing films in a pressurised atmosphere containing oxygen, perhaps 20% oxygen in nitrogen as an initial investigation. The pressurised gas may allow processing at higher fluences without causing damage to the film and this was only carried out in an argon atmosphere during this study. Other studies relating to atmosphere that would be useful to carry out include the effect of atmosphere upon changes to sheet resistance, with a full study of the effect of storing samples in a controlled vacuum environment.

Access to X-ray diffraction has been limited during the project due to departmental moves, so XRD analysis has been patchy. Full analysis, using the same XRD system and parameters, of all the samples discussed within this body of work would be useful in determining crystal structure and how it changes. It would be particularly interesting to see if changes in crystallinity are observed on thermally annealed samples which are subsequently laser processed.

While the transmission spectra has given a glimpse of the possible behaviour of the carrier concentration, it would be particularly useful to investigate the spectra at larger and smaller wavelengths to better determine the position of the plasma

wavelength and absorption edge respectively. To fully analyse the optical characteristics, absorption spectra and reflection spectra would also need to be measured. This would reveal shifts in the absorption edge indicating changes to carrier concentration, as explained by Burstein-Moss [1, 2] or changes in crystalline structure (presence of SnO). Furthermore the absorption coefficient could be determined for the UV end of the spectra and this information applied to the selection of processing laser to gain maximum penetration through the film. Shifts in the other end of the spectrum could be analysed and processes optimised to maximise carrier concentration, without reducing visible transmission. One further analysis of the transmission spectra that would be interesting relates to the shift in interference fringes shown in Figure 4-15. An investigation to determine whether this is repeatable and if so what may cause it would be useful.

7.2.2 Alternative Processes

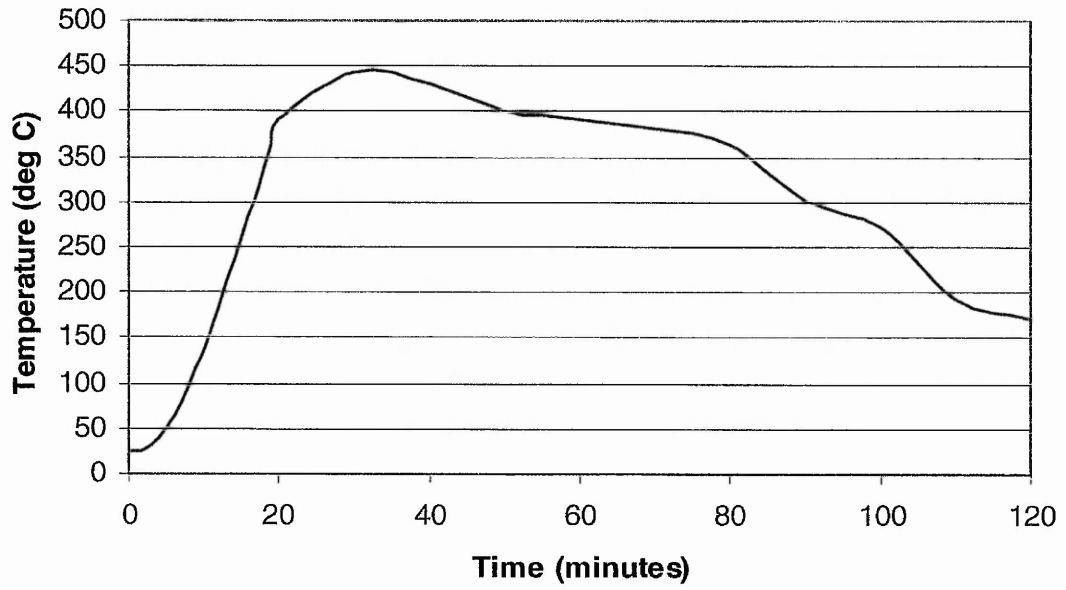
Since the energies required to affect a change in the SnO₂:Sb films are relatively low, certainly from the perspective of a high powered laser, an investigation into the effect of broad spectrum UV lamps on the films would be interesting. Considerably cheaper than an industrial UV laser, the use of a UV lamp could provide a low cost alternative, with a range of wavelengths maximising absorption into the film. Although the research in this area appears to be scant, it does appear other authors have had some degree of success with this method for sol-gel deposited ITO[3-5]. The use of a slightly longer wavelength laser (i.e. a frequency quadrupled Nd:YAG (266nm) or XeCl (308nm)), which would potentially extend further into the film, could also provide more improved results.

Finally, since the deposition method appears to largely influence the effect of the laser, an extensive study of the effect on a range of films produced by different deposition methods could be a way of determining and ultimately predicting the effect of the laser. This would of course, be no small study, but could provide a significant insight into the mechanisms by which the laser improves the properties of the films.

References

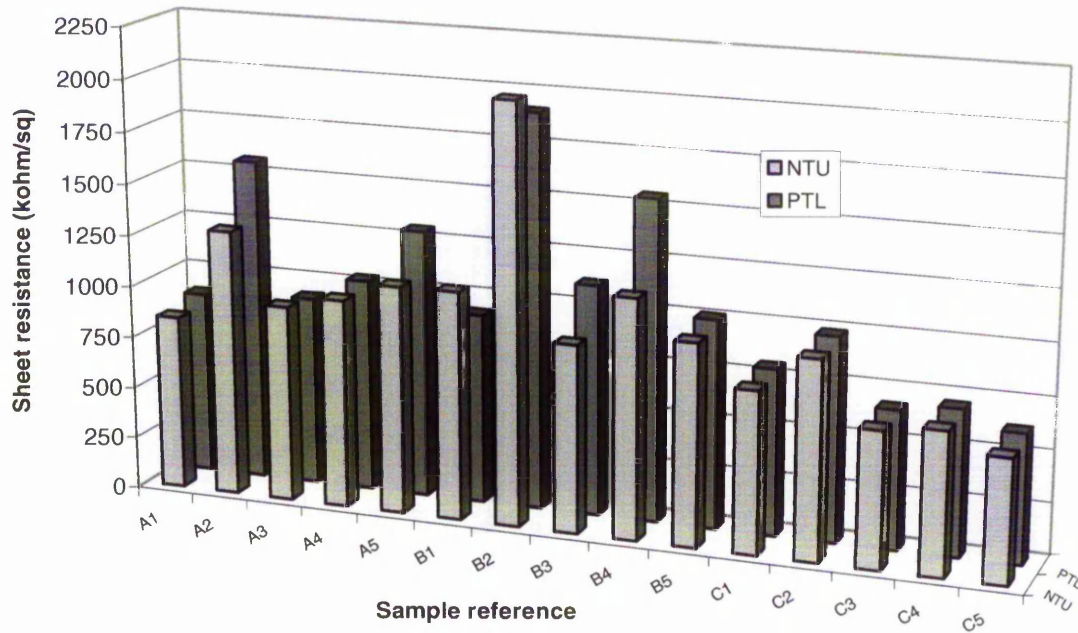
- [1] E. Burstein, "Anomalous Optical Absorption Limit in InSb," *Physical Review*, vol. 93, pp. 632, 1954.
- [2] T. S. Moss, "The Interpretation of the Properties of Indium Antimonide," *Proceedings of the Physical Society. Section B*, vol. 67, pp. 775, 1954.
- [3] H. Imai, A. Tominaga, H. Hirashima, M. Toki, and N. Asakuma, "Ultraviolet-reduced reduction and crystallization of indium oxide films," *Journal of Applied Physics*, vol. 85, pp. 203, 1999.
- [4] H. Imai, M. Yasumori, H. Hirashima, K. Awazu, and H. Onuki, "Significant densification of sol-gel derived amorphous silica films by vacuum ultraviolet irradiation," *Journal of Applied Physics*, vol. 79, pp. 8304, 1996.
- [5] V. Craciun and R. K. Singh, "Ultraviolet-assisted pulsed laser deposition of thin oxide films," *Applied Surface Science*, vol. 168, pp. 239, 2000.

APPENDIX A – Temperature Ramp for Annealing Process

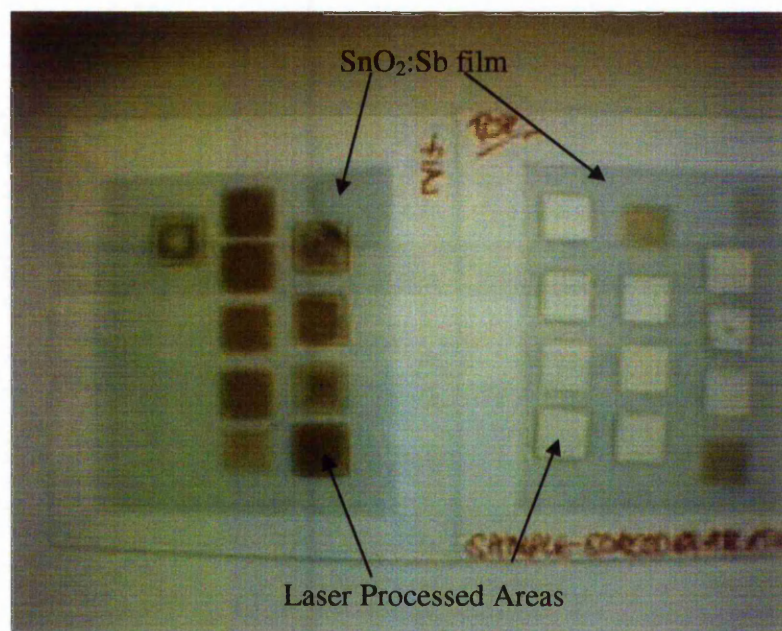


APPENDIX B – Comparison between Four Point Probe Measurements made at PTL Ltd and NTU.

Comparison between sheet resistance measured on NTU and PTL four point probes

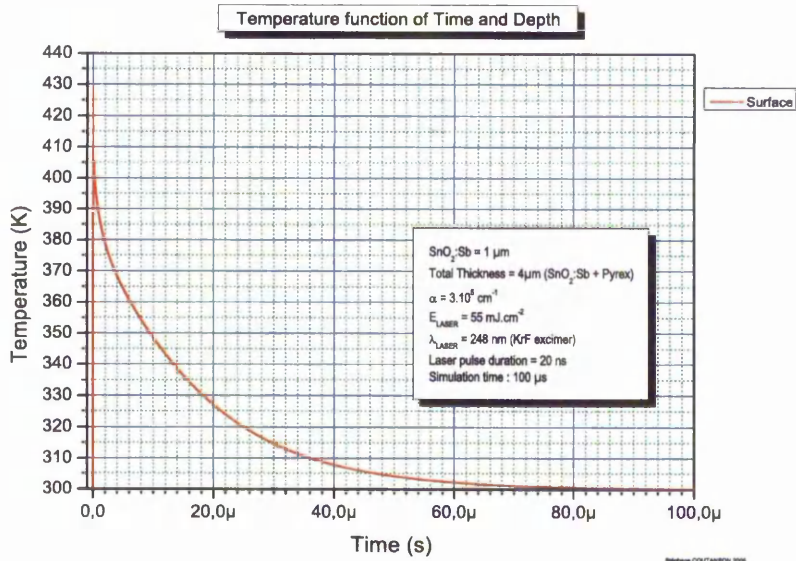
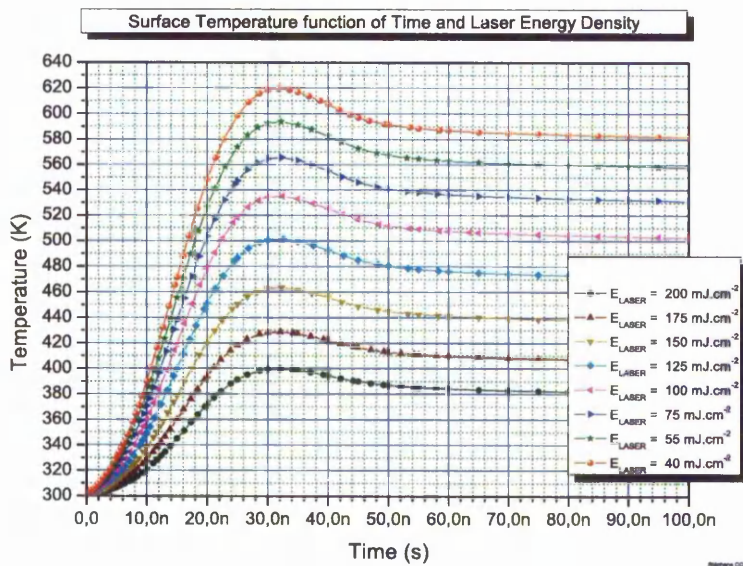
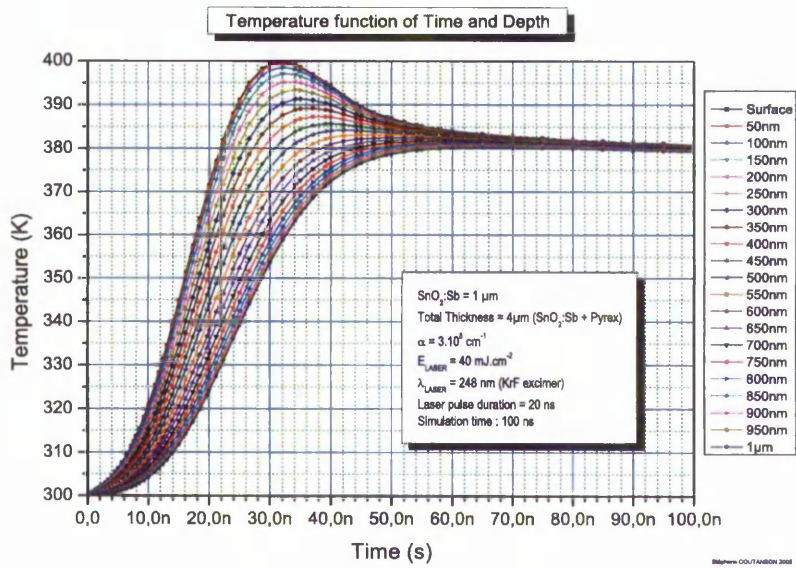


APPENDIX C – Comparison Between Water-Soaked and Dry Laser-Processed Inkjet Printed SnO₂:Sb for Removal of Film



Dry (L) and Water-soaked (R) showing clean removal of material on water soaked film of SnO₂:Sb

APPENDIX D – Thermal Model Simulations



PUBLISHED ARTICLES



ELSEVIER

Available online at www.sciencedirect.com

 ScienceDirect

Thin Solid Films 515 (2007) 8534–8538



www.elsevier.com/locate/tsf

Excimer laser processing of inkjet-printed and sputter-deposited transparent conducting SnO₂:Sb for flexible electronics

Wayne M. Cranton^{a,*}, Sharron L. Wilson^a, Robert Ranson^a, Demosthenes C. Koutsogeorgis^a,
Kuangnan Chi^b, Richard Hedgley^b, John Scott^b, Stephen Lipiec^c,
Andrew Spiller^c, Stuart Speakman^d

^a School of Computing and Informatics, Nottingham Trent University, Nottingham, NG11 8NS, UK

^b Patterning Technologies Ltd., 58 Shrivensham Hundred Business Park, Watchfield, Oxon, SN6 8TY, UK

^c Keeling & Walker Limited, Whieldon Road, Stoke-on-Trent, Staffordshire, ST4 4JA, UK

^d MDSL 7 Chapel Drive, Little Waltham, Chelmsford, Essex, CM3 3LW, UK

Available online 1 April 2007

Abstract

The feasibility of low-temperature fabrication of transparent electrode elements from thin films of antimony-doped tin oxide (SnO₂:Sb, ATO) has been investigated via inkjet printing, rf magnetron sputtering and post-deposition excimer laser processing. Laser processing of thin films on both glass and plastic substrates was performed using a Lambda Physik 305i excimer laser, with fluences in the range 20–100 mJ cm⁻² reducing sheet resistance from as-deposited values by up to 3 orders of magnitude. This is consistent with TEM analysis of the films that shows a densification of the upper 200 nm of laser-processed regions.

© 2007 Elsevier B.V. All rights reserved.

Keywords: Transparent conducting oxide; Inkjet printing; Thin film; Laser processing; Excimer laser; Displays; Flexible substrates; Conductivity

1. Introduction

In the field of plastic electronics and displays, there is a need to develop materials and processes that are compatible with large-scale, low-cost, production techniques. For plastic electronics, and particularly flexible displays, one of the major challenges that this presents is the need to produce optimised transparent electrodes and light emitting layers on low-temperature substrates. In terms of available transparent electrode materials, indium-doped tin oxide (ITO) remains the material of choice for most display and lighting applications, due to its excellent optical transparency and conductivity. However, while the deposition of ITO by sputtering is a well-developed process, it is one that poses several problems in the current and future requirements for this sector. A critical issue with

commercial ITO deposition is the materials waste generated by conventional sputtering – where up to 65% of a target is unused. With indium demand outstripping supply, the need for a viable alternative material is consequently highlighted, and ideally one that can address the materials' wastage issues associated with conventional deposition and subtractive patterning techniques.

The work presented here is the result of a collaborative investigation into the use of an alternative to indium tin oxide for a study of inkjet printing and laser processing. Antimony doped tin oxide, ATO (SnO₂:Sb) has been selected for the study, due to the feasibility of fabricating nanoparticulate source material suitable for both suspension in an aqueous solution for inkjet printing, and pressing into solid sputtering targets suitable for use in sputter deposition. The investigation has been specifically concerned with the study of low-temperature deposition and patterning techniques for the production of transparent conducting layers of ATO. The processes investigated are inkjet printing and low-temperature rf magnetron sputter deposition followed by excimer laser processing to enhance conductivity using processes that are compatible with flexible substrates.

* Corresponding author.

E-mail addresses: wayne.cranton@ntu.ac.uk (W.M. Cranton), kuangnan.chi@pattech.com (K. Chi), s.lipiec@keelingwalker.co.uk (S. Lipiec), sps7859@btconnect.com (S. Speakman).

2. Experimental details

The ATO source material was supplied by Keeling & Walker Ltd as a nano-particulate aqueous dispersion with an agglomerate size of less than 100 nm, which is sufficient to impart transparency. The aqueous solution was formulated for inkjet printing by Patterning Technologies Ltd. The formulation has been designed to provide stable jetting with good wetting characteristics on a variety of substrates and with minimal Marangoni effect. In all cases, unless otherwise stated, the ATO film was created with two wet passes in the inkjet printer, creating a single 90 mm × 70 mm layer.

For comparison with sputter deposition, the ATO powder was pressed into a 5-mm-thick, 70-mm-diameter circular target, using a hydraulic target press operating at room temperature. Sputter deposition was performed in a custom-built rf-magnetron sputtering system described previously [1] with the substrate facing down, and with no substrate heating. During the deposition process, the maximum temperature attained by the substrate is 80 °C. A range of printed and sputtered layers were deposited for the investigation onto substrates consisting of borosilicate glass and polyester flexible substrates (Cronar).

The effect of thermal and excimer laser annealing of the deposited films was investigated using atmospheric thermal annealing in a furnace, and excimer laser via KrF 248 nm irradiation. The resultant films were analysed for thickness, sheet resistance, transparency, crystallinity and microstructure. Sheet resistance (R_s) measurements were carried out using a linear four-point probe. The transmission spectrum of the sample from 400 to 1000 nm was measured using a Filmetrics F20 thin film analyser and thickness measurements were taken using a Veeco optical profilometer (NT1100). Laser processing was carried out with a LPX305i KrF Excimer laser at fluences < 100 mJ cm⁻².

The laser processing system used for both ablation and post-print processing is shown in Fig. 1. This is a configuration also used for laser processing work on thin film phosphors for displays [2,3] and has been demonstrated to facilitate large area processing of display substrates via a sample step and repeat process [4]. Lower fluences (appropriate for this work) are obtained by attenuation of the raw beam prior to homogenation using the Fresnel reflections from fused silica plates (Hoya Plates) as shown in Fig. 1. Beam energy during irradiation is monitored with an in situ energy meter, as shown in Fig. 1.

The short pulse width of the laser beam (20 ns) coupled with the high absorption coefficient of ATO at 248 nm (1.5×10^5 cm⁻¹)

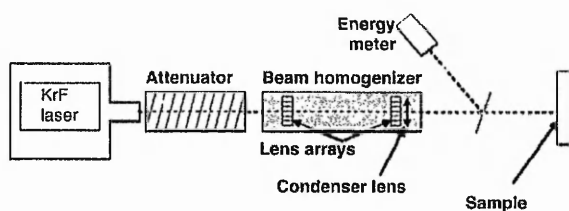


Fig. 1. Schematic diagram to show the optical system used for excimer laser processing of ATO thin films.

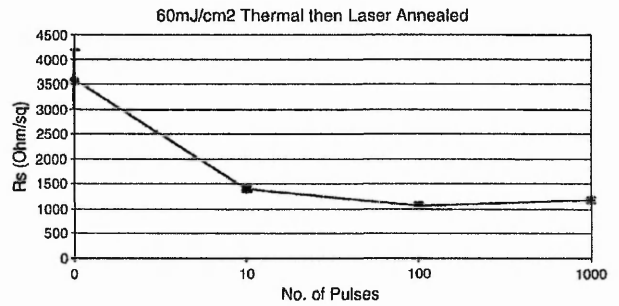


Fig. 2. Sheet resistance, R_s , as a function of laser processing irradiation pulse number, for printed ATO thin films on glass substrates that have been laser processed at 60 mJ cm⁻² following a thermal anneal to 400 °C for 1 h. The data point at 0 pulses represents the film following thermal annealing.

is expected to confine the energy dissipation due to the incident beam to the upper 150–200 nm of the film [5], with minimal effect on the substrate.

3. Results and discussion

Initial results from a study of the effect of laser processing on inkjet printed films of ATO on glass were presented previously [6]. A variety of laser irradiation parameters was investigated to study the effect of varying fluence and number of pulses incident on the samples. Irradiation was at a repetition rate of 4 Hz to avoid cumulative thermal effects [7]. The samples were processed in air at atmospheric pressure.

In all cases, laser processing of these printed ATO films resulted in reductions in sheet resistance from the as deposited figure of 4–5 MΩ/sq, with optimum values obtained at 100 pulses of 40–70 mJ cm⁻². For example, values of R_s = 300 kΩ/sq were obtained with 100 pulses at 70 mJ cm⁻². The corresponding optical transmission of these samples decreased from 94% to 90% at 550 nm following laser processing. Higher fluences or a higher number of pulses resulted in an increase in R_s and a decrease in optical transmission, concomitant with the observation of ablation and roughening of the film.

In order to provide reference samples for comparison with the low-temperature laser processing, thermal annealing of printed ATO on glass substrates was carried out in a Carbolite CWF 12/5 furnace ramping the sample from room temperature to 440 °C over 30 min and then slowly cooling back to room temperature over 90 min, resulting in a decrease in sheet resistance to typical values of 1–3 kΩ/sq. Optical transparency of the printed films was very good with 94% transmission at 550 nm, dropping to 92% after thermal annealing, which is in agreement with results reported for sol-gel films [8,9].

For the new work presented here, further batches of samples were prepared to investigate the effect of combining thermal and laser processing, and to examine the feasibility of fabricating transparent conductive films on low-temperature substrates. Laser processing was then undertaken on films that had previously been thermally annealed to 400 °C for 1 h. The results, presented in Fig. 2, show further reduction in R_s from the post-thermal anneal value of 3.6 kΩ/sq to a final figure of

1 k Ω /sq. These films were more mechanically stable than films that had not been thermally annealed prior to laser processing – indicating an enhanced bonding with the substrate. This combined process also produced the most conductive films to-date from the inkjet-printed films. A single sample was irradiated across the full sample area and R_s was measured before and after processing at 25 locations across the printed area. Uniformity of R_s was very good both before and after laser processing with average R_s =831 Ω /sq, σ (standard deviation)=183 Ω /sq, after thermal annealing, and average R_s =489 Ω /sq, σ =42 Ω /sq after subsequent laser processing with 100 pulses at 70 mJ cm⁻².

Samples that were thermally annealed following laser processing did not exhibit such an overall improvement, but attained values comparable to the results produced by thermal annealing alone, following initial reductions due to laser processing consistent with the results of the initial study reported in Sandu et al. [5].

From XRD and scanning electron microscopy studies of these films, it is evident that there is no significant increases in crystallinity, or grain size, observed for either the thermally annealed or the majority of the laser-processed films. There is, however, some limited evidence that higher fluence and/or pulse number of laser irradiations leads to enhanced crystalline ordering as indicated by a slight increase in XRD peak height, but this is inconclusive and will be the subject of a separate study using glancing XRD analysis.

Surface roughness measurements give a more direct indication of a sintering, or densification effect that correlates to improved conductivity. R_a values determined by optical profilometry and stylus profilometry show the as-deposited surface roughness varying between 20 and 35 nm across the samples, with typical post-processed R_a values (both thermal- and laser-processed) at between 3 and 10 nm. This indicates that the increase in conductivity is probably linked to the reduction of energy barriers at grain boundaries, possibly in combination with the modification of charge carrier densities due to the formation of enhanced donor sites via thermal processes. The low surface roughness measurements are also of interest for device fabrication – particularly display devices. Indeed, ATO deposited by sol–gel processes has recently been used to improve the surface roughness of ITO films for use in display applications, since with ITO films, localised spikes are an issue [10].

The ultimate aim of this work is to identify processes that could be used to fabricate transparent conductive layers by inkjet printing onto flexible substrates, rather than glass. This consequently requires a low-temperature process that is compatible with the substrates used. Polyester substrates are of interest for use in flexible display and electronics manufacture, but require processing temperatures to be maintained at temperatures typically less than 150 °C–200 °C. The potential for excimer laser processing of inkjet printed ATO on polyester is thus of interest for the feasibility of transparent conductive layers being patterned via an additive rather than subtractive process, and also for the benefit of low-temperature processing. For this phase of the investigation, a range of ATO layers and patterns were printed onto polyester (Cronar) substrates at room temperature, with no post-deposition thermal processing. Printing was under-

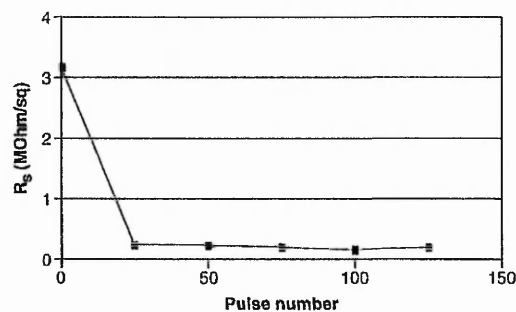


Fig. 3. Sheet resistance, R_s , as a function of laser processing irradiation pulse number, for printed ATO thin films on polyester substrates following laser processing at 20 mJ cm⁻². The data point at 0 pulses represents the as-deposited film.

taken using the same two pass processes as performed previously on the glass substrates. Measured sheet resistance values across printed 3 cm×3 cm samples give an average R_s of 2.7 M Ω /sq with σ =0.324 M Ω /sq.

Laser processing of these films was performed at 20 mJ cm⁻² and 100 mJ cm⁻² for a range of total pulse number irradiations, with the results showing good reduction of R_s as a function of processing parameters, as shown in Fig. 3, with optimum conditions resulting in printed films with an optical transparency of 89% at 550 nm, and R_s =200 k Ω /sq. In all cases, irradiation at 20 mJ cm⁻² did not produce any visible damage to the substrates or film. At 100 mJ cm⁻², some roughening of the film surface was observed, but there was no damage to the substrate. Hence, while further investigation and refinement is necessary to reduce R_s further, these results clearly demonstrate the feasibility of using excimer laser processing, or an equivalent flash annealing process, combined with inkjet printing for the fabrication of transparent conducting electrodes onto flexible substrates.

Fig. 4 shows the result of high-resolution transmission electron microscope analysis of inkjet-printed ATO films on polyester substrates before and after laser processing. The nanoparticulate structure of the ATO film is clearly visible in the micrographs, confirming the primary particle size to be ~10 nm. Following laser processing at 70 mJ cm⁻² 1000 pulses, Fig. 4b shows a clear region of densification at the surface of the film that is consistent with the expected penetration depth of the 248 nm irradiation – to ~200 nm. This physical transformation of the upper surface correlates to the improvement in conductivity observed, and indicates that there is a probable reduction in electron barrier height between grains as a result of defect and void removal via this densification. Similar results were observed by SEM analysis of samples on glass substrates – indicating a densification at the film surface following laser processing, but the results shown in Fig. 4 are more conclusive, due to the ease of preparing TEM samples from the films on polyester. Further analysis is underway, and there is evidently an opportunity to examine the use of longer wavelength irradiation in combination with the 248 nm process, in an attempt to increase the conductivity by a more thorough in-depth densification of the ATO.

Finally, as a comparison to the inkjet printed thin films, a series of samples were deposited onto borosilicate glass substrates using a custom-built rf-magnetron thin film deposition system [1]. Films were deposited using the following parameters: Ar/O₂, 10% O₂ sputtering gas maintained at 5 mTorr pressure, with 100 W rf power applied to the 70-mm-diameter pressed powder sputtering target, mounted onto a Kurt Lesker Torus electrode. The substrate was mounted onto a heated rotating substrate holder facing down, with the electrode head 15 cm from the substrate at an angle of 30° to the normal. For this work, the heater was not used, but monitoring of the substrate temperature during deposition indicates that the maximum temperature attained due to the plasma heating effect is 80 °C. Films were deposited to a thickness of 350–400 nm. The resultant films were conductive with sheet resistances of the order of 3–10 kΩ/sq, and optical transparency at 550 nm of 88%. Hence, in comparison to the printed films, the as-deposited conductivity is enhanced, but transparency is reduced. SEM observation reveals the expected columnar polycrystalline structure of sputtered films.

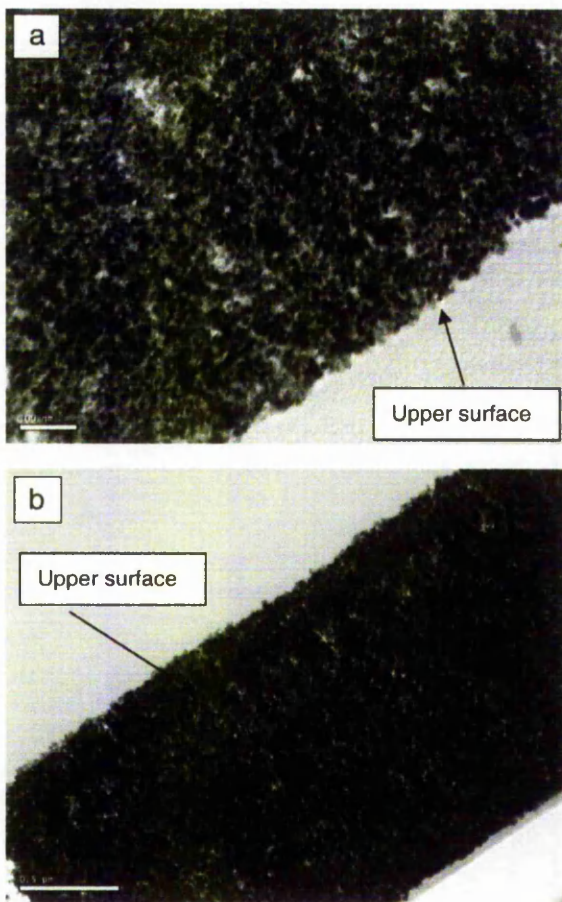


Fig. 4. Transmission electron micrographs showing cross-sectional images of 1- μm -thick ATO thin films inkjet printed onto polyester substrates: (a) as-deposited film illustrating primary nanoparticulate structure of the film; (b) identical sample following laser processing at 70 mJ cm^{-2} , 1000 pulses, indicating enhanced densification of upper 200 nm.

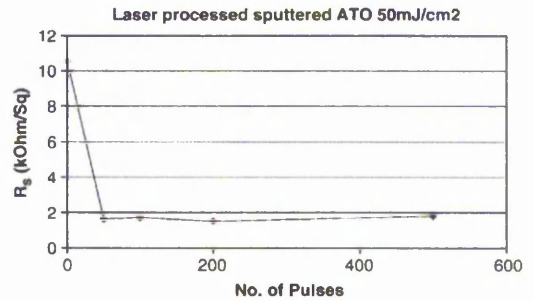


Fig. 5. Sheet resistance, R_s , as a function of laser processing irradiation pulse number, for rf-sputtered ATO thin films on glass substrates, following laser processing at 80 mJ cm^{-2} . The data point at 0 pulses represents the as-deposited film.

Post-deposition laser processing was performed as with the printed films. In all cases, the use of 248 nm irradiation resulted in an improvement in conductivity, with the best improvements at fluences and pulse number similar to the optimum demonstrated for the printed films. A typical result is shown in Fig. 5 where the initial sheet resistance of $10.7 \text{ k}\Omega/\text{sq} \pm 0.2 \text{ k}\Omega/\text{sq}$ is reduced to $1.7 \text{ k}\Omega/\text{sq} \pm 0.02 \text{ k}\Omega/\text{sq}$ following 100 pulses at 50 mJ cm^{-2} . Unlike with the printed films, initial electron microscopy analysis does not indicate a dramatic change in the film density at the upper surface, but it is suspected that a similar process of defect removal is occurring to reduce energy barriers at grain boundaries, and this is currently being investigated further.

4. Conclusions

A study of potential low-temperature techniques for use in the fabrication of transparent conducting oxides on flexible substrates has been undertaken. Inkjet printing of ATO films has been demonstrated as a viable technique for the additive patterning of transparent conducting layers onto glass and polyester substrates. Thermal annealing of these films at 400 °C results in useful conductivities in the range of $\leq 1 \text{ k}\Omega/\text{sq}$, which is applicable to device work on glass substrates, and which indeed has been used as a basis for the fabrication of inorganic electroluminescent display demonstrators [11]. The use of thermal annealing, however, precludes use of low-temperature substrates, but laser processing with 248 nm KrF irradiation has been demonstrated to be a viable method for reducing the as-printed sheet resistance by an order of magnitude. This improvement is consistent with an observed densification of the upper 200 nm of the ATO films following the irradiation treatment. The reduced R_s values are due to a low-resistance upper layer in parallel with the higher resistance lower section of the film. It is thus expected that this effect can be exploited by the use of variable wavelength irradiation in an attempt to process the full depth of the film for higher conductivities. In addition, the fluence levels that have been demonstrated to be optimum for this work are $< 100 \text{ mJ cm}^{-2}$, which implies that alternative UV-based pulsed annealing techniques could be suitable for this application. Finally, the use of excimer laser processing to realise conductive transparent films deposited by low-temperature rf-magnetron sputter deposition has been demonstrated, based on

sputter deposition of the ATO nanoparticulate powder that has been used for the inkjet printing trials. Optimum laser processing parameters are similar to those appropriate for the printed films.

Acknowledgements

The authors would like to thank the UK Department of Trade and Industry and the Engineering and Physical Sciences Research Council for the funding support that has enabled this collaborative research project. This work was undertaken as part of the DTI ISD Link Programme – ELJET – Electroluminescent Displays by Inkjet Printing.

References

- [1] W.M. Cranton, D.M. Spink, R. Stevens, C.B. Thomas, *Thin Solid Films* 226 (1) (April 15 1993) 156.
- [2] E.A. Mastio, M.R. Craven, W.M. Cranton, C.B. Thomas, M. Robino, E. Forgarassy, *J. Appl. Phys.* 86 (5) (1999) 2562.
- [3] D.C. Koutsogeorgis, E.A. Mastio, W.M. Cranton, C.B. Thomas, *Thin Solid Films* 383 (1–2) (Feb. 15, 2001) 31.
- [4] D. Koutsogeorgis, PhD Thesis, Nottingham Trent University, 2004.
- [5] C.S. Sandu, V.S. Teodorescu, C. Ghica, B. Canut, M.G. Blanchin, J.A. Roger, A. Brioude, T. Bret, P. Hoffmann, C. Garapon, *Appl. Surf. Sci.* 208–209 (2003) 382.
- [6] S.L. Wilson, W.M. Cranton, R. Ranson, D.C. Koutsogeorgis, A. Mosley, C.B. Thomas, G. Boutaud, S. Wagland, E.A. Mastio, S. Lipiec, A. Spiller, J. Scott, S. Stoute, *SID Symp. Dig.* 35 (1) (2005) 530.
- [7] C.S. Sandu, V.S. Teodorescu, C. Ghica, P. Hoffmann, T. Bret, A. Brioude, M.G. Blanchin, J.A. Roger, B. Canut, *J. Sol–Gel Sci. Technol.* 28 (2003) 227.
- [8] T. Boudiar, C.S. Sandu, B. Canut, M.G. Blanchin, V.S. Teodorescu, J.A. Roger, *J. Sol–Gel Sci. Technol.* 26 (2003) 1067.
- [9] M.I.B. Bernardi, L.E. Soledade, I.A. Santos, E.R. Leite, E. Longo, J.A. Varela, *Thin Solid Films* 405 (2002) 228.
- [10] G. Guzman, B. Dahmani, J. Puetz, M.A. Aegerter, *Thin Solid Films* 502 (2006) 281.
- [11] S. Wagland, MSc. Dissertation, University of Dundee, October 2005.

P-169: Optimization of the Electrical and Optical Properties of Ink-Jet-Printed SnO(2):Sb using Thermal Annealing and Excimer-Laser Processing

S. L. Wilson, W. M. Cranton, R. Ranson, D. C. Koutsogeorgis, A. Mosley, C.B. Thomas, G. Boutaud, S. Wagland, E.A. Mastio

Displays Research Group, School of Computing and Informatics, Nottingham Trent University, Nottingham, Nottinghamshire, UK

T: +44 (0) 115 8482885, Email: N0022984@ntu.ac.uk, wayne.cranton@ntu.ac.uk, robert.ranson@ntu.ac.uk

S. Lipiec, A. Spiller

Keeling & Walker Limited, Whieldon Road, Stoke-on-Trent, Staffordshire, ST4 4JA, UK.

T: +44(0) 1782 744136, Email: s.lipiec@keelingwalker.co.uk, a.spiller@keelingwalker.co.uk

J.Scott, S. Stoute

Patterning Technologies Limited, Fujifilm House, Boundary Way, Hemel Hempstead, Hertfordshire, HP2 7RH, UK

T: +44(0) 1442 251720, Email: john.scott@pattech.com, sheldon.stoute@pattech.com

Abstract

Sb doped SnO₂ has been formulated and inkjet printed onto borosilicate glass substrates. The resultant films have been post processed using traditional thermal annealing up to 440°C and laser processing with a KrF excimer laser ($\lambda = 248\text{nm}$). Sheet resistance values of $700\Omega/\square$ have been achieved with thermal annealing, whilst transparency remains $>85\%$ in the visible region. As a result of laser processing significant decreases in sheet resistance of the inkjet printed layers have been demonstrated indicating the viability of inkjet printing onto flexible substrates. The optical transmittance of the laser processed films has been shown to remain $>85\%$. Initial measurements indicate that thermal and laser post processes reduce surface roughness.

1. Introduction

Transparent Conducting Oxides (TCOs) have been extensively studied[1-5] because their excellent transparency and conductive properties are ideal for use in applications such as electronic displays, solar cells and photodetectors, where they typically form electrodes. There are many methods of depositing the electrodes including spray pyrolysis[6], r.f. sputtering[7], chemical vapour deposition[8] and spin coating[9]. However, conventional TCO deposition methods are usually subtractive processes requiring either a masking and etching process (photolithography) or laser ablation in order to form patterned electrodes. The manufacture of such devices therefore requires additional processes, time and ultimately cost. Identification of a suitable direct printing process for patterned TCO layers would be advantageous, with minimal material wastage and cost benefits and thus forms the basis of this work, where the TCO is required to be deposited onto flexible substrates.

The present work is the result of a collaborative project investigating the material science and processing techniques required to achieve viable inkjet printing of Sb doped SnO₂ to

produce electrodes suitable for use in display fabrication. Antimony Tin Oxide (ATO) has been identified as a suitable material because of its lower cost in comparison to Indium Tin Oxide (ITO) and the relative ease with which it can be suspended to formulate the ink. The initial target for films to be used in AC Electroluminescent displays is a transparency $> 85\%$ across the visible spectrum, and a sheet resistance of better than $300\Omega/\square$. This paper presents the preliminary results of the investigation and demonstrates the viability of the combined inkjet printing and laser irradiation process to achieve conductive transparent thin films on low temperature substrates.

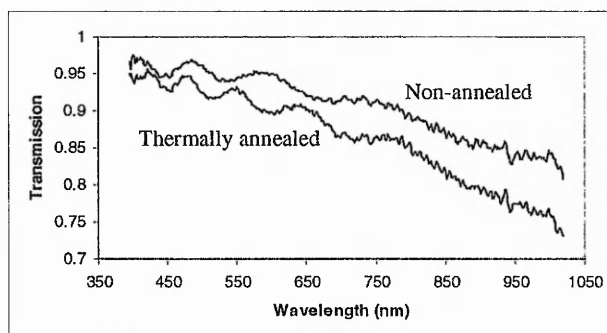
2. Experiment

For the purposes of the presented work, the ATO was inkjet printed as a 90x70mm rectangle onto Borosilicate slides. The ink was based on an electrically conductive ATO powder produced from separate chemical precursors of antimony oxide and tin oxide. These precursors were precipitated and chemically combined, pH adjusted and washed to remove impurities. The resulting powder was dried and calcined to form the electrically conductive ATO material. The resultant material, comprising aggregates of nano-sized primary ATO particles, was milled to an agglomerate size of less than 100nm which is sufficient to impart transparency to coated films. This was formed into an aqueous dispersion, which was subsequently formulated for ink jet printing. The formulation has been designed to provide stable jetting with good wetting characteristics on a variety of substrates and with minimal Marangoni effect (coffee staining). In all cases, unless otherwise stated, the ATO film was created with two wet passes in the inkjet printer, creating a single layer.

Following a drying stage, the inkjet printed ATO samples were thermally annealed and laser processed. The resultant films were analysed for sheet resistance, transparency, surface roughness and thickness.

Sheet resistance (Rs) values measured at Nottingham Trent

University (NTU) and Patterning Technologies Ltd (PTL) were carried out using a linear and square four-point probe respectively. The transmission spectrum of the sample from 400 – 1000nm was measured using a Filmetrics F20 thin film analyser and thickness measurements were taken using a Veeco optical profilometer (NT1100) after a step was ablated in the ATO using a LPX300 KrF Excimer laser. Ablation of the ATO thin film was performed using the laser at a typical fluence of 150mJcm⁻², which did not result in the ablation of the substrate surface. Thermal annealing was carried out in a Carbolite CWF 12/5 furnace ramping the sample from room temperature to 440°C over half an hour and then slowly cooling back to room temperature over 90 minutes. Laser processing was carried out with the LPX300 KrF Excimer laser. The laser processing system used for both ablation and post print processing is shown in Figure 1.



Transmission spectra of inkjet printed ATO, pre and post thermal annealing.

Figure 2

3.1.3 Surface roughness

The typical surface roughness, Ra, of a non-annealed, as-printed sample is of the order of 30nm.

Following the thermal annealing process, the surface roughness was consistently reduced, to a typical value of 10 - 15nm indicative of a densification / sintering process, although, as mentioned above, this did not produce any observable grain size increase.

3.2 Laser Processing

Since the aim of this work is to develop an electrode fabrication and patterning process that would be suitable for use on low temperature substrates, there is a need for alternative conductivity enhancing techniques to replace the thermal processing. From the previous work undertaken by the authors on the use of excimer laser processing to enhance thin film phosphors with minimal effect on the underlying electronic interfaces[13], we have developed a technique that would also be suitable for use on inkjet printed thin films. The system shown in Figure 1 was used to irradiate samples of the inkjet printed ATO to investigate the viability of this technique. KrF (248nm) irradiation was used at 4Hz to avoid cumulative thermal effects[14]. At this wavelength, the absorption characteristics of ATO thin films would ensure that the energy is absorbed within the upper 150 - 200nm of the thin film layer, depending on density[15]. Nine samples were laser processed with the range of different parameters shown in Table 1. A five by five array of laser processed areas was created on each sample to give five repeat samples of each annealing condition on each sample. For this preliminary investigation, the samples were processed in air at atmospheric pressure.

Table 1

Beam Energy \ N ^o of Pulses	N ^o of Pulses		
	1-10	10-100	100-1000
20mJ/cm ²	Sample 1	Sample 2	Sample 3
40mJ/cm ²	Sample 4	Sample 5	Sample 6
70mJ/cm ²	Sample 7	Sample 8	Sample 9

Parameters used to irradiate the inkjet printed ATO with the KrF 248nm pulsed laser

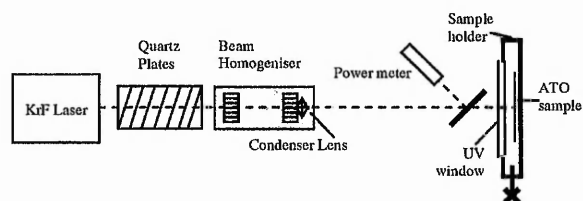


Figure 1

3. Results

Typical inkjet printed ATO thicknesses were in the region of 1µm, ± 10%. The thickness showed no appreciable variation with post processing.

3.1 Thermal Annealing

3.1.1 Sheet Resistance

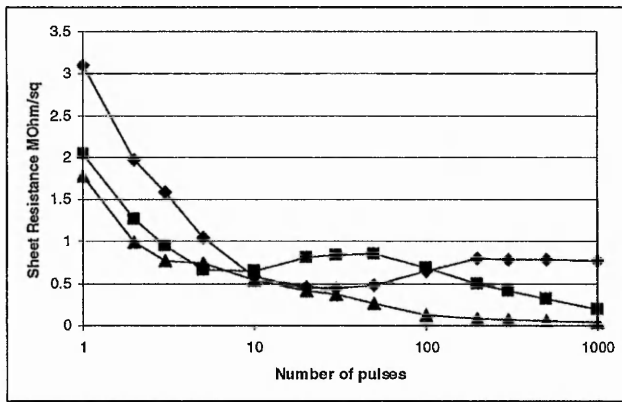
The sheet resistance of the samples was measured before and after thermal annealing. As-deposited films have a high sheet resistance, of the order of 4MΩ/□. However, in all instances of thermal annealing, a significant decrease in Rs was observed, with recent films exhibiting sheet resistances of 700Ω/□. X-ray diffraction and scanning electron microscopy studies were performed on the films before and after annealing, but there were no significant increases in crystallinity, or grain size observed for the thermally annealed films, although there is evidence of some sintering occurring, as would be expected[10]. This indicates that the increase in conductivity is probably linked to the reduction of energy barriers at grain boundaries, or to the modification of the charge carrier density due to enhanced donor sites.

3.1.2 Transparency

The transparency of the as-deposited ATO was good, with 94% transmission at 550nm. Following thermal annealing a small reduction in transparency was observed to an average at 550nm of 92%. This is comparable to many reported values by other deposition methods[10-12]. The typical transmission spectra for an as-deposited and thermally annealed sample is shown in Figure 2, showing that the transparency across the visible spectrum is in the target region of >85%.

3.2.1 Sheet Resistance

The sheet resistance of each processed area was measured using the four-point probe. The results demonstrated that all laser-processed areas exhibited a decrease in sheet resistance compared with pre-processed values of $4\text{M}\Omega/\square$. The variation in sheet resistance with number of pulses and fluence is shown in Figure 3. The lowest value of R_s occurred in the areas processed with 1000 pulses. The greatest change in R_s occurred within the first 1-3 pulses with a general decrease to 1000 pulses. Between 10 and 100 pulses, there appears to be little effect. The further increase in number of pulses above 100 shows a continuing decrease in R_s which appears not yet to plateau at 1000 pulses. This suggests that the investigation should be extended until a rise or plateau in R_s is achieved and is an important consideration for future work.



The variation in sheet resistance post laser processing as a function of number of pulses and laser energy. $\diamond = 20\text{mJ}/\text{cm}^2$, $\blacksquare = 40\text{mJ}/\text{cm}^2$, and $\blacktriangle = 70\text{mJ}/\text{cm}^2$. The sheet resistance of these samples prior to annealing was typically $4\text{M}\Omega/\square$

Figure 3

3.2.2 Transparency

The transmission spectra of the laser processed ATO showed a decrease in transmission across the visible range with increasing number of pulses. For example, for the sample processed with a $40\text{mJ}/\text{cm}^2$ beam, the average transmission for 10, 100 and 1000 pulses across the visible spectrum was measured to be 89.9%, 89.6% and 85.2% respectively. These are comparable with typical values reported elsewhere of $>85\%$ [16].

The transmission spectra of inkjet printed ATO processed with 10, 100 and 1000 laser pulses is shown in Figure 4.

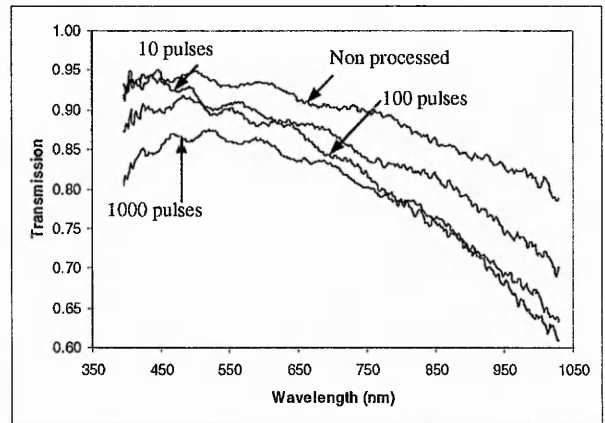
3.2.3 Surface Roughness

A limited number of samples have been measured for surface roughness post laser processing. These measurements indicate surface roughness is improved by laser processing, with typical post processing R_a values of 5-10nm.

3.2.4 Laser Processing Following Thermal Annealing

As a second phase of investigation, samples that had been

thermally annealed were then laser annealed to determine if further improvements could be gained. Initial experimentation was carried out with samples on borosilicate and having been annealed up to 440°C . It was demonstrated that further improvements in R_s could be made, with post laser processing providing a sheet resistance three times better than with thermal annealing only. Using this method R_s values of between $1\text{K}\Omega/\square$ and $450\Omega/\square$ were achieved. This is a promising trend that would need further investigation for applicability to thermally sensitive substrates with initial thermal annealing temperatures not exceeding 200°C .



Transmission spectra, post laser-processing, of the inkjet printed ATO for 10, 100 and 1000 pulses at $40\text{mJ}/\text{cm}^2$.

Figure 4

4. Conclusions

4.1 Sheet Resistance

The combined processes of inkjet printing and thermal annealing and / or laser processing have been demonstrated to produce conducting thin films with excellent visible spectrum transparency. The reduction in R_s from an initial $4\text{M}\Omega/\square$ to values of the order of several hundred Ω/\square indicate that these combined processes can produce films close to the target range of $300\Omega/\square$, $>85\%$ transmission. However, for practical and more diverse application, the sheet resistance must be reduced, ideally by a further order of magnitude. Current investigations are concerned with the use of reactive and reducing environments during the thermal and/or laser processing in order to reduce the final value of R_s . In addition, demonstrations of display devices fabricated from this inkjet printed TCO are currently being produced. In summary, the decreases in R_s reported in this paper are a promising indication of the possibilities of a low cost deposition method for a transparent conductor that would be suitable for use with low temperature substrates. The exact mechanisms at work are not yet clear, however it is thought that the post processing helps eliminate grain boundary defects that can otherwise increase the sheet resistance of the ATO. SEM images, not published here, show no discernable increase in grain size following either thermal or laser post processing. This demonstrates that grain growth is unlikely to be the source of

sheet resistance improvements and provides some support to the idea that grain boundary changes are occurring.

Although much of the work described here concerns thermal annealing, it also shows that significant reductions in R_s are achievable using laser processing to modify the properties of the as-deposited ATO layer. The use of the laser, rather than thermal processing, will enable deposition of the ATO on temperature sensitive substrates.

An investigation into multiple layer deposition has also begun and is showing R_s values of sub $300\Omega/\square$ following repeated thermal processing. Further laser work is required to investigate optimum parameters, including processing at pressure and in various gases as well as repeat processing, increasing number of pulses and processing after lower thermal annealing temperatures.

4.2 Transparency

The transparency of the as-deposited inkjet printed ATO is good with transmission in the visible region typically above 90%. With thermal processing there is an observable decrease in transmission, but only 2-3%. The values of transparency reported in this paper are comparable with many published and commercial values reported for more expensive and time-consuming deposition methods[17, 18].

Laser processing has been shown to be effective in reducing sheet resistance whilst still maintaining good transparency. Transmission in the visible region is >85% even with the highest number of pulses.

4.3 Surface Roughness

Surface roughness is an important parameter for display applications. As deposited, the average surface roughness is typically 30nm. Initial measurements of thermally annealed inkjet printed ATO indicate that R_a is reduced by up to two thirds by the annealing process. Furthermore, similar measurements on laser processed inkjet printed ATO show a greater reduction in R_a to values around 5nm. This is indicative of a sintering or densification process, although not easily detectable by SEM. The current post-processed values are of appropriate order of magnitude for most display applications (the notable exception being OLED[19]).

5. Summary

This paper highlights the progress of the work of a DTI funded consortium called ELJET. Recent work has demonstrated the feasibility of a low cost inkjet printed transparent conductor, with most recent single layer results achieving sheet resistances as low as $450\Omega/\square$ whilst still maintaining good transparencies of >85%. Furthermore, laser processing has demonstrated that it can be used as an effective post process to reduce sheet resistance, thus enabling the production of inkjet printed ATO on flexible and temperature sensitive substrates. Whilst further work is required to optimize these processes, all the results and indications are so far very encouraging.

6. Acknowledgements

Our thanks to DTI and EPSRC for the funding that has enabled this project: This project has been supported by the DTI LINK programme and by the COMIT Faraday Partnership/EPSRC.

7. References

- [1] S. Shanthi, C. Subramanian, P. Ramasamy. *Materials Science & Engineering B*. 57 (1999) 127
- [2] Sung-Soon Park, J.D. Mackenzie. *Thin Solid Films*. 258 (1995) 268
- [3] X. Hao, J. Ma, D. Zhang, X. Xu, Y. Yang, H. Ma, S. Ai. *Applied Physics A*. 75 (2002) 397
- [4] Xiaotao Hao, Jin Ma, Deheng Zhang, Yingge Yang, Xiangang Xu, Feng Chen, Honglei Ma. *Applied Surface Science*. 189 (2002) 157
- [5] G. Gasparro, J.Pütz, D. Ganz, M.A. Aegerter. *Solar Energy Materials & Solar Cells*. 54 (1998) 287
- [6] Garima Jain, R. Kumar. *Optical Materials*. 26 (2004) 27
- [7] Jow-Lay Huang, Yi Pan, Jia Yuan Chang, Bao-Shun Yau. *Surface & Coatings Technology*. 184 (2004) 188
- [8] Keun-Soo Kim, Seog-Young Yoon, Won-Jae Lee, Kwang Ho Kim. *Surface & Coatings Technology*. 138 (2001) 229
- [9] C. Goebbert, R. Nonninger, M.A. Aegerter, H. Schmidt. *Thin Solid Films*. 351 (1999) 79
- [10] M.J. Van Bommel, W.A. Groen, H.A.M. Van Hal, W.C. Keur, T.N.M. Bernards. *Journal of Materials Science*. 34 (1999) 4803
- [11] T. Boudiar, C.S. Sandu, B. Canut, M.G. Blanchin, V.S. Teodorescu, J.A. Roger. *Journal of Sol-Gel Science and Technology*. 26 (2003) 1067
- [12] M.I.B. Bernardi, L.E. Soledade, I.A. Santos, E.R. Leite, E. Longo, J.A.Varela. *Thin Solid Films*. 405 (2002) 228
- [13] E.A. Mastio, M.R. Craven, W.M. Cranton, C.B. Thomas, M. Robino, E. Forgarassy. *Journal of Applied Physics*. 86, 5 (1999) 2562
- [14] C.S. Sandu, V.S. Teodorescu, C. Ghica, P. Hoffmann, T. Bret, A. Brioude, M.G. Blanchin, J.A. Roger, B. Canut. *Journal of Sol-Gel Science and Technology*. 28 (2003). 227
- [15] C.S. Sandu, V.S. Teodorescu, C. Ghica, B. Canut, M.G. Blanchin, J.A. Roger, A. Brioude, T. Bret, P. Hoffmann, C. Garapon. *Applied Surface Science*. 208-209 (2003) 382
- [16] S.Shanthi, C. Subramian, P. Ramasamy. *Journal of Crystal Growth*. 197 (1999) 858
- [17] Jow-Lay Huang, Yi Pan, Jia Yuan Chang, Bao-Shun Yau. *Surface & Coatings Technology*. 184 (2004) 188
- [18] Jin Ma, Xiaotao Hao, Shulai Huang, Jie Huang, Yingge Yang, Honglei Ma. *Applied Surface Science*. 214 (2003) 208
- [19] Yoon-Heung Tak, Ki-Beom Kim, Hyoung-Guen Park, Kwang-Ho Lee, Jong-Ram Lee. *Thin Solid Films*, 411 (2002) 12